

POLITECNICO DI TORINO

Master's Degree
in Mechanical Engineering

Master's Degree Thesis

**Study of connections between modules
of an articulated vehicle using
multibody approach**



Supervisor

Prof. Aurelio Somà

Co-Supervisor

Ing. Nicolò Zampieri

Candidate

Carlo Galfione

A.Y. 2020-2021

October 2021

*“There is no passion to be found playing
small - in settling for a life that is less
than the one you are capable of living.”*
Nelson Mandela

Summary

This thesis work is the result of the internship carried out at the company Blue Engineering SRL.

The objective of this thesis is to determine the position, value and type of connection between the different modules of an articulated vehicle through the use of a multibody software called "Simpack". In detail, the mean of transport that has been considered is a trolleybus moved by electric motors and equipped with autonomous driving. All the data have been provided by the company mentioned above, in fact, some parts could not be included for issues of corporate secrecy.

During the discussion, it is explained how the following work is placed in the world's literature, starting with an analysis of the articles about autonomous driving and articulated vehicles; then, a detailed description of the trolleybus is made followed by the mathematical treatment of the elements used in the model such as the tire-asphalt contact, the longitudinal dampers and the tracks used to validate the results. Afterwards, the multibody approach is explained in a summary way, to give an idea of how it works and why it is used, and then moving on to the construction of the real model using the dedicated software; in this chapter the various steps useful to complete the model are explained in detail, starting from the construction of the various modules, the connection up to the use of speed control and steering systems. Finally, starting from the model in its entirety, the elements of connection are optimized thanks to the workspace in Simpack called "DoE" (Design of Experiment) which allows you to perform sensitivity analysis; in this chapter is optimized one element at a time, so the interaction between the various elements is not taken into account, this is because the optimization is performed on a path built ad hoc to excite a precise degree of freedom that is precisely regulated by the element of connection considered. Once all the elements are optimized, the forces exchanged by the spherical joint are extracted.

Table of Contents

List of Tables	VII
List of Figures	VIII
1 Introduction	1
1.1 State of the art of self-driving vehicles	1
1.1.1 Autonomous driving applications	6
1.2 State of the art of articulated vehicles	12
2 Vehicle description	15
2.1 Tire model	17
2.1.1 Reference system	18
2.1.2 Brush model	21
2.2 Longitudinal dampers	27
2.3 Creation of the paths	31
2.3.1 Track	31
2.3.2 Superelevation	33
2.3.3 Vertical direction	33
2.3.4 Road	34
2.3.5 Road excitations	35
2.4 Track used	37
3 Multibody architecture of the vehicle	43
3.1 Model construction	47
3.2 Reference frame of the model	47
3.3 Driving module	48
3.4 Data used	57
3.5 Assembly generation	57
3.6 Configurations studied	59
3.7 Connection between modules	60
3.7.1 Rigid connection	61

3.7.2	Lower connections - Joint	62
3.7.3	Longitudinal dampers (upper and lower)	63
3.7.4	Longitudinal springs	66
3.7.5	Configuration 1	68
3.7.6	Configuration 2	69
3.8	Preload	71
3.9	Steering system	73
3.10	Speed control	76
4	Optimisation	81
4.1	DoE in Simpack	83
4.2	Longitudinal springs	88
4.3	Silent block	90
4.3.1	Rolling stiffness	90
4.3.2	Pitch stiffness	94
4.4	Longitudinal dampers	98
4.5	Final configuration	104
4.6	Choice of the mechanical joint	105
4.7	Active dampers	108
5	Conclusion	114
	Bibliography	116

List of Tables

3.1	Markers distance from ISYS	52
3.2	Subvar used	56
3.3	Data used to build the model in terms of inertia and center of mass	57
3.4	From and To Markers positions	67
3.5	Longitudinal springs stiffnesses, nominal lengths and preloads . . .	67
3.6	Silent block Markers location	69
3.7	Free and locked d.o.f. constraint in order to perform preload	72
4.1	Connection Subvars used to optimize longitudinal springs	88
4.2	Variation of longitudinal springs stiffness for the analisis	89
4.3	Subvars used for the analysis	91
4.4	Variation of the parameter $\$_k_alfa$ for the optimization analysis .	91
4.5	Connection subvar used	95
4.6	Variation of the parameter $\$_k_beta$ for the optimization analysis	95
4.7	Values of optimised SubVars for longitudinal dampers	99
4.8	Variation of damping coefficient	100
4.9	Parameters used for the sensitivity analysis of longitudinal dampers	103
4.10	Input subvars explained	104
4.11	Optimized configuration for longitudinal dampers	104
4.12	Optimized connection subvar values	104
4.13	Longitudinal dampers positions	105
4.14	Maximum force in each direction for joint characterization	106

List of Figures

1.1	Sensors widely used in autonomous driving[2]	3
1.2	Gaussian pyramid image processing	7
1.3	Hough transform straight line detection	8
1.4	Lane boundary detection [6]	9
1.5	Hyperbola fitting [6]	9
1.6	YOLO working flow[8]	10
1.7	Articulated vehicles forms of instability [20]	13
2.1	NVIDIA DRIVE AGX Developer Kit	16
2.2	Reference frame	18
2.3	Deformable wheel with bristles [25]	20
2.4	Brush model pure longitudinal slip	22
2.5	μ_x function of longitudinal slip	23
2.6	Lateral Force and self-aligning moment with respect to the slip angle varying the vertical load	25
2.7	Force trend varying a parameter	28
2.8	1 d.o.f. mass-spring-damper system	29
2.9	Free response	30
2.10	Track segment types for superelevation	34
2.11	Track segment types for vertical direction	34
2.12	Road type parameters for vertical excitation	36
2.13	Track excitation	36
2.14	Road vertical excitation	37
2.15	Track road	37
2.16	Google Earth view of Corso Casterlfidardo roundabout	38
2.17	Roundabout geometry reconstruction	39
2.18	Data export from Solidworks	39
2.19	Double curve horizontal data	40
2.20	Double curve track characteristics	41
2.21	Vertical slope track construction	42

3.1	Body creation in Simpack	44
3.2	Assembly modules	47
3.3	Reference frame used in the construction of the model	48
3.4	Solidworks model built	49
3.5	Extraction of the center of mass and of the inertia matrix	50
3.6	COM Marker	50
3.7	Chassis mass properties	51
3.8	Degrees of freedom allowed for the chassis	51
3.9	Wheel hub mass properties	52
3.10	Wheel hub joint description	53
3.11	Geometric position of the marker belonging to the chassis (From)	53
3.12	Wheel mass properties	54
3.13	Wheel joint description	54
3.14	Suspension parameters used	55
3.15	Tire parameters used	56
3.16	Before translation	58
3.17	After translation	58
3.18	Configuration of the lower connections CM-TM/TrM	59
3.19	Configuration 1	60
3.20	Configuration 2	60
3.21	Front and rear rigid connection	61
3.22	0 d.o.f. Simpack definition	62
3.23	Joint Simpack definition	63
3.24	Force-speed trend through input function	64
3.25	α and β definition for longitudinal dampers	65
3.26	Definition of dampers in Simpack	65
3.27	Longitudinal springs From (in red) and To (in green) Markers	66
3.28	Longitudinal springs Simpack definition	67
3.29	Silent block definition in Simpack	68
3.30	Silent block location	68
3.31	Springs - Configuration 2	70
3.32	Creation in Simpack of the inclined springs elements	70
3.33	Constraint used to lock the wheel	72
3.34	Preload calculation	72
3.35	Steering marker	73
3.36	Steering Sensor definition	74
3.37	Steering Controller definition	75
3.38	Steering marker definition	76
3.39	Steering Left Constraint definition	76
3.40	Reference transient dynamics	77
3.41	Speed profile input function	78

3.42	Speed profile function of time	79
3.43	Proportional controller	79
3.44	Proportional actuator	80
3.45	Measured vehicle dynamics performance	80
4.1	Longitudinal springs top view	82
4.2	Sensitivity analysis post-processing	83
4.3	Experiment workspace	84
4.4	Input values properties	85
4.5	Result Element Properties	86
4.6	Responses workspace	87
4.7	Tasks workspace	87
4.8	Post-processing comparisons by varying stiffnesses	90
4.9	Vertical force on the wheel as the stiffness varies	92
4.10	Roll angle as the stiffness varies	93
4.11	Lateral slip and spring length as the stiffness varies	94
4.12	Vehicle behaviour approaching vertical slope	96
4.13	Influence of the maximum and minimum stiffness parameter on the vertical load (CM)	96
4.14	Influence of the maximum and minimum stiffness parameter on the vertical load (DM and DM2)	97
4.15	Influence of stiffness parameter on the vertical load (CM)	97
4.16	Step excitation to optimize longitudinal dampers	99
4.17	Yaw angle response to step excitation	100
4.18	Damper force response to step excitation	101
4.19	Comparison varying damping coefficient	102
4.20	Longitudinal dampers sensitivity analysis post-processing	103
4.21	Trend of the forces exchanged by the front joint over time	106
4.22	Trend of the forces exchanged by the rear joint over time	107
4.23	Front and rear joint force trend in y direction	107
4.24	Impulse applied through input function	109
4.25	PD calibrated compared with passive dampers	110
4.26	Trajectory comparison	111
4.27	R.M.S. vertical acceleration of the different modules	112
4.28	Roll, pitch and yaw angle responses to the impulse	113

Chapter 1

Introduction

1.1 State of the art of self-driving vehicles

An autonomous car is an automated vehicle that include the main transportation capabilities of a traditional car with little (or without) human inputs. Autonomous driving technologies are gradually gaining ground in the automotive industry. Just think about the fact that traffic could potentially be significantly reduced to zero if all people were equipped with self-driving vehicles, accidents could be avoided, and from a fuel consumption point of view, there could be benefits. In fact, in 2018, according to the Global Status Report published by the World Health Organization (WHO), the number of annual deaths from traffic accidents reached 1.35 million; that of traffic accidents has become one of the leading causes of unnatural death, which is also why, thanks to technology, there is the need for a change of course [1]. These are the most important reasons why self-driving vehicles are increasingly becoming a necessity and why companies are investing so much in this area.

In January 2014, SAE International released a classification called J3016 that defined six different levels for self-driving. Each level corresponds to what the driver needs to intervene in vehicle dynamics, meaning steering, acceleration and braking. A first classification is that of monitoring the surrounding environment, in fact from level 0 to level 2 this task is carried out by the driver. From level 3 to 6, instead, the monitoring of the driving environment is automated. This classification has allowed to clarify the technical and bureaucratic aspects related to the subject.

- Level 0: the automated system issues warnings and can intervene momentarily but does not have sustained control of the vehicle.
- Level 1: this level does not yet have any type of automation but is of assistance to the driver, who is supported through audible or visual alerts; an example

may be cruise control or Park Assist where responsibility for steering and speed is imposed by the driver who is aided by technology in certain circumstances.

- Level 2: It has one or more partial automations to support the driver; as mentioned, it does not yet have monitoring systems such that it is able to drive autonomously in even the simplest circumstances. However, the vehicle does have automated safety systems such as assisted braking or collision avoidance emergency braking. At this level, the maximum automation is when the signals are visible and at this point, the system can steer in a partially automated manner.
- Level 3: This level is the first to be equipped with systems that allow autonomous driving, this condition occurs only in special circumstances where environmental conditions allow it.
- Level 4: The automated system can provide a high degree of automation. However, this level has limitations; it can be used in certain geo-referenced areas or in traffic jams. If the car is not in a specific area or in a traffic jam, the system can rescue the driver in an emergency.
- Level 5: full automation.

When it comes to autonomous driving, the heavy use of sensory elements is a parameter to consider. Basically, they are used to analyze the conditions of the environment surrounding the car and the sensors' interaction of these are of primary importance for the reliability of an AV (Autonomous Vehicle). In this regard it is necessary to first make a distinction between the types of sensors, they can be divided for this discussion into two main types, intelligent sensors, and non-intelligent sensors. The definition of "smart sensor" has evolved over the past few decades along with the emergence of the Internet of Things (IoT), a system of interconnected and Internet-connected objects (devices) that can collect and transfer data over the wireless network without human intervention. In the IoT context, a smart sensor is a device that can condition input signals, process and interpret data, and make decisions without a separate computer. Furthermore, in the AV context, range sensors for environmental perception, e.g., cameras, LiDAR, and radar, can be considered "smart" when the sensors provide, for example, target tracking, event descriptions, and other information, as part of their output. In contrast, an "unintelligent" sensor is a device that only conditions raw sensor data or waveforms and transfers the data for remote processing. It requires external computing resources to process and interpret the data to provide additional information about the environment. Ultimately, a sensor is only considered "smart" when computing resources are integral to the physical design of the sensor [2]. Primarily the sensors used are:

- LiDAR
- Radar
- Sonar
- Cameras
- GNSS+INS

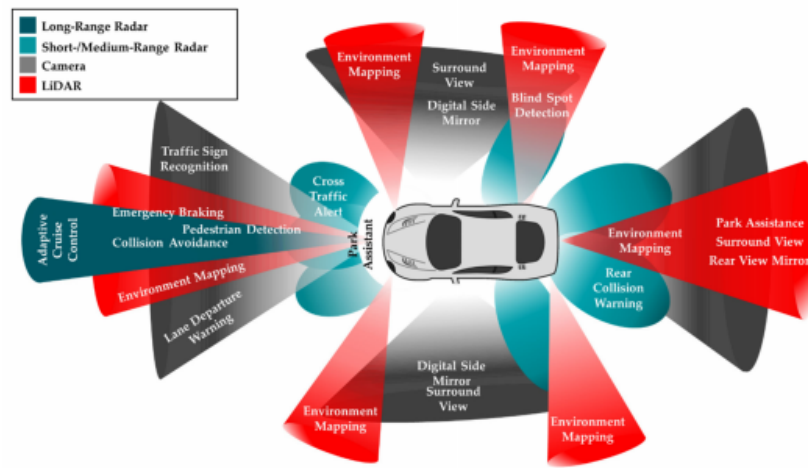


Figure 1.1: Sensors widely used in autonomous driving[2]

In Figure 1.1 are shown the most widely used systems for AV, depending on the different technologies used by the companies. For example, Tesla’s autopilot uses video cameras and ultrasonic sensors, in contrast, Google has developed a self-driving car called Waymo that uses LiDAR and Radar technology. Each of these technologies brings with it positive aspects and some negative starting from size and cost. This discussion will only explain the technologies used by modern manufacturers building these prototypes, without making detailed comparisons.

LiDAR

LiDAR (**L**aser **I**maging **D**etection **A**nd **R**anging) is a remote sensing technology that works on the principle of emitting pulses of infrared rays or laser light that reflect off target objects. These reflections are detected by the instrument and the interval between the emission and reception of the light pulse allows the distance to be estimated. As the LiDAR scans its surroundings, it generates a 3D representation of the scene in the form of a point cloud, the distance to the object is determined

by measuring the time elapsed between the emission of the pulse and the reception of the backscattered signal[3]. It uses a laser beam, which is a beam of light with a precise wavelength; unlike radar, LiDAR allows for the identification of much smaller objects because it uses infrared wavelengths. This is an advantage, but it can also play an opposite role when there is fog or rain, it will be identified because it is larger than the wavelength used. In the automotive industry, the wavelength used for LiDAR is 900nm, sometimes higher to suffer less from bad weather conditions. In general, LiDARs can be mainly divided into two categories, mechanical LiDAR and solid-state LiDAR. In mechanical/rotational LiDARs, the laser is emitted and received into the environment through rotating lenses driven by an electric motor to capture the desired field of view (FoV) around the ego vehicle. Solid-state LiDARs (SSLs) do not have rotating lenses to direct the laser light; instead, they direct the laser lights electronically. These LiDARs are more robust, reliable, and less expensive than their mechanical counterparts, but their disadvantage is their smaller and limited FoV compared to mechanical LiDARs [4].

Radar

Radar (**R**adio **d**etecting **a**nd **r**anging) uses radio waves to detect the position and speed of fixed or moving objects. For AVs, radars are used that exploit the Doppler effect, i.e., constantly monitor the speed and position of bodies. The Doppler effect works in the following way: a radar beam is launched against a moving object, in this way the return waves will all be different; in detail if the object, for example, is moving away, the return wave had to travel more space than the previous one, so the frequency changes. Thanks to the Doppler equation it is possible to obtain the frequency:

$$f_D = \frac{2 * V_r * f}{C} = \frac{2 * V_r}{\lambda} \quad (1.1)$$

where f_D is the Doppler frequency in Hertz (Hz); V_r is the relative velocity of the target; f is the frequency of the transmitted signal; C is the speed of light ($3 * 10^8$ m/s) and λ is the wavelength of the emitted energy. In practice, the Doppler frequency shift in a radar occurs twice; first, when EM waves are emitted toward the target and second, during Doppler reflection the energy is shifted toward the radar (source)[2]. From the equation 1.1 knowing the frequency f_D which can be measured, the velocity of the body can be found. These radars also operate at frequencies of 24 GigaHertz (GHz), 77 GHz and 79 GHz. The GHz frequency corresponds to millimeter wavelengths; therefore, they are also called millimeter-wave radars (MMW) [4]. Radars are used for distances and are not particularly useful for identifying bodies.

Sonar

Sonar (**S**ound **n**avigation **a**nd **r**anging) uses sound waves to detect or communicate with objects. Sonars can be divided into active or passive, the active ones propagate a sound wave or ultrasonic that through the echo you can immediately know the position and speed of the body, the operation is the same as radar. Passive ones on the other hand capture the waves of bodies that emit sound waves. Self-driving cars can use sonar to detect large objects made of solid materials (e.g., metal, ceramic) at short distances. Sonar sensors do not require light to operate. However, sonar sensors are limited by the speed of sound (which is slower than the speed of light) and sometimes mistakenly detect nonexistent objects.

Cameras

A camera works on the principle of detecting light emitted from the surroundings on a photosensitive surface through a camera lens (installed in front of the sensor) to produce clear images of the surroundings. Since camera performance and high-fidelity image creation are highly dependent on environmental conditions and illumination, the image data are often fused with other sensor data such as radar and LiDAR data to generate a reliable perception of the environment and accurate in AD [2].

GNSS+INS

GNSS is the acronym for **G**lobal **N**avigation **S**atellite **S**ystem is a geo-radiolocation system that allows, with the help of orbiting satellites or pseudo-satellites (GPS, Global Positioning System, transmitter installed on the ground) to identify the position in terms of geographical coordinates on the earth or atmosphere with an error of a few meters. GNSS navigation has excellent accuracy provided the antenna has line-of-sight visibility with at least four satellites. When the satellites' line of sight is blocked by obstacles such as trees or buildings, navigation becomes unreliable or impossible [5]. An inertial navigation system uses information from sensors to find information about rotation and acceleration. Accelerometers and gyroscopes are placed on all three axes of the vehicle's coordinate system, with the former measuring linear acceleration and the latter rotational acceleration. The INS system translates this information into a local reference system. This is important for various applications, for example, not only is the position of the camera at a given time important, but also its angular position relative to the ground.

1.1.1 Autonomous driving applications

The state of the art of autonomous driving applications will be presented in this part, precisely:

- Lane detection
- Object detection
- Localization and mapping
- Prediction and planning
- Vehicle control

Lane detection

Lane detection usually requires the use of relevant algorithms to extract the pixel features of the lane line, and then the appropriate pixel fitting algorithm is used to complete the lane detection. Traditional lane detection uses "Canny edge" extraction algorithm or "Sobel edge" extraction algorithm to obtain lane line candidate points and uses Hough transform for lane feature detection. The approach followed by these techniques is as follows [6]:

1. Image capturing

The image of the road is captured thanks to the front camera, which is reduced to 620x480 pixels thanks to the Gaussian pyramid (Figure 1.2) in which the elements are smoothed copies of the original image, it is used in image processing instead of subsampling because the latter leads to aliasing errors; smoothing means reducing the maximum frequency of the image features to avoid aliasing errors, smoothing is done with an appropriate filter and then subsampling of the smoothed image (no more aliasing problems). This is done both to reduce calculation times and to obtain more accurate results.

2. Conversion to gray scale

The previously processed image is transformed into gray scale; this is because detecting the line of the road using colours is very complicated because the road will be made up of many colours due to shadows, furthermore, using colours the calculation times are considerably lengthened.

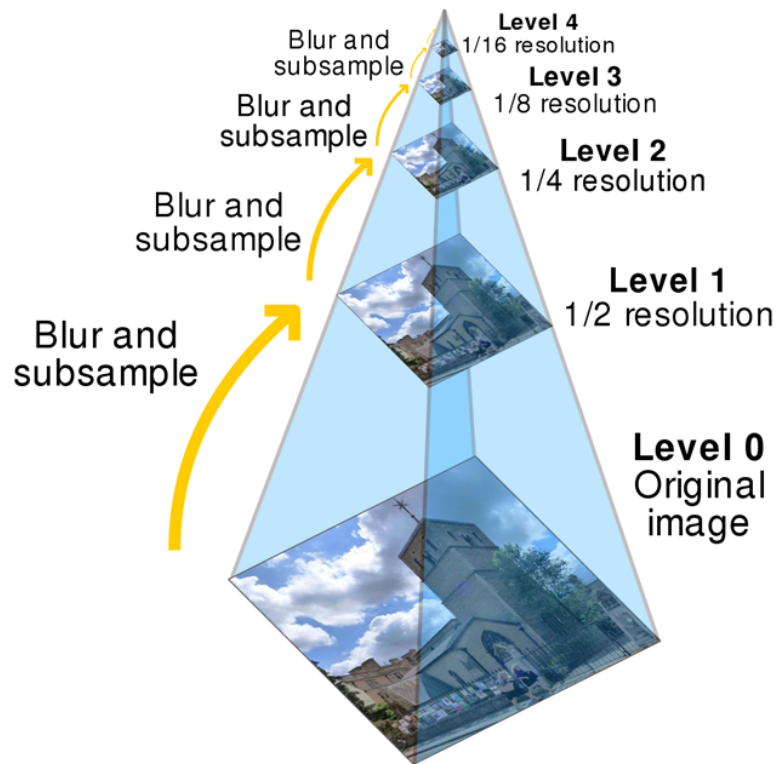


Figure 1.2: Gaussian pyramid image processing

3. Noise reduction

As presence of noise in our system will hinder the correct edge detection, so that noise removal is a prerequisite for efficient edge detection with the help of (F.H.D.) algorithm that removes strong shadows from a single image.

4. Edge detection

Road edges are recognized by the contrast between the line and the road surface, this contrast is referred to as a line. To do this, algorithms are used, in this case, the "Canny edge" detector will be mentioned. In a nutshell, it works by comparing the value of the gradient of each point with thresholds defined as high or low, if the value of the gradient of the point considered is below the low threshold this point is discarded, if instead, the gradient is above the threshold high the point is accepted; if the gradient is included between the two thresholds, the point is accepted only if in a certain neighbourhood of the previously accepted point.

5. Line detection

The "Hough transform"[7] is used to extract the line from the image. It searches for lines using the equation 1.2 (in case of straight line):

$$r = x\cos\theta + y\sin\theta \quad (1.2)$$

as seen in the figure. For the purpose for which it is used the Hough transform

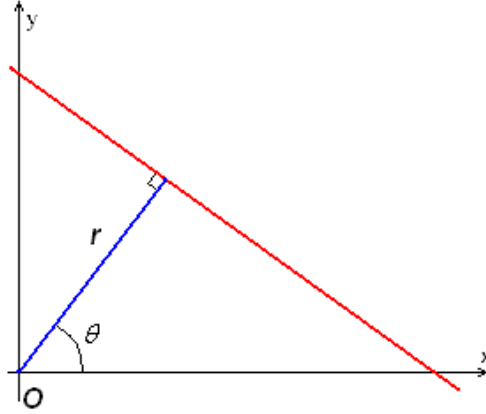


Figure 1.3: Hough transform straight line detection

is modified to discard any line that falls outside a certain range, for example, a horizontal line will certainly not be a useful or real line, therefore it is discarded. The restricted Hough transform was modified to limit the search space to 45° for each side.

6. Lane boundary scan

It uses the horizon line, edge image and line image previously extrapolated as input data, the intersection between the Hough line and the edge of the image is found, this is considered the starting point. From the starting point, the pixels belonging to the line are searched for, moving in the central direction until reaching the horizon line. The points making up the line are then ordered and inserted into two vectors.

$$L^{(l)} = \{(u_1^{(l)}, v_1^{(l)}), (u_2^{(l)}, v_2^{(l)}), \dots, (u_m^{(l)}, v_m^{(l)})\} \quad (1.3)$$

$$L^{(r)} = \{(u_1^{(r)}, v_1^{(r)}), (u_2^{(r)}, v_2^{(r)}), \dots, (u_m^{(r)}, v_m^{(r)})\} \quad (1.4)$$

Where Equation 1.3 contains all the coordinate of the left line (superscript l) while Equation 1.4 the right one (superscript r). The letters u and v stand for the coordinate of the point considered.

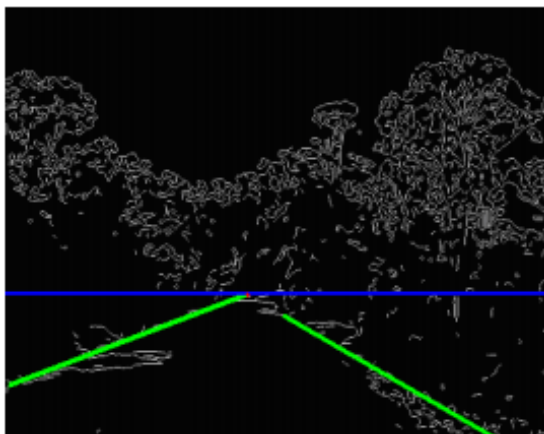


Figure 1.4: Lane boundary detection [6]

7. Hyperbola fitting

Starting from the vectors representing the scanned lines, the least squares technique is used to fit a hyperbola to the data. The parameters of the two hyperbolas are related because they must converge to the same point, due to the geometry of the roadway as shown in Figure 1.5. The formula for expressing the lane boundary as a hyperbola, given by the the road boundary point (u, v) in image plane is:

$$u = \frac{k}{u-h} + b(v-h) + c \quad (1.5)$$

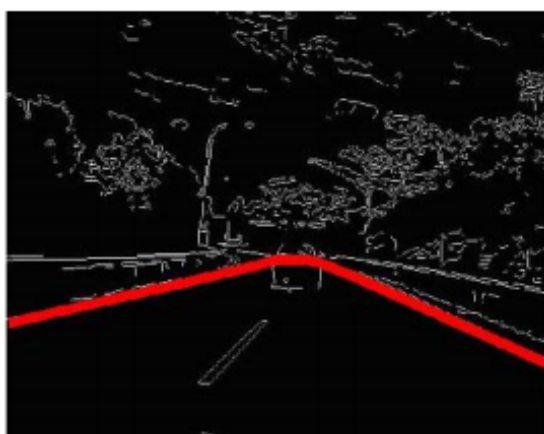


Figure 1.5: Hyperbola fitting [6]

Object detection

Obstacle detection is of paramount importance when it comes to autonomous driving. In general, it is widely accepted that the development of object detection algorithms has gone through two typical phases: (1) conventional object detection phase, and (2) object detection phase supported by deep learning. In this discussion, the second one will be described in detail as the literature scenario is gradually moving in that direction.

To perform the object detection operation, sensors are required to scan the surrounding area, usually LiDAR and cameras are used. In detail, the information coming from these sensors are processed, the elements are recognized, then classified and subsequently the position and speed of these is calculated. Recognizing different objects from a single image is a very complex task, first algorithms are used to extract features from the input images. Next, these features are used to classify objects; at this point, the gradual growth that deep learning has seen has led to the creation of algorithms that can detect objects using feature extraction. These algorithms are called convolutional neural networks (CNN) is a type of artificial neural network inspired by the organization of the animal visual cortex whose individual neurons are arranged to respond to the overlapping regions that make up the visual field. The algorithms used are different, from R-CNN (Region-based Convolutional Neural Network) to YOLO (You Only Look Once).

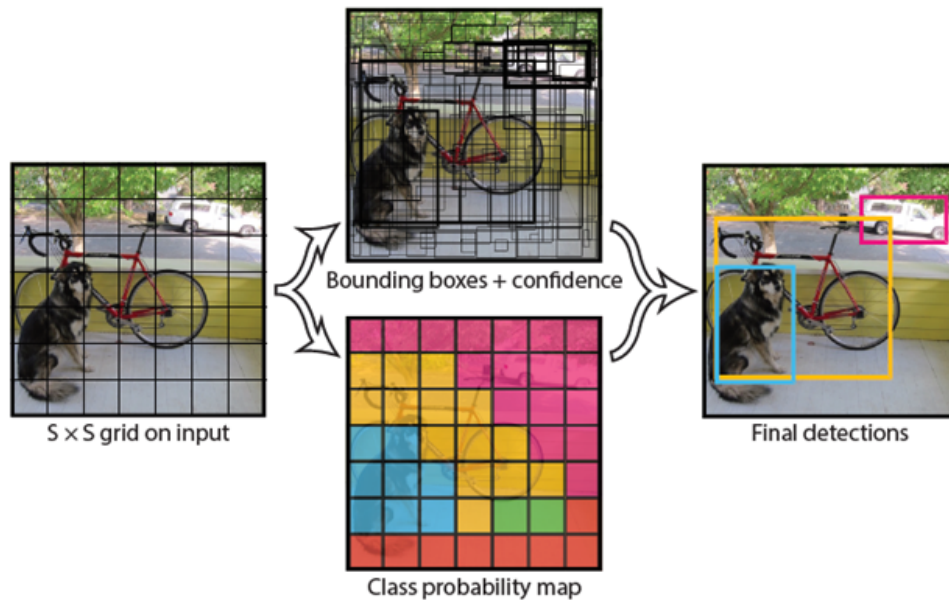


Figure 1.6: YOLO working flow[8]

YOLO is the fastest algorithm as thanks to a single image it can identify all the objects represented. In fact, the approach is different from all the other algorithms, it exploits the use of a single neural network to the full image. This network divides the image into regions and predicts bounding boxes and probabilities for each region.

These bounding boxes are weighted by the predicted probabilities[9]. The other algorithms are longer because once the possible bounding boxes have been generated, they are subsequently classified. After classification during post-processing, bounding boxes are refined, duplicates are eliminated, and boxes are resized. The YOLO works by taking the image and dividing it with an $S \times S$ grid, the bounding box, the confidence level, and the probability class are predicted for each cell created. Objects are recognized when bounding boxes have a probability class above a certain threshold value, this treatment is shown in Figure 1.6.

Localization and mapping

Localization and mapping are essential when it comes to autonomous driving, as the accuracy of the data affects the reliability of the system. GPS-IMU systems are widely used, but for urban driving conditions where more accurate measurements are needed for the safety of the car passengers but also for the people outside. In the literature, there are several systems for localization and mapping of a new environment, such as systems using pre-built HD maps that can be based on vision [10], point cloud [11] or landmarks [12] all three can be realized with the help of cameras or LiDAR. In contrast to this technique, there is SLAM which simultaneously builds the map and locates the vehicle, this technology will be described to understand how it works. SLAM stands for "Simultaneous Localization and Mapping" is the computational problem of building or updating a map of an unknown environment while simultaneously tracking the location of an agent within it [13]. This technology allows not only for self-driving devices to be used in places where GPS does not work because the signal is covered by something or in wooded areas, but also in places such as built-up areas where signal accuracy is of paramount importance, as mentioned above. Like the above systems, SLAM can also work using both LiDAR sensors and cameras, they are called SLAM and VSLAM (Visual Simultaneous Localization and Mapping) respectively. The VSLAM, thanks to the camera, takes photos that, through an algorithm, combines to form a map of the environment, it can be coupled to an IMU to obtain a digital map with the right proportions. The SLAM works in a similar way but instead of photos, the environment is reconstructed thanks to a laser scan, also in this case it can be used an IMU system to increase the accuracy. The techniques used to solve the visual SLAM problem can be divided into three main groups: (a) the classical ones, based on probabilistic filters, by which the system maintains a probabilistic

representation of both the robot pose and the position of the landmarks in the environment, (b) the techniques that employ Structure from Motion (SfM) in an incremental (causal) way, and finally (c) the techniques inspired by biology [14].

Prediction and Planning

Prediction means observing and evaluating the behavior of surrounding cars and pedestrians so that their trajectory and speed can be predicted in advance for risk assessment operations. For this purpose, the so-called HMM (Hidden Markov Model) is used to predict behavior, especially lane change events. Planning means finding the best route from where you start to where you arrive, usually GPS is used but these do not have sufficient accuracy, so usually local planners are used, which can be divided into three groups [15]:

1. Graph-based planners that give the best route to the destination.
2. Sampling-based planners that randomly scan environments and find only one feasible path.
3. Interpolated curve planners that are proposed to smooth out the path.

Vehicle Control

This application allows you to perform steering, acceleration and braking operations. Usually, vehicle control is performed on longitudinal and lateral coordinates. In detail, the control laws that allow following a certain trajectory are for example PID control [16], fuzzy control [17], Stanley control [18] and MPC (Model predictive control)[19].

1.2 State of the art of articulated vehicles

Articulated vehicles have a different dynamic behaviour if compared to the isolated vehicle, both for the dimensions involved and for the weight distribution. The detailed study of the dynamics of articulated vehicles is therefore of particular importance, especially about the stability conditions of the latter. Also, regarding autonomous driving, such vehicles are of particular interest, especially self-driving trucks. These vehicles have the same driving conditions as cars, but due to their weight, size, the presence of a tow bar, they need to perform more complex maneuvers. From this point of view, technology still needs time to be able to deal with these types of vehicles reliably. On the other hand, however, articulated vehicles, mainly used for transport will have to travel for most of the time outside urban centers, and since these are the most difficult challenge for AVs, both for the

variables involved, and for the unexpected situations that could arise, articulated vehicles with autonomous driving (level 5) could enter the market before self-driving cars, just for the characteristics described above. Study models in the literature are divided into vehicles with one joint and those with two joints; vehicles with multiple joints are an extension of the second. Single-jointed vehicles, such as tractor-semi-trailers, can be studied analytically using the model that is commonly referred to as the "bicycle model". In general, the types of instability associated with these vehicles are related to yaw angle and are mainly due to the presence of the linkage joint. The different forms of instabilities of this type are (see figure 1.7):

1. Jackknife, often happens at the side slip of the rear wheels of the tractor.
2. Trailer swing, appears at the side slip of the wheels of the trailer.
3. Trailer oscillation, is related to the rearward amplification.

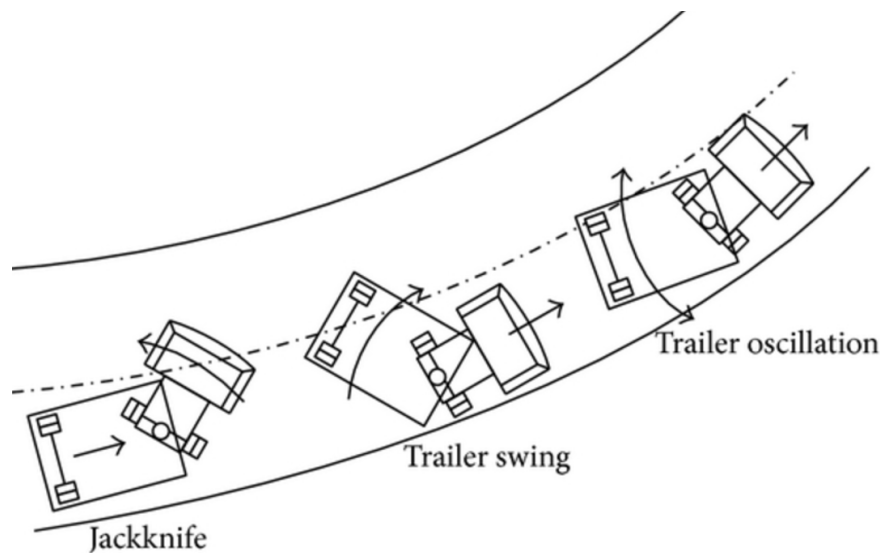


Figure 1.7: Articulated vehicles forms of instability [20]

Double-jointed vehicles exhibit the same instability phenomena, related to yaw angle. The most dangerous from the point of view of dynamic instability is the last one, since the oscillations can continue with an exponential law and lead to the loss of control of the entire vehicle. The trailer and jackknife have similar effects, both oscillate when there is a loss of lateral forces on the rear axle of the vehicle and trailer respectively; this type of uncontrolled growth of the angle between tractor and trailer can be associated with what is called static instability in systems, it occurs when a dynamic perturbation changes a state of the system

and when this ceases the states tend to diverge from infinity. There are numerous articles in the literature dealing with the lateral stability and maneuverability of self-trailer combinations, in [21] a state of the art analysis is made with attention to specific active and passive control techniques. In [22] an active steering controller is designated, based on a 3-DOF analytical model. In [23], the directional stability of articulated vehicles with one or more joints is analyzed. In this thesis, no analytical model was constructed. Based on the data provided by the company Blue Engineering Srl, a multibody model of an articulated vehicle has been built, which is very different from the previously mentioned ones; in fact, it is built by modules. Each module has a maximum of one pair of wheels, which makes the configuration very particular both from a theoretical and practical point of view. In the following chapters we describe the vehicle and the construction of the model and then we arrive at the optimization of the connections between the various modules which is the primary objective of the thesis.

Chapter 2

Vehicle description

The BTB (BLUE TROLLEY BUS) project is configured as highly innovative in view of the plurality of technological contents that it will exhibit, including contactless battery charging, piloted driving. In this way we speak of a green, flexible and configurable public transport vehicle that allows the same density of transport of people while maintaining a high degree of comfort and usability on board for passengers, together with a significant economy of operation. The BTB project is an advanced and innovative solution that is fully part of the future zero-emission urban and suburban transport systems, which are an integral part of the Smart City concept and the reduction of pollutant emissions from the atmosphere. A very interesting goal is to develop a product that allows mass transport, with minimal impact on the infrastructure [24]. The term trolleybus refers to an electric vehicle that draws power from dual overhead wires (usually suspended from street poles) via spring-loaded poles. The BTB, on the other hand, is equipped with an electric motor, allowing it to travel on any type of route. It is an articulated vehicle and is composed of several modules, specifically five which in order are:

- Driving module
- Transit module
- Connection module
- Transit rear module
- Driving module 2

The first two modules are connected to each other with a rigid connection, as are the last two, so the model can be studied through three macro-groups, the Connection module and the two groups of rigid modules, respectively. They are connected by a joint, in this discussion spherical joint, longitudinal stiffnesses and

dampers. The BTB is a three-axle articulated bus and there is one axle with wheels for each macro-group. As for the vehicle data, it has dimensions of 9 m in length, 2 m in width and 2.9 m in height (above ground) for a total unladen weight of over 6 tons . During the mission it will reach a maximum speed of $35 - 40\text{ km/h}$ with a maximum acceleration of 0.5 m/s^2 , while the emergency braking rate is 1.2 m/s^2 . All these data were simulated in a single test, it was explained in detail in the section 3.10. The vehicle in question for the moment represents a prototype, so even the autonomous driving technologies have been developed to perform tests without passengers on board except the driver who can intervene at any time on the guide for operations in which the vehicle does not follow the desired trajectory or some sensor fails to detect obstacles. The sensors used are four front cameras placed two in the center and two others moved laterally (wide angle type), these are necessary for the detection of obstacles. More front cameras were included to get a more accurate view of the road, especially for driving operations where the presence of wide-angle cameras is essential. As the autonomous driving of this vehicle is designed, once an obstacle is detected, the vehicle stops and waits until the obstacle is no longer there to restart, so there are no automatic line change systems. As for the route to follow, it uses a GPS/INS to get information about the status of the vehicle. For the route to be followed, initially a test drive is made in which the vehicle is driven by the driver during which the vehicle status information is acquired moment by moment by the GPS/INS system and the data is saved, then this route is automatically driven by the vehicle. While driving, the driver's operations have a higher priority than those of the autonomous driving system so that any command can be overridden at any time, essentially for safety reasons. Processing the input data to then perform all acceleration, braking and steering operations is entirely dedicated to the NVIDIA DRIVE AGX board, which is shown in the figure 2.1.



Figure 2.1: NVIDIA DRIVE AGX Developer Kit

NVIDIA DRIVE AGX Xavier™ delivers 30 trillion operations per second (TOPS) for Level 2 and Level 3 automated driving. It is based on the first auto-level Xavier SoC, which integrates six different types of processors, including CPU, GPU, Deep Learning Accelerator (DLA), Programmable Vision Accelerator (PVA), Image Signal Processor (ISP), and nvidia stereo/optical flow accelerator. All sensors (the ones mentioned and explained in the paragraph 1.1) used are connected to the inputs of the board; outputs are produced that control the acceleration, braking and steering operations. Each command given by the driver has priority over the outputs of the board, as mentioned above. To conclude the discussion, in this chapter the main elements that influence the vehicle dynamics will be explained, describing the theory that characterizes them which will then be the basis of the model in multibody environment. The elements considered are:

- Tire
- Longitudinal dampers

In this part we will also describe in detail the creation of different traces that will be will then be the basis from which we will start to perform the sensitivity analysis to obtain the best configuration regarding the connections between the modules. Regarding the suspension, will not be explained in detail as it was the task of the company to size this element, for this thesis it was decided to impose a value of stiffness of the suspension so that the first natural frequency was around 1.5 Hz and the optimal damping was given in first approximation, knowing the mass and stiffness. The calculations were done using the model called "quarter-car" although in this case there are six wheels. The calculation of stiffness and damping have been done for each axle, as said this approach is very approximate but still allows to make a reliable analysis. The values of the suspended and unsprung masses have been obtained once the model has been built and transported on the axle.

2.1 Tire model

The tire model is of fundamental importance for the study of the dynamics of the vehicle considered, in Simpack there are several packages able to simulate the contact between asphalt and tire; specifically a tire model called "Pacejka Similarity" has been used, of which in this paragraph we will try to explain the physics of the coefficients used for modeling. This model is a simplified version of the Pacejka model and closely follows the physical model explained in this discussion. In order to explain the role of the tire in detail, it is necessary to first describe the peculiarities of the tire-asphalt contact. A model that explains the key features and allows to understand the fundamental parameters of the considered contact is the so-called "Brush model". The one-dimensional brush model is the

simplest tire-asphalt contact model capable of considering the deformability of the bodies in contact. This chapter will deal with the tire-asphalt contact starting from the wheel up to the definition of the fundamental parameters for the study of this phenomenon. It is not the object of this article to study in detail the behavior of the tire, therefore only some fundamental concepts will be mentioned, moreover the combined slip will not be treated.

In this paper the "Pacejka Similarity" model has been used, although it brings with it some approximations, it has been used for two reasons; the main reason is the lack of data in the literature of tires using the coefficients that constitute the so-called "Pacejka magic formula", moreover considering the elements that must be sized and the dynamics to which the vehicle must be subjected the model taken into consideration is satisfactory.

2.1.1 Reference system

To characterize the vehicle dynamics it is necessary to impose an absolute reference system, in order not to generate confusion and to be consistent we chose to take as reference the ISO 8855-2011 (reference system used by Simpack) as shown in Figure 2.2. Three main reference systems can be defined:

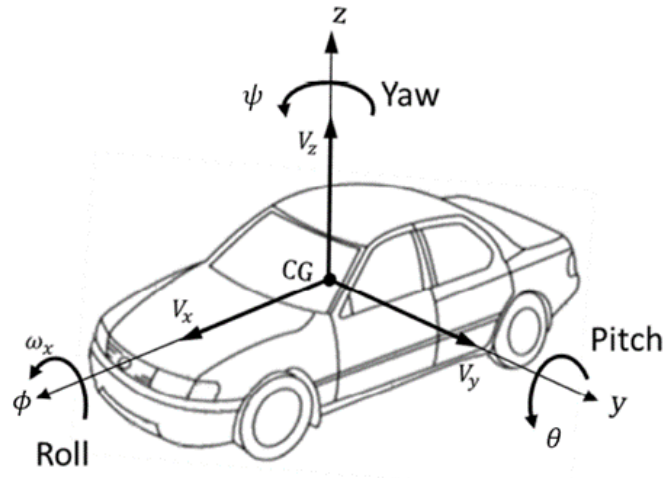


Figure 2.2: Reference frame

1. Absolute reference system (X, Y, Z)
2. Vehicle reference system (x : longitudinal coordinate, z : coordinate perpendicular to x and directed upwards, y : lateral direction identified starting from the other two and applying the right-hand rule)

3. Reference system applied to the wheels, represents a reference system integral with the wheel in question and which rotates around the steering axis (x_w , y_w and z_w) these three axes are parallel to the absolute reference system for $x = 0$.

Forces and moments applied to the vehicle are defined as:

- F_x : Longitudinal Force
- F_y : Lateral Force
- F_z : Vertical Force
- M_x : Roll Moment
- M_y : Pitch Moment
- M_z : Yaw Moment

The wheel

Generally, the set of elements formed by disc, rim and tire is referred to as wheel; the first two are considered rigid elements while the last one is considered deformable. The tire is a fundamental element since it allows the vehicle to adhere to the ground. The wheel can be modeled as a rigid element (point contact with the ground) or as a deformable element (what happens in reality). In detail, we will evaluate the situation of the deformable wheel because it better reflects the characteristics that must be evaluated in the physics of contact, so in this case the contact area is represented by the footprint of the tire on the ground, the contact area depends on the stiffness of the tire and the inflation pressure. The deformable wheel takes into account the actual distribution of contact forces along the footprint area of the tire while the rigid one considers only a point contact characterized by Coulomb friction. In Figure 2.3 three radii are distinguished: the radius of the undeformed wheel R_0 , the radius under load r and the effective rolling radius r_e . The point S is an imaginary point and is at zero speed. The radius under load, which identifies the distance of the wheel center from the road surface where the contact forces develop, is directly affected by the vertical load F_z applied to the axle, it is assumed as a first approximation that the radial stiffness of the tire K_r constant:

$$r = R_0 - \frac{F_z}{K_r} \quad (2.1)$$

In this case, the pure rolling condition is no longer uniquely defined by the geometry of the system as for rigid wheel, but to identify it, reference must be made to the longitudinal force developed on the ground. It can be defined:

$$V_{sx} = V_x - \omega r_e \quad (2.2)$$

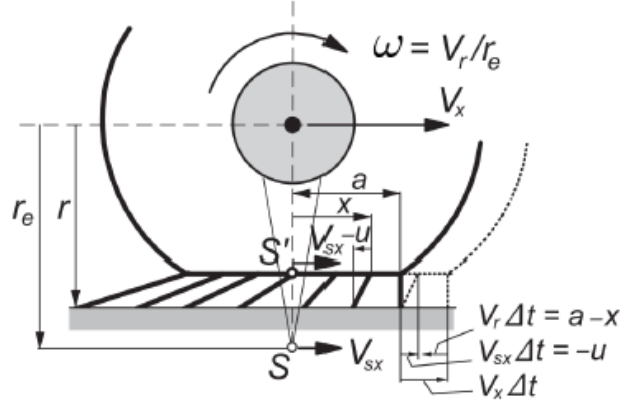


Figure 2.3: Deformable wheel with bristles [25]

While V_r called the linear speed of rolling is defined as:

$$V_r = \omega r_e = V_x - V_{sx} \quad (2.3)$$

to study the condition of pure rolling it is necessary to refer to the longitudinal force developed on the ground, the generation of such force requires a sliding in the longitudinal direction which can be expressed as:

$$\sigma = \frac{V - \omega r_e}{V} \quad (2.4)$$

From this last equation two limit conditions can be considered:

- Locking of the wheel under braking in which $\omega = 0$ and the speed is greater than zero so that $\sigma = 1$
- Skidding of the driving wheels during the start in which $\omega > 0$ and $V = 0$ so that $\sigma = -\infty$

Another parameter of fundamental importance is the tire inflation pressure which determines the footprint on the ground, the contact area is mainly influenced by two factors which are the stiffness of the tire and precisely the pressure with which the wheels have been inflated.

To this end we write:

$$p_{gas} A + K_p \Delta z = p_S A = F_z \quad (2.5)$$

So applying a vertical load the tire will react with a force coming from the inflating pressure multiplied by the area of the footprint plus the stiffness of the tire multiplied by the vertical deformation.

2.1.2 Brush model

The brush model consists of a row of elastic bristles that touches the road plane and can deflect in a direction parallel to the road surface. These bristles may be called tread elements. Their compliance represents the elasticity of the combination of the carcass, belt, and actual tread elements of the rear tire. [25] The friction model used is the Coulomb model as it is applied locally (on each brush) and this allows to correctly describe the generation of lateral and longitudinal forces, this would not happen if this friction model were applied to the global level on the wheel. With this model, the horizontal force is limited by the vertical force on the wheel and by the coefficient of friction. An assumption is that the pressure profile is parabolic over the contact length. The value turns out to be:

$$p(x, y) = p(x) = p_0[1 - (\frac{x}{a})^2] \quad (2.6)$$

Where a represents the half-length of the contact area and x is the free coordinate, so we have that $L = 2a$ while the width is called $f = 2b$ which represents the width of the tire where the pressure trend is considered constant. We define:

$$\xi = x + a \quad (2.7)$$

It is assumed that, when the wheel turns, the bristle entering the contact area is in a perpendicular position concerning the road surface, supposed to be perfectly horizontal.

Pure longitudinal slip

Considering the Figure 2.4, ω and V are imposed so that sliding occurs so that the wheel is not driven but a driving torque is applied. Considering the deformation of the brushes through shear stress generates a speed difference at the ends of the bristle. $u(\xi)$ is defined as the displacement of the end of the brush considered which, when derived over time, gives shape to the deformation rate that is generated. So, we can find the speed of the bristle in contact with the ground:

$$v(\xi) = V - \omega r_e + \frac{du}{dt} = V - \omega r_e + \frac{\partial u}{\partial \xi} \frac{\partial \xi}{\partial t} \quad (2.8)$$

$$v(\xi) = V \left(\frac{V - \omega r_e}{V} + \frac{\partial u}{\partial \xi} \right) \quad (2.9)$$

V is defined as the speed of the wheel centre and is usually an approximate speed that derives from the travel speed of the vehicle while ω is the angular speed measured on the considered wheel, therefore ωr_e represents the speed at the attack

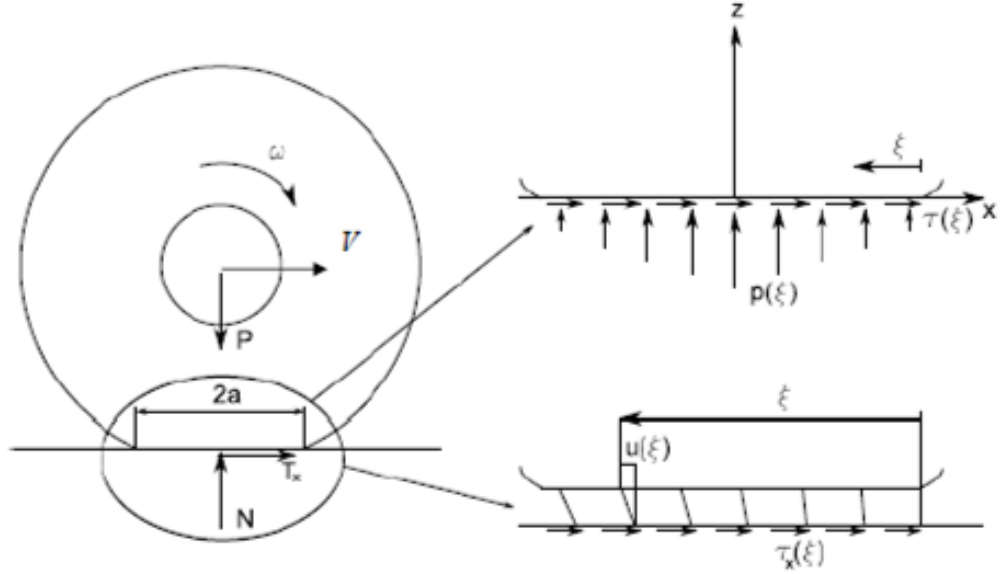


Figure 2.4: Brush model pure longitudinal slip

of the bristles and finally $\frac{du}{dt}$ as previously said it represents the deformation speed of the brushes. By imposing the arduous condition for which zero speed of the brushes in contact with the ground, the equation can be defined:

$$\frac{V - \omega r_e}{V} = -\frac{\partial u}{\partial \xi} \quad (2.10)$$

Using the constitutive equation of the material used for the tread, the tension/tangential deformation link can be defined as follows:

$$\tau_x = G \gamma_x = G \frac{u}{l} = k_x u \quad (2.11)$$

Where G is the modulus of tangential elasticity, γ_x the angular sliding, k_x the longitudinal stiffness of the tread, u the deformation of the bristle and l the length of the latter. At this point, we find the relationship between the slip and the tangential tension starting from Eq.2.10:

$$\sigma = -\frac{1}{k_x} \frac{\partial \tau_x}{\partial \xi} \quad (2.12)$$

$$\frac{\partial \tau_x}{\partial \xi} = k_x \sigma \quad (2.13)$$

By integrating the equation 2.13 between 0 and ζ we obtain:

$$\tau_x(\xi) = \tau_x(0) - k_x \sigma \xi \quad (2.14)$$

$$\tau_x(\xi) = -k_x \sigma \xi \quad (2.15)$$

We pass from the first to the second equation as the tangential tension at the zero coordinate is zero as it comes from an area not in contact with the ground. From Eq.2.15 two different tension distributions are distinguished, one of adhesion in which, while for the sliding condition there is $\tau_x(\xi) = -f_D p(\xi)$ imposing that the dynamic friction coefficient is lower than the static one. By integrating the relationship found on the contact area (constant width) we obtain:

$$T_x = F_x = 2b \int_0^{2a} \tau_x(\xi) d\xi = 2b \left[\int_0^{L_A} \tau_{x,A}(\xi) d\xi + \int_{L_A}^{2a} \tau_{x,S}(\xi) d\xi \right] \quad (2.16)$$

Now, we can diagram the trend between the longitudinal force just obtained and the longitudinal sliding but usually the longitudinal force $|T_x|$ is normalized with respect to the vertical force F_z acting on the tire, we define this ratio as μ_x .

$$\mu_x = \frac{|T_x|}{F_z} \quad (2.17)$$

In Figure 2.5 is plotted the trend between the 2.17 and the longitudinal slip.

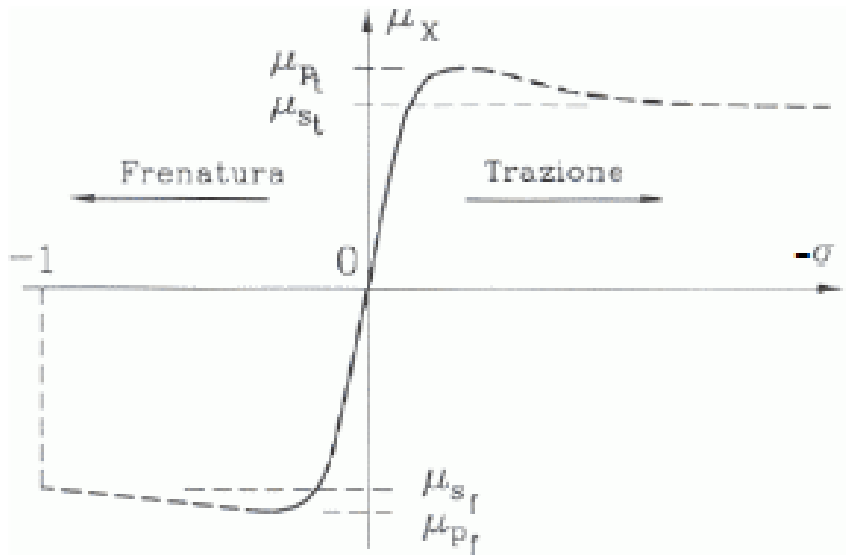


Figure 2.5: μ_x function of longitudinal slip

From the figure you can see that the right side is the one with positive slip, therefore it represents the part in which there is traction while with negative slip it represents the braking phase. It is noted that for low slip values the trend between longitudinal and sliding force is approximately linear and is defined as $C(\sigma)$: longitudinal slip stiffness, so we can write that for low values of longitudinal slip $|T_x| = C_\sigma \sigma$. We can say that the first part of the diagram (low σ values) the diagram force-slip is mainly due to structural characteristics of the tire including the tire inflating pressure, while the last part of the diagram is only depending by the adhesion conditions by the equation $T_x = f_d F_z$.

Pure slide slip

To model this condition, we consider the wheel that translates with a speed v in pure rolling conditions, in which a force T_y is applied to the wheel hub in the transverse direction and a moment to prevent it from overturning. In this way there will be a deformation of the brushes that try to realign themselves with the direction imposed by the speed. As the bristles move, they increase the tension until reaching the adhesion limit beyond which there will be creep. For the study, the longitudinal component of the null force is assumed to study the simple side slip. The angle is defined:

$$\alpha = \text{arctg}\left(\frac{V_y}{V_x}\right) \approx \frac{V_y}{V_x} \quad (2.18)$$

Like the approach previously used, we can define:

$$w(\xi) = -\alpha \xi \quad (2.19)$$

The distribution of tensions, as it is legitimate to imagine, is asymmetrical and for this reason a moment called self-aligning torque is generated which can be defined as:

$$M_z = T_y t \quad (2.20)$$

The pneumatic trail t , which indicates the distance behind the contact centre C where the resultant side force T_y is acting. Using the same approach adopted for the longitudinal slip we can write:

$$v_y = V \sin \alpha + \frac{dw}{dt} \quad (2.21)$$

$$v_y = V \sin \alpha + \frac{\partial w}{\partial \xi} \frac{\partial \xi}{\partial t} = V \alpha + \frac{\partial w}{\partial \xi} V = V \left(\alpha + \frac{\partial w}{\partial \xi} \right) \quad (2.22)$$

If we consider the conditions of adherence ($v_y = 0$) we can write:

$$\frac{\partial w}{\partial \xi} = -\alpha \quad (2.23)$$

Integrating ($w(0) = 0$) we obtain:

$$w(\xi) = -\alpha \xi \quad (2.24)$$

Analyzing the stress-strain relationship (k_y is the radial stiffness of the tread) we can write:

$$\tau_y = k_y w = -k_y \alpha \xi \quad (2.25)$$

$$\tau_y = -f_D p(\xi) \quad (2.26)$$

The Eq. 2.25 represents the adherence condition in which $|\tau_y| \leq f_s p(\xi)$, while the Eq. 2.26 represents the creep condition. By integrating the lateral force we obtain:

$$T_y = 2b \int_0^{2a} \tau_y(\xi) d\xi \quad (2.27)$$

Also, in this case it is possible to plot the trend of the lateral force as function of the slip angle varies and a trend is obtained that is completely like that of the longitudinal slip as can be seen in Figure 2.6. In the case of the lateral force, as

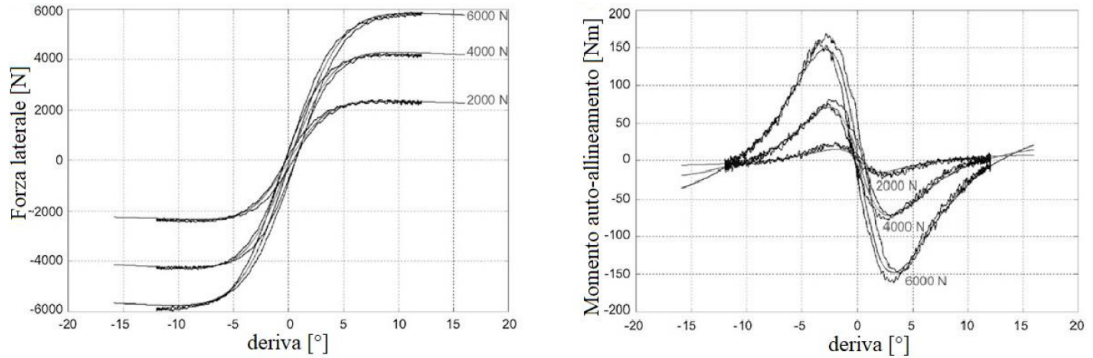


Figure 2.6: Lateral Force and self-aligning moment with respect to the slip angle varying the vertical load

in Figure 2.5, the inclination of the straight line for small angles is approximately constant and the angular coefficient C_α called Cornering Stiffness can be defined. Similarly to the previous case we can define:

$$F_y = -C_\alpha \alpha \quad (2.28)$$

$$\mu_y = \frac{F_y}{F_z} \quad (2.29)$$

Data used

The text file containing all the data useful to study the behavior of the tire using the "Pacejka Similarity" model is included below. It can be seen that the physical quantities to be entered as input data fully follow the physical model just described. As for the data used, they were extracted from the literature.

```

**MODELPARAMETERS 16
ovalldia Overall Diameter m 0.6539
fkrr Factor for kin. roll. Radius - 1.0
cz Vertical Stiffness N/m 900000.0
dz Vertical Damping Ns/m 2000.0
crr Rolling Resistance Coeff. - 0.001
nomwidth Nominal Section Width m 0.23
inflpres Inflation Pressure kPa 900.0
cy Lateral Stiffness N/m 900000.0
F_z0 Nominal vertical Load N 13000.0
mu_0 Nominal Friction Coefficient - 1
C_sigx0 Gradient of Fx(sx) for sx=0 N 180000
! Gradient of the nominal
! longitudinal Force F_x over
! the longitudinal Slip sigma_x
! (for alpha=0) at sigma_x = 0
C_sigy0 Gradient of Fy(sy) for sy=0 N 180000
! Gradient of the nominal
! lateral Force F_y over the
! lateral Slip sigma_y
! at sigma_y = 0
sig_sly Lateral Gliding Slip - 0.15
! Lateral Slip of the nominal
! lateral Force F_y over the
! lateral Slip sigma_y at which
! there is complete Gliding
F_sly Lateral Gliding Force sy=syg N 11400
! Lateral Force at which
! sigma_y = sig_sly
F_infy Lateral Gliding Force sy=inf N 7475
! Lateral Force for
! sigma_y => inf
dC_sigy0 Derivative of Gradient Fy(sy) - 5.0
! Derivative of the Gradient
! C_sigy of the lateral Force
! Fy over the lateral Slip
! sigma_y w.r.t. the vertical
! Force F_z for F_z = F_z0
    
```

2.2 Longitudinal dampers

The longitudinal dampers were simulated in this treatment in three different ways, initially they were simulated as ideal, so the damping coefficient was given only as an input parameter and in output, the damping force is calculated by the software trivially as a product of force and relative velocity, then a linear correlation between the two; in this way, however, you could potentially get an infinite force. For this reason the second step was to treat the dampers as real elements and therefore with the impossibility of obtaining a potentially infinite force, in fact in the real dampers the force after a certain relative velocity tends to saturate up to a maximum value beyond which it is physically impossible to go. For the sizing of these elements have been used the ideal dampers because the range in which the damper works in this elaborate has very low relative velocities, this means that in most cases works in the linear section, the damper reaches saturation only in adverse conditions such as a pothole or a very high excitation, then in the tracks where the vehicle has been sized, the treatment carried out is a good approximation. As a final step, however, the dampers were simulated as active, thus with the damping coefficient varying depending on the surrounding conditions and adapting, providing the optimal moment-to-moment value. The latter path was followed initially by imposing a PID type control on the relative velocity, as an error, the velocity difference was given at the ends of the damper so that the control tends to impose a zero velocity, this strategy was followed by placing a control force at each point where there is a damper. The velocity cannot be zero, because otherwise the vehicle dynamics would vary and the steering operations could not be followed correctly because it would tend to remain rigid. Therefore, it is not possible to enter a high proportional control value, in this way the high frequency oscillations are eliminated and the travel comfort is also improved. With this technique, it is possible to choose an active damper or to ask the manufacturer for a purpose-built damper, since, in the post-processing environment, it is possible to plot the trend of the force resulting from the PID as a function of the relative velocity through the damper. In this discussion, the passive damper is described as the one used in all the tests performed, as for the active dampers a dedicated paragraph will be presented (4.7) in which the results obtained will be shown. Longitudinal dampers take care of damping, precisely, the oscillation motion that is generated during the vehicle dynamics; this motion, without the correct damping, risks leading the system to dynamic instability (oscillations grow exponentially). A system is dynamically unstable if, after of a perturbation, the oscillation grows according to an exponential law. Dynamic instability is mainly attributable to the yaw angle at the joint, since this is the degree of freedom useful for driving the vehicle, it is the one that has a higher range of angles and also the one that could potentially lead to instability (e.g. side wind gusts). For this reason, a sensitivity analysis will

subsequently be performed to overcome this problem and designate the optimal parameters for these dampers. The dampers, as defined by the software used, are represented as ideal, so the force grows progressively as the velocity changes using a linear law such as:

$$F = C * v \quad (2.30)$$

Where F is the damping force, C is the damping coefficient and v is the relative velocity obtained as the difference of velocities through the damper. However, the damping force does not grow linearly, or rather it grows linearly only for a certain velocity range, once this range is exceeded it will tend to saturate. The model used to simulate real dampers was as follows:

$$F = \frac{Cv}{\sqrt{1 + a * v^2}} \quad (2.31)$$

It is noted that when the speed tends to infinity, the saturation force becomes:

$$F_{v \rightarrow \infty} = \frac{C}{\sqrt{a}} \quad (2.32)$$

Therefore, having optimized the value of C , it is known, consequently setting the value of the required saturation force is obtained. In this regard, a graph showing the trend of the curve as the parameter a varies is presented in the figure 2.7.

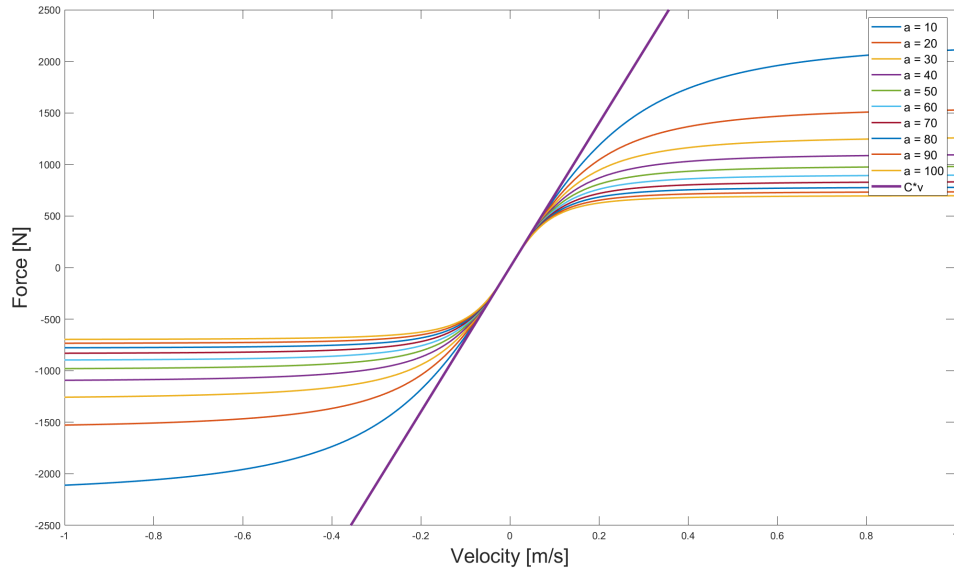


Figure 2.7: Force trend varying a parameter

In this case, a value for the damping coefficient $C = 7000Ns/m$ was used. As can be seen in Figure 2.7, the model used is linear only for a small velocity range, beyond which the force trend tends to saturate. For this discussion, a value of parameter a equal to $30 s^2/m^2$ was chosen.

Mathematical model

Dampers have the role of decreasing the amplitude of oscillations over time to avoid instability phenomena and improve comfort in the various areas in which they are used. In this section, longitudinal dampers will be discussed, but the discussion can be extended to all damping elements. To explain the terms used, the mass-spring-damper paradigm is presented, which is very useful in understanding the role of the various elements that comprise it. The mathematical model of a single degree of freedom translating horizontally will be explained without the application of external forcing terms, for which the oscillations are given only by the initial conditions representing a displacement from the equilibrium position or an initial velocity. In this way, it is possible to understand the role of damping within the system, the treatment used in this thesis from this point of view is very quick and only some information about it is given; since this is not the main objective of the article. Figure 2.8 shows the system used to explain the influence parameters, in this regard x represents the horizontal translation coordinate and is defined as a function of time, it represents the position of the mass from the static equilibrium conditions, k represents the spring stiffness while c represents the damping coefficient of the damper.

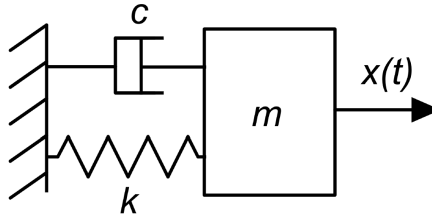


Figure 2.8: 1 d.o.f. mass-spring-damper system

$$m\ddot{x} + c\dot{x} + kx = 0 \quad (2.33)$$

The equation is of the second-order differential type with constant coefficients whose solution is in the form:

$$x(t) = Ae^{st} \quad (2.34)$$

Deriving to get \dot{x} and \ddot{x} and replacing inside 2.33 we get:

$$A(ms^2 + cs + k) = 0 \quad (2.35)$$

Avoiding the trivial solution of $A = 0$ we study the polynomial enclosed in parentheses and we arrive at the algebraic solution of the second-degree polynomial:

$$s_{1,2} = \frac{-c \pm \sqrt{c^2 - 4km}}{2m} \quad (2.36)$$

The solution of (2.33) is therefore:

$$x(t) = A_1 e^{s_1 t} + A_2 e^{s_2 t} \quad (2.37)$$

The constants A_1 and A_2 are determined due to the initial conditions. At this point we can define $\zeta = c/c_{cr}$ where c is the damping coefficient of the damper while c_{cr} represents the value of the so-called "critical" damping coefficient that depends on mass and stiffness according to the relation $c_{cr} = 2\sqrt{km}$. It is defined as critical because it cancels the radical of the equation (2.36), this equation can be rewritten using the damping factor ζ :

$$s_{1,2} = -\zeta\omega_n \pm \omega_n\sqrt{\zeta^2 - 1} \quad (2.38)$$

The evolution of the x coordinate varies with the variation of the radicand; in detail it is expressed:

- If $\zeta > 1$ the system is said to be overdamped.
- If $\zeta = 1$ the system is said to be critically damped.
- If $\zeta < 1$ the system is said to be undamped.

Knowing ζ ; imposing the initial conditions we find the constants A_1 and A_2 and then substituting in equation (2.37) we find the trend of the coordinate x as time varies. Obviously, to have a solution other than the trivial one, the velocity or the initial position must be different from zero. Figure 2.9 shows the three cases listed above, in practice most of the cases are represented by overdamped systems.

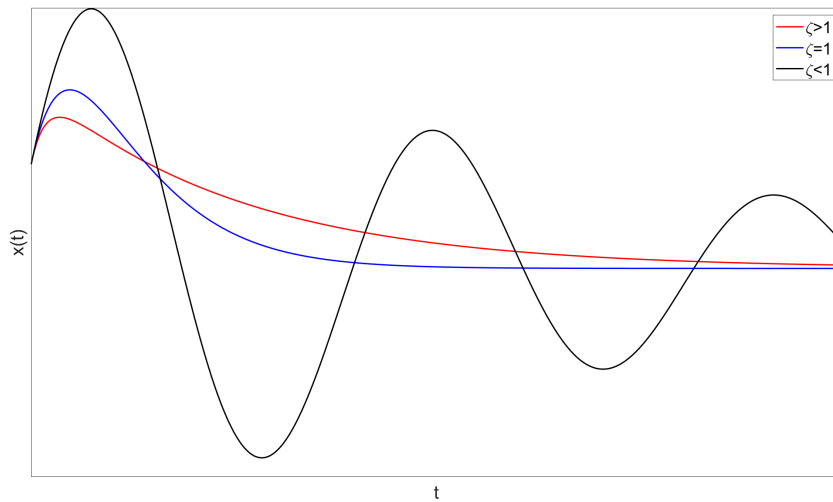


Figure 2.9: Free response

As said, this treatment is only illustrative and serves to describe the terms related to the choice of damping, however it gives an idea of how the parameters involved influence each other; in fact, this paradigm is the most used in the field of dynamics also with regard to the behavior of suspensions. It certainly has its limitations, but it allows us to understand the physics behind it.

2.3 Creation of the paths

To correctly size the various connection elements between the modules, tracks have been constructed to study in detail the behaviour of these elements when the input conditions vary. Subsequently, once the parameters to be used have been chosen, sensitivity analyzes are performed using these traces to optimize the element taken into consideration. First of all, it should be explained how it is possible to insert a path within the software and how these elements work, especially the interaction with the Road element. In order to explain in detail the operation of these elements, the definitions have been taken from the Simpack help [26].

2.3.1 Track

A Track defines the three-dimensional run of a route, the track line, in space. Tracks are usually intended for providing a virtual guideway for vehicles. The track is represented by six functions:

- The position coordinates with respect to the global reference system:
 1. $x(s)$
 2. $y(s)$
 3. $z(s)$
- The orientation angles in aerospace convention sequence:
 1. $\psi(s)$, the yaw angle about $z - axis$
 2. $\theta(s)$, the pitch angle about the new $y - axis$
 3. $\phi(s)$, the roll angle about the new $x - axis$

The independent coordinate s is either the approximated curve length along the track line or its horizontal projection (into the $x - y$ plane), dependent upon which of the kind of track is used. Positions and orientations usually arise from the three main directions of the Track layout:

- Horizontal, given by the horizontal radius or curvature.

- Vertical, given by the vertical slope, the vertical radius or curvature.
- Superelevation, given by the level difference along a lateral baseline, the superelevation reference length.

The horizontal and the superelevation layout are linked together because the latter follows the trend of the former, while the vertical one is totally separated from the other two. The types of track that can be used in the Simpack environment are:

- Cartographic Track
- Measured Track
- Measured CRG Track

In this discussion, the first two will be used; the first allows you to build a path directly within the work environment, while the second was used to import a path; then the types of routes used and the type of Track chosen will be explained. The horizontal layout can be constructed by means of different segments, joining them together to generate the desired profile. These segments are divided into:

- Straight track
- Circular arc
- Clothoid transition
- Bloss transition
- Sine transition
- Cosine transition

The elements used to generate the desired profile were the straight track which, as the term itself implies, generates a segment of length L between the starting point and the ending point (determined by the tangent of the previous segment); the circular arc defined by the length of the arc and the radius; the Clothoid transition allows to connect two segments with two connections at the ends, it is defined by the two radii and by the length of the clothoid. This last element described is particularly useful in the case of superelevation as it allows in the clothoid area to pass from a point at zero height to a second point of a certain height (height of the superelevation), in doing so there is a certain slope and not a step as it would be without.

2.3.2 Superelevation

Superelevation in curve is one of the most important features to consider when new roads are created. This is true because when a vehicle is in curve, according to physics, it is forced outward by centrifugal force. The purpose of superelevation in curve is to counteract the centripetal acceleration generated when a vehicle round. The calculation of the superelevation depends by the radius of the curve due to centripetal force, the friction coefficient according to the following formula [27]:

$$e + f = \frac{v^2}{gR} = \frac{0.0079V^2}{R} = \frac{V^2}{127R} \quad (2.39)$$

Where e is the rate of superelevation (m), f is the side friction factor, v is the vehicle speed (m/s), V is the vehicle speed (Km/h), g is the gravitational constant ($9.81 m/s^2$) and R is the radius of the curve (m). In Simpack the superelevation is implemented starting from the definition of the horizontal Track, in fact the approach for this discussion is to keep the superelevation constant during the straight sections, instead using the clothoid as a connecting element. It allows to pass from zero to the actual value of superelevation, and vice versa, linearly. Subsequently the constant value is maintained for the actual curve. The elements that define superelevation are:

- L is the segment length, projected in the horizontal $x - y$ plane.
- u is the superelevation.
- $u1$ and $u2$ are the initial and final value of superelevation of a transition segment.

While the segment types are depicted in Figure 2.10

2.3.3 Vertical direction

The vertical direction instead is completely independent from the other two elements, it is defined by:

- L is the segment length, projected in the horizontal $x - y$ plane.
- p is the slope.
- $p1$ and $p2$ are the initial and end slope of a transition segment.

While the types of vertical track segments are depicted in Figure 2.11

Abbr.	Description	Par. 1	Par. 2	Par. 3
CST	Constant superelevation	L	u_1	
LIR	Linear ramp, the superelevation increases or decreases linearly from u_1 to u_2	L	u_1	u_2
BLO	Bloss ramp, the superelevation increases or decreases according to the formula $u(\tilde{s}) = -2\frac{u_2 - u_1}{L^3}\tilde{s}^3 + 3\frac{u_2 - u_1}{L^2}\tilde{s}^2 + u_1$ providing a smoother transition to the previous and next segment than a linear ramp. (Note that an additional smoothing is still required because the second derivative is still not continuous.)	L	u_1	u_2
SIN	Sine ramp, the superelevation increases or decreases according to the formula $u(\tilde{s}) = (u_2 - u_1) \left(\frac{\tilde{s}}{L} - \frac{1}{2\pi} \sin\left(2\pi\frac{\tilde{s}}{L}\right) \right) + u_1$	L	u_1	u_2
COS	Cosine ramp, the superelevation increases or decreases according to the formula $u(\tilde{s}) = \frac{u_2 - u_1}{2} \left(1 - \cos\left(\pi\frac{\tilde{s}}{L}\right) \right) + u_1$	L	u_1	u_2

Figure 2.10: Track segment types for superelevation

Abbr.	Description	Par. 1	Par. 2	Par. 3
CSL	Constant slope	L	p	
PL2	Parabolic transition, the slope increases or decreases linearly from p_1 to p_2	L	p_1	p_2
CIR	Circular arc transition defined by the length and the initial and end slope, the slope increases or decreases according to the formula $p(\tilde{s}) = \frac{\tilde{s}}{\sqrt{R^2 - \tilde{s}^2}} + p_1$ The (projected) length L to be entered is related to the transition radius R by $L = 2R \cos\left(\frac{\theta_1 + \theta_2}{2}\right) \sin\left(\frac{\theta_2 - \theta_1}{2}\right)$ $\approx 2R \cos\left(\frac{p_1 + p_2}{2}\right) \sin\left(\frac{p_2 - p_1}{2}\right)$ for small slopes, where $p_i = \tan \theta_i \approx \theta_i$.	L	p_1	p_2

Figure 2.11: Track segment types for vertical direction

2.3.4 Road

Roads in Simpack represent the surface on which the vehicle can travel and a certain coefficient of friction or excitations due to the real representation of the road surface, which can be more or less worn, can be applied to them. Roads serve as an input to the tires and operate via an excitation in the distance domain. Usually, the Road is used in tandem with the Tracks, but they are two completely different elements. The former is used to excite the tires, so it is used to simulate obstacles, road profiles, etc. while the latter is used to impose a path for the generated vehicle to follow. Track was used in this work because it was decided to adopt the "Automotive Track Joint" as the main body joint. This Joint describes the motion of a road vehicle in space. The coordinates used to describe the movement are not tied to a global Cartesian coordinate system, but to the trend of the currently

active Track (2.3.1). This allows the user to define and see track-related positions directly in the states of the joint:

- s -along the track line
- y -lateral in the location track system
- z -vertical in the location track system
- ϕ -roll angle about the local longitudinal axis
- θ -pitch or rotation angle about the local lateral axis
- ψ -yaw angle about the local vertical axis

The joint is often used with six degrees of freedom. In this work, the "Track Road" was used as a road type, which allows defining the friction coefficient and a road profile, this command generates a road surface that follows the active track of the model. This element also allows the implementation of a vertical excitation within the model due to the irregularities of the road.

2.3.5 Road excitations

This section will discuss the vertical excitation imposed by the road profile. The road surface is not smooth but has asperities, the nature of these irregularities varies depending on the conditions and the conformation of its surface. Therefore, the study of the excitations induced on the vehicle due to motion on an uneven road is of fundamental importance both from the point of view of comfort and of the ability of the tires to exert forces in the x and y directions, since the vertical load component F_z varies. Typically, these excitations are studied through a nondeterministic approach that is treated using random vibrations. The tool that will be used is called a power spectral density. A power spectral density (or PSD) describes the frequency-dependent power content of a stationary stochastic signal. "Stationary" means that the mean value and variance of the signal do not change over time. "Power" means the actual physical power (energy per time) or a more abstract form, which is simply the square of the amplitude of the signal. "Density" means that the power per frequency range is returned and not the actual power. Therefore, the total power of the signal (i.e., its variance) can be determined by integrating the PSD over the frequency. The approach used for random vibrations will not be discussed in this section. PSDs are not limited to the time frequency domain, there are also many applications in the distance frequency domain, e.g., for road excitation.

From experimental measurements of the road profile, a law $h(x)$ can be defined, and its power spectral density obtained through harmonic analysis. The profile

is function of space, and the frequency (*rad/m* or *cycles/m*) is referred to it. According with the Simpack notation the PSD can be expressed like:

$$S(\Omega) = \frac{b_0}{a_0 + a_2\Omega^2 + a_4\Omega^4} \quad (2.40)$$

The coefficients are as follows (Figure 2.12):

Road Type	b_0	a_0	a_2	a_4
Very good cement concrete	0.002129632	1.804124	453.5357	1
Good cement concrete	0.04521842	107.7899	9629.229	1
Good asphalt concrete	0.004627566	5.058896	917.2805	1
Good Macadam	0.003864958	2.339663	539.7142	1
Medium asphalt concrete	0.01696774	5.058896	917.2805	1
Medium pavement	0.04831402	38.09674	1454.728	1
Bad pavement	0.08305384	36.21485	1760.542	1
Very bad Macadam	0.1585651	7.058781	1164.409	1
Bad unfortified road	0.6648117	7.950653	1270.181	1
Very bad unfortified road	18.00072	7.950653	1270.181	1

Figure 2.12: Road type parameters for vertical excitation

Where $\Omega = 2\pi F$ and F is the inverse of the wavelength in m^{-1} . The procedure used to introduce a vertical excitation was to choose the Road type from Figure 2.12, in detail a "medium asphalt concrete" was chosen as seen in Figure 2.13. Vertical excitation was subsequently generated (Type: Stochastic from PSD). This

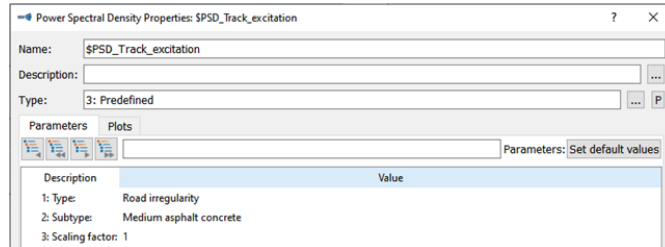


Figure 2.13: Track excitation

Excitation takes a Power Spectral Density as input and creates on this basis a pseudo stochastic signal in the distance domain, which can be directly applied to a Road or Track. The modelling elements that provide the contact of the wheel to the Road or Track will convert the distance domain excitation into the according to time-domain excitation according to their current travel speed. The power spectral density function is sampled at a given number n_F of discrete frequencies within a given band from F_{min} to F_{max} . This is illustrated in Figure 2.14. At this point,

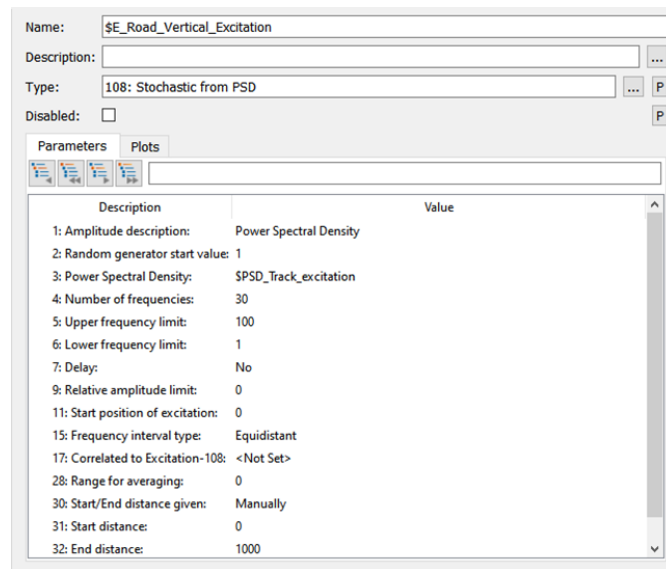


Figure 2.14: Road vertical excitation

this excitation is applied to the road profile directly using the Road element and selecting the previously created excitation, as shown in figure 2.15. Parameter 11 is

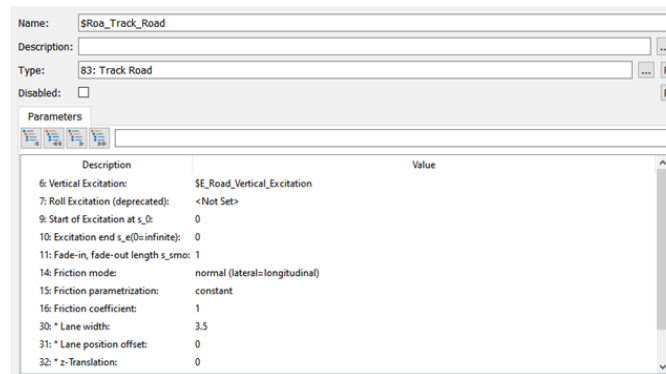


Figure 2.15: Track road

used only when a vertical excitation is entered, it means the length over which the irregularities are faded in from zero to their full extent and faded out again to zero.

2.4 Track used

Using the previously explained elements it is possible to reconstruct any type of track, those that are used for the study of the connecting elements are the following:

- Castelfidardo roundabout
- Double curve
- Vertical slope (2% and 4%)
- Straight track

Each track was developed for a particular element, in detail, the simulated roundabout was the test for the various elements as the vehicle will have to cover it, it represents the worst condition for several situations. The first three track will be explained in detail, the last being the path that is set by default by the software, will be taken for granted.

Corso Castelfidardo roundabout

Corso Castelfidardo roundabout has been simulated; as previously said it will have to be physically travelled during the test of the vehicle. To implement the roundabout within the Simpack code, the "Google Earth" software was used in the first instance to make a top view of the roundabout and obtain reference measurements as shown in Figure 2.16.

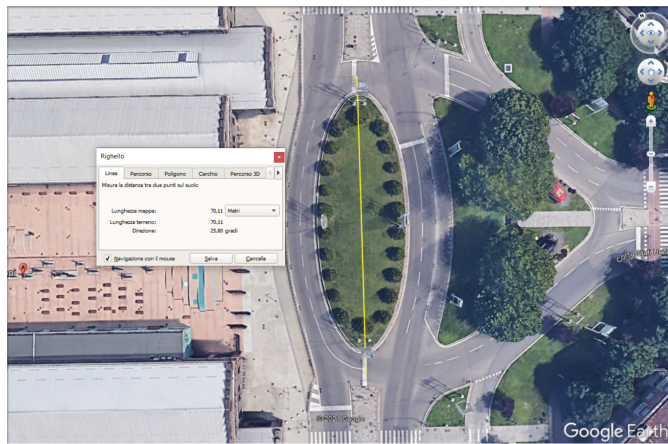


Figure 2.16: Google Earth view of Corso Casterlfidardo roundabout

It is noted that the length taken as a reference is that of the upper semi-axis, which turns out to be 70.11 m . Once the reference has been taken, the image has been imported into Solidworks where the geometry has been reconstructed as in Figure 2.17, taking the path delimited by the dotted line as the path the dimension is relative to that.

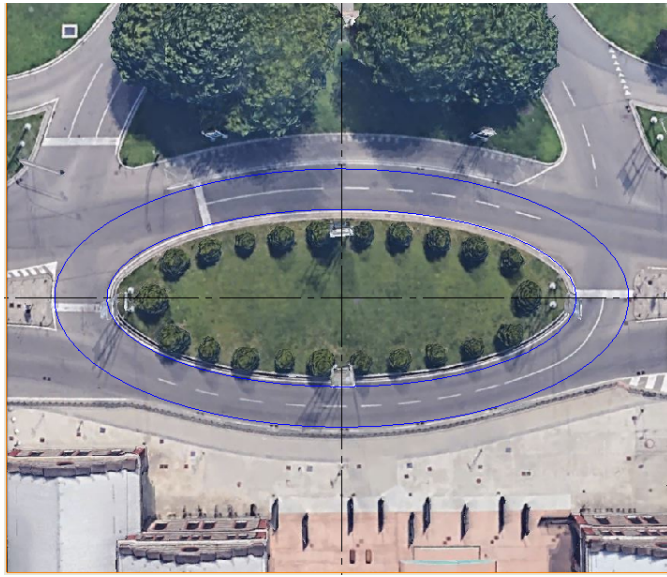


Figure 2.17: Roundabout geometry reconstruction

Once the geometry has been reconstructed, it has been scaled to bring the upper axle shaft back to the measured value, in this way the real measurements of the roundabout are obtained. To export this data to Simpack some points have been arranged along the path, furthermore, it has been modified to be easier to follow, the configuration used was the one represented in Figure 2.18.

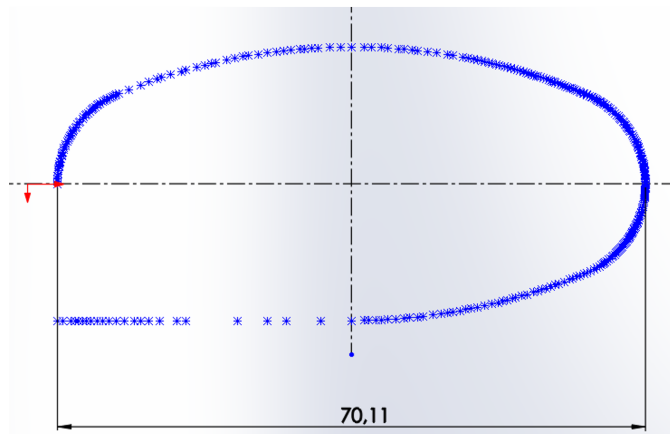


Figure 2.18: Data export from Solidworks

At this point, thanks to a macro, the coordinates of the points are extracted in Excel, at this point the coordinates can be entered into a text file with the ".trm" extension so that it can be read by the software and at this point, you can get the

roundabout within the Simpack workspace. No superelevation in the curve has been inserted for this route since the roundabout is located in an urban area it was assumed that it was negligible as it was travelled at low speeds.

Double curve

A track with a double curve with a radius of curvature of 60 m for both curves was reproduced within the software; this track is of particular importance as it represents a verification of the fact that the vehicle must exhibit the same dynamics while driving whether it is cornering to the right or to the left. In this case, a superelevation has been inserted in the curve, as happens in reality to counteract the centrifugal force that develops and to guarantee a higher speed. In this case, we have set a superelevation value of 0.1 m. The construction of the path containing the double curve is represented in Figure 2.19.

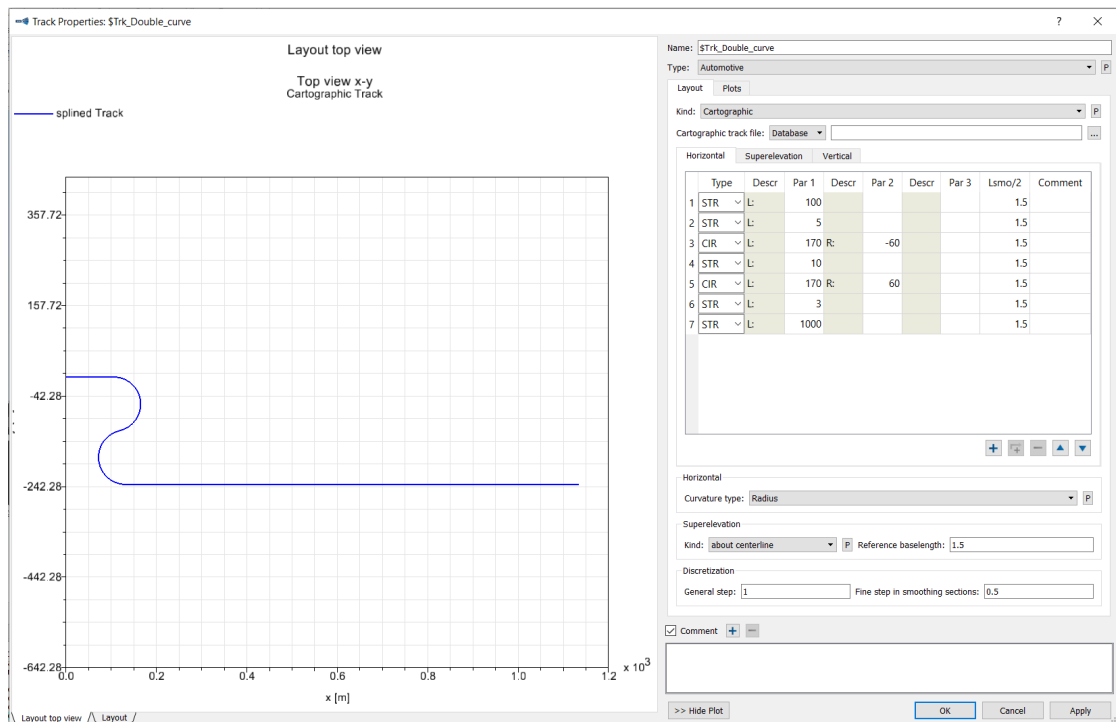


Figure 2.19: Double curve horizontal data

Then, once the horizontal path has been constructed, the superelevation is inserted; it is introduced as a linear segment that goes from a null value to the required value. As it can be seen in line number four, there is the connecting stretch between the two curves, a straight road of 10m has been chosen in which the sign of the superelevation is changed as the direction of curvature of the road varies.

As can be seen, the horizontal and superelevation sections are closely related, since one influences the other.

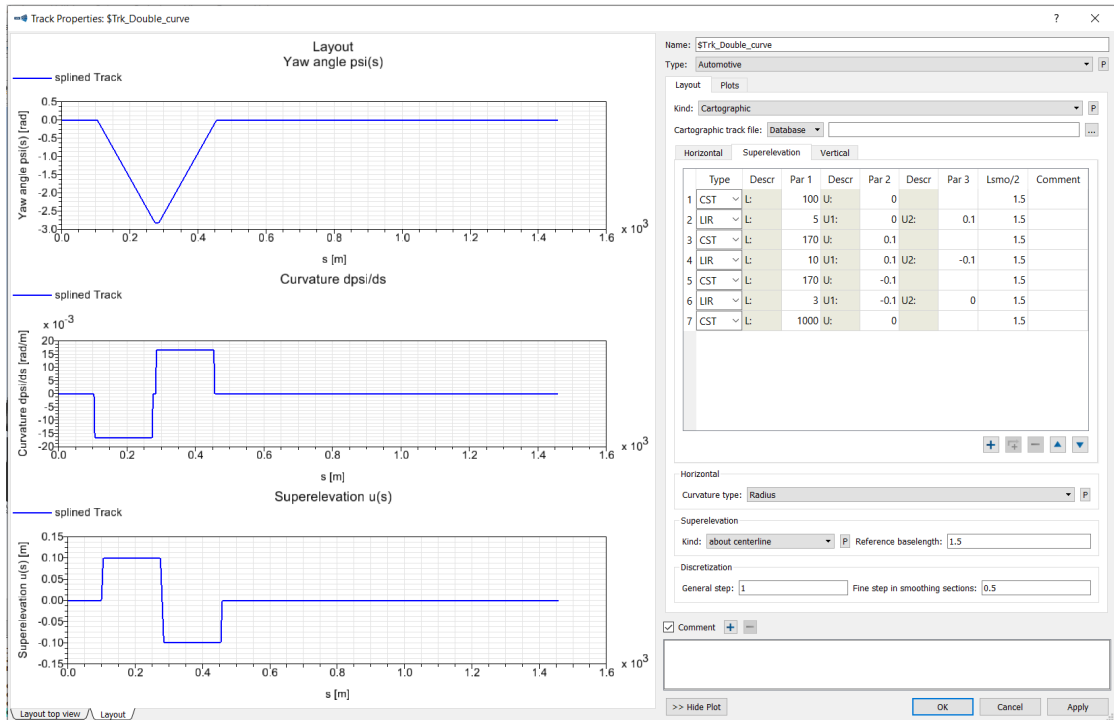


Figure 2.20: Double curve track characteristics

Figure 2.20 shows some parameters that describe the characteristics of the path, also useful for the interpretation of the output values.

Track with vertical slope

This path has only a variation along the vertical coordinate, represented by the z -axis. In detail, the track shows a net variation from the slope of 2% to that of 4%, in this way it is as if there were a kind of step and it will be useful to optimize the elements that will be subsequently implemented and optimized. As can be seen, the variation that has been imposed is constant, i.e. the first zero coordinate section of length 50 m, subsequently an inclination of 2% long 100 m is imposed and finally the last section with inclination 4% also it along 100 m. as far as the horizontal is concerned, it is represented by a straight path for the entire duration of the imposed slope.

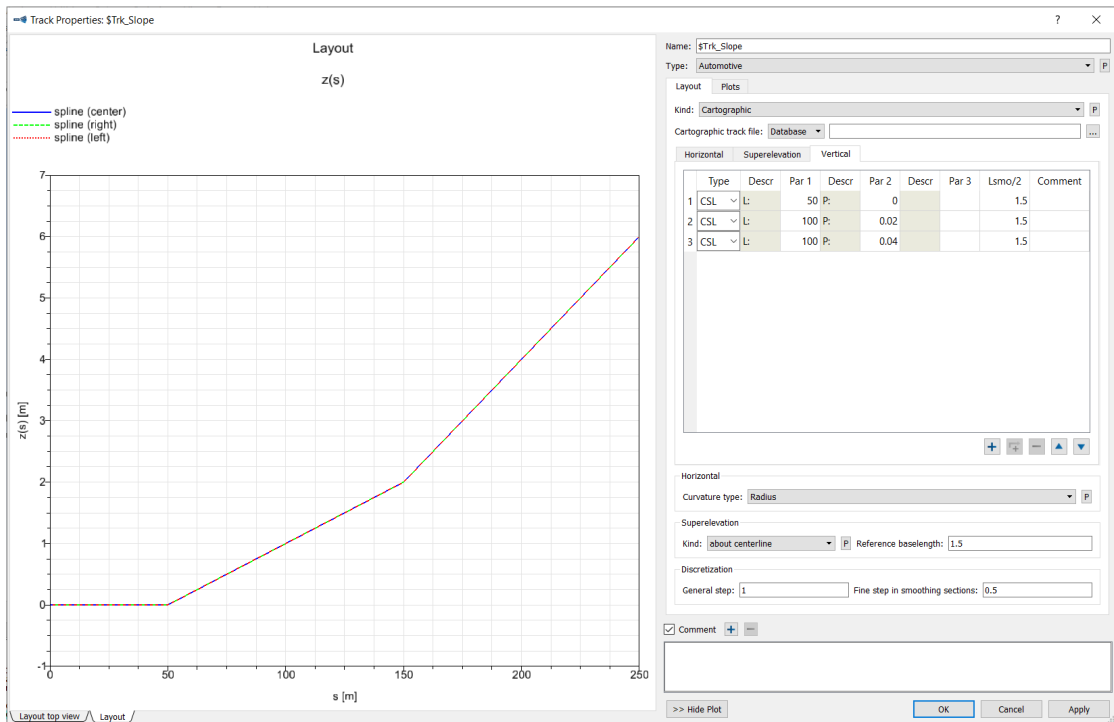


Figure 2.21: Vertical slope track construction

Chapter 3

Multibody architecture of the vehicle

A multibody system is a representation of a mechanical system based on a set of rigid (or possibly flexible) bodies connected by kinematic constraints and subjected to a series of external forces. Kinematic constraints are rigid connections that limit the degrees of freedom of the system (hinges, carriages, imposed motions, etc.). It is therefore a lumped-parameter approach, which allows the creation of relatively simple models of the structures under examination. The term rigid body means that the deformation of the body under consideration is assumed small such that the body deformation does not affect the gross body motion. Hence, for a rigid body, the distance between any two of its arbitrary points always remains constant and all configurations. The motion of a rigid body in space can be completely described by using six generalized coordinates and so every rigid body in the space has six degrees of freedom. The most recent multibody codes allow treating contemporary rigid and flexible body together to better simulate reality. How the code treats the flexible element is different from the FEM approach, in fact in the multibody code the user has to pass a certain number of flexible modes of the system under study to properly describe the physics of the body. The model must be developed to analyse a specific problem, and the simplifications introduced must be considered so that they do not negatively affect the simulation results. For example, since the bodies and constraints introduced have no flexibility, it is necessary to evaluate in advance whether this flexibility is negligible, otherwise, it is still possible to introduce it using elastic elements. Multibody software is widely used in companies due to its great versatility ranging from the aeronautical field to the railway one with specific applications for each sector. The way to work is to start from a very simplified model of the system under consideration to have orders of magnitude of the results to be obtained and then add more and more details to the model.

These types of codes are mainly used for the dynamic and kinematic analyzes of the systems under consideration, particularly when large displacements come into play such as a simulation of a train on a rail or a vehicle on a track. As mentioned, every field of study be it automotive, railway etc. introduces dedicated packages that allow the study of the peculiarities of the area studied in detail, such as the contact between tire and asphalt in the automotive field or the wheel-rail contact in the railway sector. The software used for this thesis has been Simpack, a leading software in the multibody field, it differs from the main competitor MSC Adams for some peculiarities that make it preferable for studying in certain areas. Simpack software will be described in detail. Bodies are described by the following elements:

- Local reference system (MSYS)
- Absolute reference system (ISYS)
- Inertial properties
- Initial conditions

Also, can be added if necessary:

- Marker
- Geometries
- Sensors

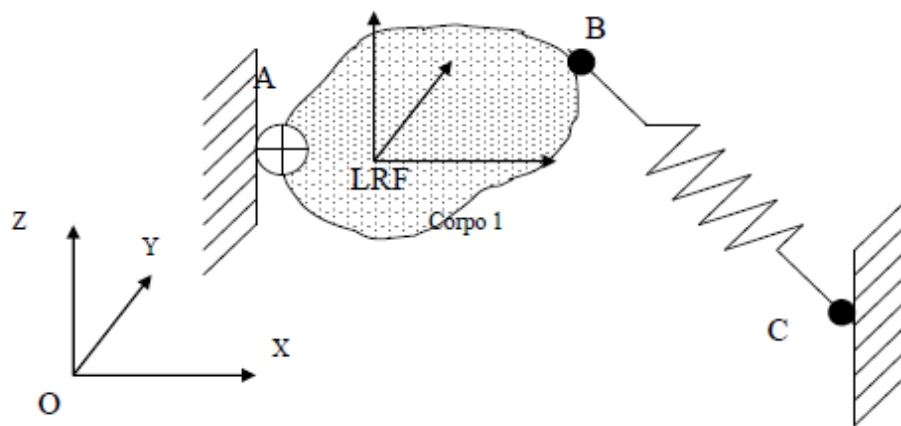


Figure 3.1: Body creation in Simpack

The Figure 3.1 shows the creation of a new body in the work environment, in detail it can be seen that by default the Simpack software inserts a Joint connecting

the body and Ground (when inserted it compensates for 6 d.o.f. but can be modified based on the d.o.f. owned by the considered body), therefore it is implicitly bound, subsequently if the body has other connections a Marker is inserted, represented in the Figure 3.1 by point B which is a local reference system defined concerning the LPRF of the body to which it belongs and the connection is made through Constraints or a Force elements depending on the physics of the system. Each time a new body is inserted, a new set of variables are automatically generated and added to the state vector. The location vector can be expressed like:

$$q = [x \ y \ z \ \alpha_\lambda \ \alpha_\mu \ \alpha_v]^T \quad (3.1)$$

$$\dot{q} = [\dot{x} \ \dot{y} \ \dot{z} \ \omega_\lambda \ \omega_\mu \ \omega_v]^T \quad (3.2)$$

The first three column of equations 3.1 and 3.2 represents the translation and the velocity referred to the local reference frame, while the last three column of equations 3.1 and 3.2 represents the rotation and the angular velocity referred again with respect to the local RF. The real orientation is given by the Euler's angles through the following definition:

$$\Theta = [\theta \ \phi \ \psi]^T \quad (3.3)$$

The state vector for a rigid body results to be:

$$y = [\dot{q}^T \ \dot{\Theta}^T \ q^T \ \Theta^T]^T \quad (3.4)$$

In multibody systems, the body's motion is constrained due to its mechanical joints such as prismatic, cylindrical, spherical etc. From a mathematical point of view constraints are elements that introduces in the system an algebraic connection between different state vector and reducing the d.o.f. of the system. There are two main approaches to describe mathematically the constraints:

1. Lagrange multiplier
2. Generalized coordinate partitioning

the first one allows to solve the problem by adding an algebraic equation and a variable so called Lagrange multiplier. At the end, the system will be formed by algebraic and differential equation that must be solved simultaneously with respect to time (DAE) and so this approach is more time demanding with respect to the second one to be solved. For every degree of constraint, the second approach allows to delete a row and a column of the dynamic matrix of the system, obtaining a dynamic system of ordinary differential equations (ODE) and a set of algebraic equations to be solved in cascade. As previously explained, the Simpack software

differentiates Joint and Constraint, in fact from the mathematical point of view the former (unavoidable constraints) use a coordinate partitioning (ODE) while the latter use Lagrange multipliers (DAE).

The real strength of multibody software lies in the definition of the equations of motion; this expression allows to treat independently equations of linear and non-linear type. The equations of motion can be expressed as Newton-Euler:

- Translation

$$\begin{aligned}
 m\ddot{x} - F_x &= 0 \\
 m\ddot{y} - F_y &= 0 \\
 m\ddot{z} - F_z &= 0
 \end{aligned}
 \tag{3.5}$$

- Rotation

$$\begin{aligned}
 J_\lambda \dot{\omega}_\lambda - J_\mu \omega_\mu^2 - J_\nu \omega_\nu^2 - T_\lambda &= 0 \\
 J_\nu \dot{\omega}_\nu - J_\mu \omega_\mu^2 - J_\lambda \omega_\lambda^2 - T_\nu &= 0 \\
 J_\mu \dot{\omega}_\mu - J_\lambda \omega_\lambda^2 - J_\nu \omega_\nu^2 - T_\mu &= 0
 \end{aligned}
 \tag{3.6}$$

As we can notice in the equations 3.5 and 3.6 the forces and torques are expressed as generalized one, this allows to treat independently linear and non linear systems.

3.1 Model construction

Considering the structure of the model to be created, see figure 3.2; it lends itself particularly well to the creation of the complete assembly using substructures. This allows you to generate a file for each module studied and then, by combining the various files, you arrive at the realization of the assembly. The substructures make it possible to maintain a link between the file initially created and the complete assembly, in fact, by varying the conditions of the former, these will also be applied to the latter. Once the assembly has been generated in its entirety, the substructures can be resolved and any link with the initial files can be eliminated. In constructing the various modules, initially, some a priori assumptions must be made; one must decide what to simulate and what to group as a single body, this approach is all that encapsulates the essence of multibody codes, these assumptions will be described later. To build the model, the inertial properties of the considered bodies (mass, center of mass and moments of inertia) were initially applied, these properties depend on the geometry and material used. For the calculation, the modulus was recreated in Solidworks, the density was applied and then the inertia matrix referring to the center of mass was extracted. At this point, the constraints are applied through the joint and then the various bodies are connected through the force elements. The complete assembly and the various modules to be constructed are shown in figure 3.2. The description will not explain the construction of the model on Solidworks as it is not useful for this article.

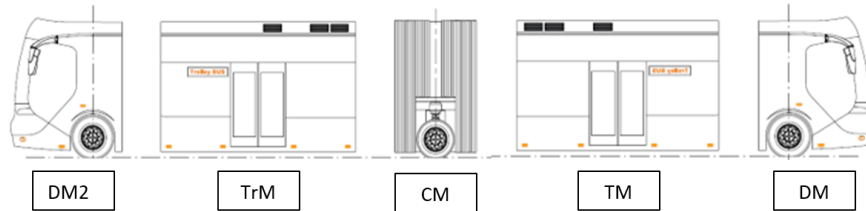


Figure 3.2: Assembly modules

3.2 Reference frame of the model

An important step is the definition of the reference system. The absolute reference system used in this discussion coincides with the Simpack reference system and is placed on the front axle of the DM along the longitudinal coordinate x , y is zero at the center of the vehicle while the z -axis coincides with the ground level (this is shown in Figure 3.3). The chosen reference system coincides with that of the multibody software but differs with the 3D model from which the data and measurements for the construction of the prototype in question were derived. The

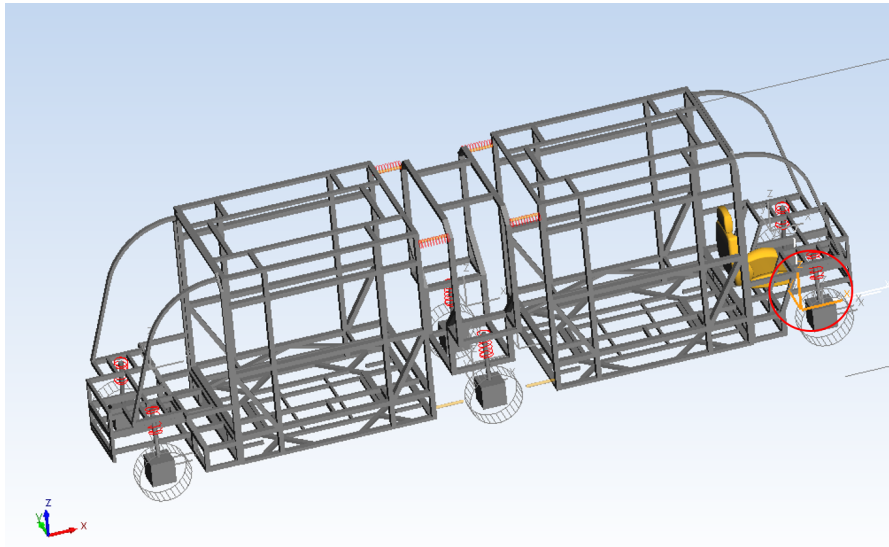


Figure 3.3: Reference frame used in the construction of the model

latter reference system is placed in the front axle but the x -axis is inverted with respect to the one used and the z -axis coincides with the coordinate of the axle. In the following discussion, all COM values were shifted along z of the distance between the axle and the road ($\$_Z_0$), to change from the CAD reference system to the one used in Simpack. As far as the longitudinal coordinate is concerned, it has been inverted for the reasons explained above and a parameter has been added to translate and move the vehicle along the path ($\$_X_0$). In detail, the creation of the most complex substructure, namely the DM, is explained; in order not to repeat things, the other modules will not be discussed because they are very similar in creation.

3.3 Driving module

The first substructure created is the Driving module (DM) as it was decided to follow the order shown in Figure 3.2. It represents the most complex module to represent as it contains many elements. For the calculation of the inertia, a simplified file was created that could consider both the geometry and the material used. Everything was referred to the frame, of which the inertia matrix and the centre of mass were calculated, for elements such as springs it was not necessary to reconstruct them through CAD software as they were of negligible mass and inertia. To create the model we used a new file, as a template we chose “Automotive_Track” which by default inserts the elements necessary for the specifications of the automotive field. At this point, the model was generated on Solidworks by imposing the material

and geometry of the various bodies and then calculating their inertia.

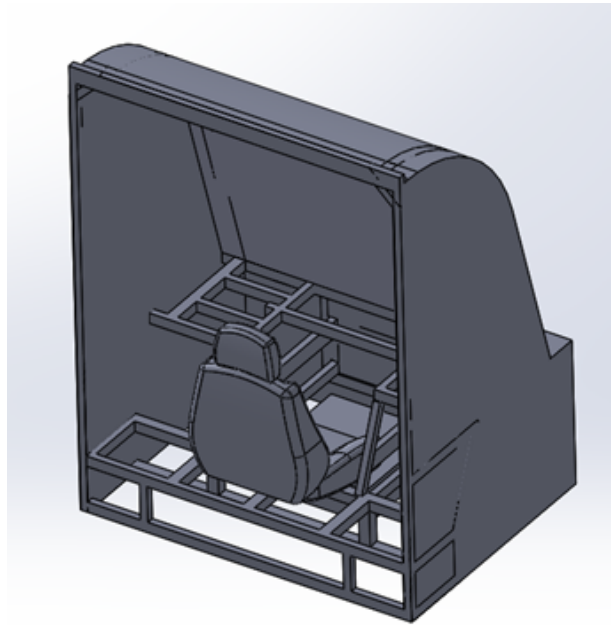


Figure 3.4: Solidworks model built

As you can see in the Figure 3.4, the frame, the seat, the external covering, the engine and steering elements were created. From these elements, the inertial properties to be implemented in Simpack are extrapolated, to the total has been given the name 'Chassis'. These elements have been considered as rigid elements for which the calculated inertia takes into account both geometry and materials of these elements and for how they have been calculated, it is as if they behave as a single body. The most important thing is to calculate the inertia concerning the centre of mass as Simpack requires this treatment. As can be seen from Figure 3.3, the first box represents the centre of mass while the second represents the inertia matrix referred to the COM.

At this point, the extrapolated data can be used and implemented in Simpack. First of all, a new body called 'Chassis' is created, a Marker called \$M_Chassis_COM (Figure 3.6) is created and the coordinates of the centre of mass are assigned as in Figure 3.3. Subsequently, the properties of the body are applied by assigning the mass (calculated in Figure 3.3), the position of the centre of mass (referred to the previously created Marker) and the inertia matrix referred to the COM; this is shown in Figure 3.7.

All variables have been parameterized so that it is easier to change their properties. At this point the constraints are applied through a joint, as regards the "Chassis" an "Automotive Track Joint" is used, this element describes the movement

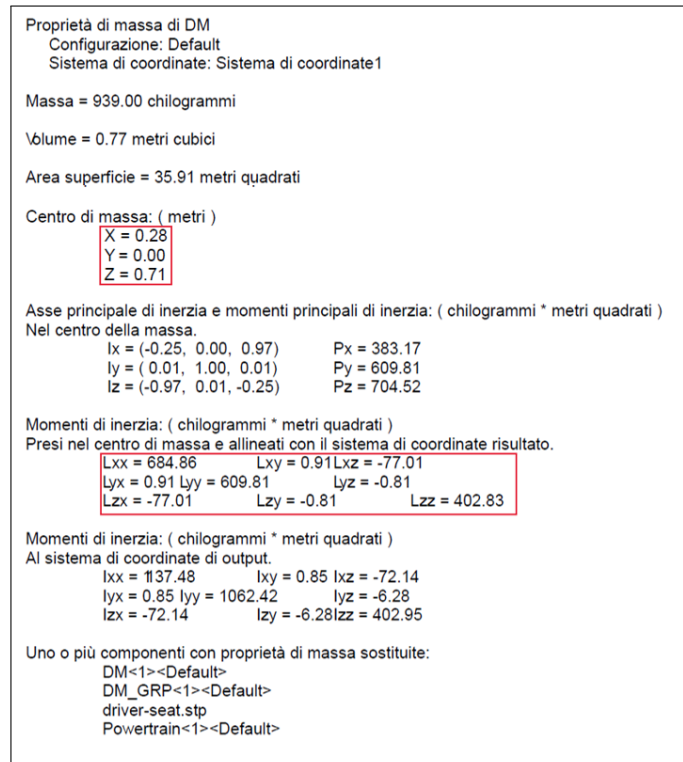


Figure 3.5: Extraction of the center of mass and of the inertia matrix

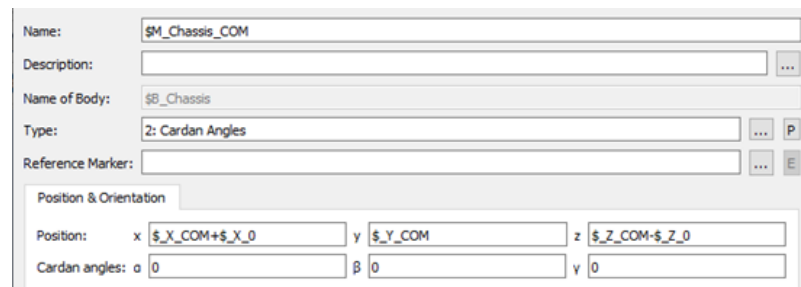


Figure 3.6: COM Marker

of a road vehicle in space. The joint represents a 6 d.o.f. in which the longitudinal direction is represented by the s -coordinate along with the path (Figure 3.8) and therefore, consequently, the other coordinates will no longer be referred to the absolute reference system but to that of the path.

At this point the "Chassis" has been completely defined, the next body created is the wheel hub of which only one side will be treated as the vehicle is symmetrical; the same approach will be used for the wheels. As regards the hub, an estimate was made starting from the data provided by the company Blue Engineering Srl,

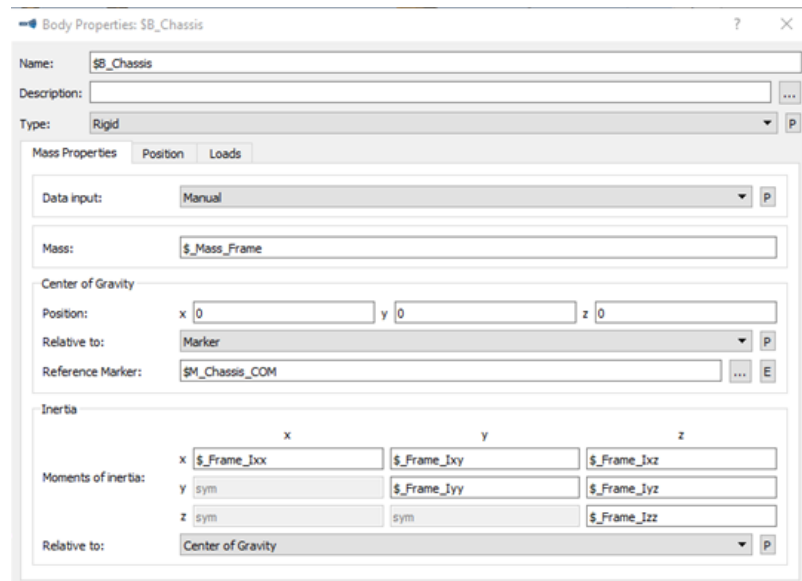


Figure 3.7: Chassis mass properties

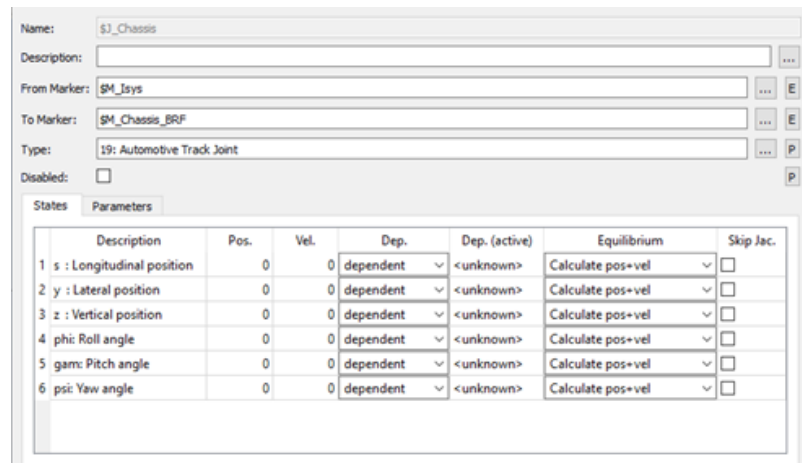


Figure 3.8: Degrees of freedom allowed for the chassis

knowing the sprung and unsprung mass, it was possible to define the mass and inertia characteristics of the wheel hub; as regards the centre of mass, it has been reported concerning the BRF of the body as can be seen in the Figure 3.9. While the inertia as in the previous case is calculated with respect to the COM. The degrees of freedom assigned through the Joint are two, since the DM is equipped with steering, the wheel hub must be able to rotate around the z – axis and translate vertically, for this purpose a Joint called ‘User defined’ has been used, as shown in Figure 3.10. The geometric position of the From Marker (Figure 3.10)

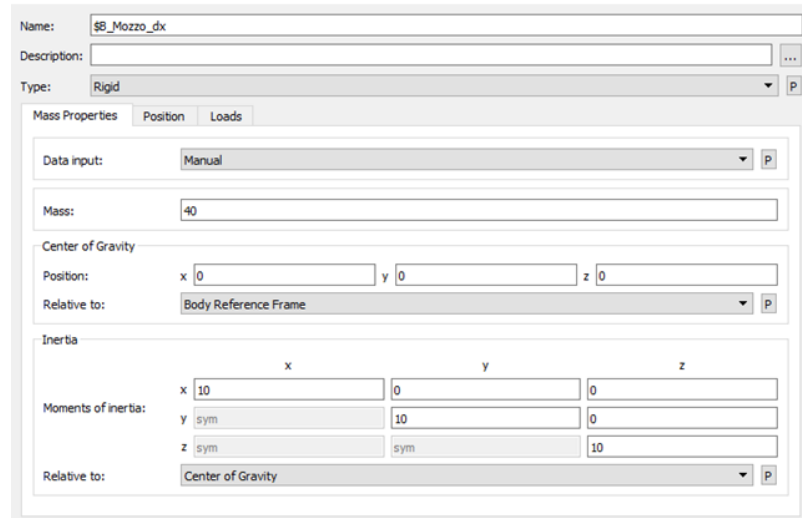


Figure 3.9: Wheel hub mass properties

has been obtained from the file provided by the company previously cited, the dimensions of the markers created for the generation of the DM are presented in Table 3.1. From the dimensions exported by the file CAD it is possible to note that

Table 3.1: Markers distance from ISYS

Marker's name	x [m]	y [m]	z [m]
\$M_Chassis_COM	-0.28	0	1.16688
\$M_Chassis_attacco_mozzo_dx	0.0536	-0.7524	0.32695
\$M_Mozzo_dx_att_ruota	0.0536	-0.839	0.32695
\$M_Chassis_att_sospensione_dx	0.0536	-0.615	1.09
\$M_Mozzo_dx_att_sosp	0.0536	-0.6895	0.80395

the distance from the inertial reference of frame to the axis of the wheels, hub and suspension (these three elements share the same longitudinal coordinate) turns out to be 53.6 mm. As can be seen by Table 3.1, the x axis has been inverted and the z -axis has been shifted upward with respect to the Figure , as previously explained. The position of the Marker \$M_Chassis_attacco_mozzo_dx is shown in Figure 3.11 in which it can be seen as previously mentioned that it has been parameterized to be able to move the vehicle along the track. The last body to be created is the wheel, also in this case the centre of gravity has been made to coincide with the BRF. As far as the wheel Joint is concerned, only the rotation around β has been given as the degree of freedom, this implies that the hub and the wheel are rigidly connected. The From Marker belongs to the hub and geometrically corresponds to the right end of the element, in this case, the To Marker instead represents the

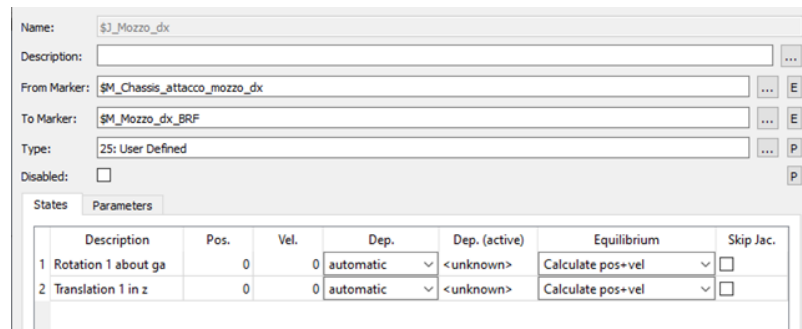


Figure 3.10: Wheel hub joint description

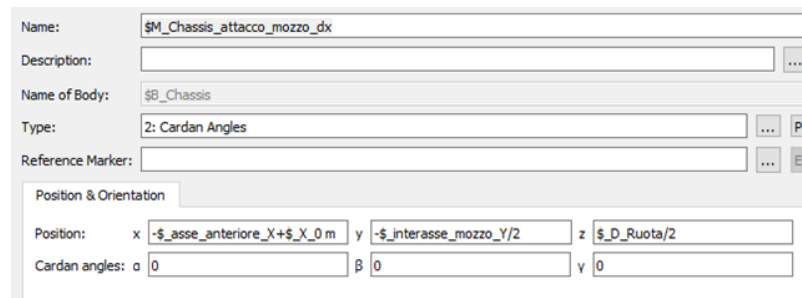


Figure 3.11: Geometric position of the marker belonging to the chassis (From)

BRF of the wheel, in this case since the centre of mass and the BRF coincide there are no problems; if the two do not coincide this would lead to an eccentricity, but considering the wheel as an ideal element from the geometric and material point of view, its COM will certainly lie in the centre of the wheel (plane $z - x$ as the eccentricity depends on such coordinates). So far, the various bodies belonging to the DM have been described and the constraints that are applied to them, from this moment the generation of the suspensions and the model of the tire used will be described. As regards the geometric position in which the suspension is located and the length of the spring and damper, they have been obtained from the CAD file and subsequently implemented in Simpack. So now we define the two Markers from which the suspension will then be created, one will belong to the Chassis while the other to the hub following the measurements taken from the drawing. At this point the Force Element can be created, the Spring-Damper Parallel PtP has been chosen, whose behaviour follows the real one of the suspensions. This modeling element is a simple spring (massless) and damper in parallel which can be either linear or nonlinear in both the stiffness and damping; end moments are ignored. Spring and damper can be active for compression and/or tension. Also, in this case, only one side of the vehicle will be treated as it is symmetrical. For this type of element, the free length of the spring, the value of the stiffness and the damping

Name: \$B_Ruota_dx

Description: ...

Type: Rigid P

Mass Properties Position Loads

Data input: Manual P

Mass: 60

Center of Gravity

Position: x 0 y 0 z 0

Relative to: Body Reference Frame P

Inertia

	x	y	z
Moments of inertia: x	2.69	0	0
y	sym	4.71	0
z	sym	sym	2.69

Relative to: Center of Gravity P

Figure 3.12: Wheel mass properties

From Marker: \$M_Mozzo_dx_att_ruota E

To Marker: \$M_Ruota_dx_BRF E

Type: 2: Revolute be P

Disabled: P

States Parameters

	Description	Pos.	Vel.	Dep.	Dep. (active)	Equilibrium	Skip Jac.
1	Rotation about be	0	0	automatic	<unknown>	Calculate pos+vel	<input type="checkbox"/>

Figure 3.13: Wheel joint description

must be entered as input data; instead of these data, the trend of the stiffness as a function of the displacement and damping as a function of the speed can be entered directly through some input functions in positions 4 and 5 of Figure 3.14. The value of damping and stiffness or their behaviour is of fundamental importance for the dynamics of the vehicle, as it affects comfort, road holding and the unloading of forces on the ground. It is not the purpose of this paper to dimension the suspensions in detail, also because for this purpose, they should be simulated more precisely. As for the preload, it is also very important as it allows to avoid an initial adjustment phase, which without damping would oscillate indefinitely. For this purpose, it will be treated later and the modalities with which the preload in the simulation environment was carried out will be explained, to do this, however, it is necessary to have a complete model in which the distribution of forces is influenced by the interconnected modules. For the moment, the preload is set equal to zero as can be seen from Figure 3.14. Parameter number 10 means that the operation of the spring and the damper are valid even with negative displacement and velocity,

i.e., in lengthening or shortening. In Figure 3.14 the suspension is represented, for

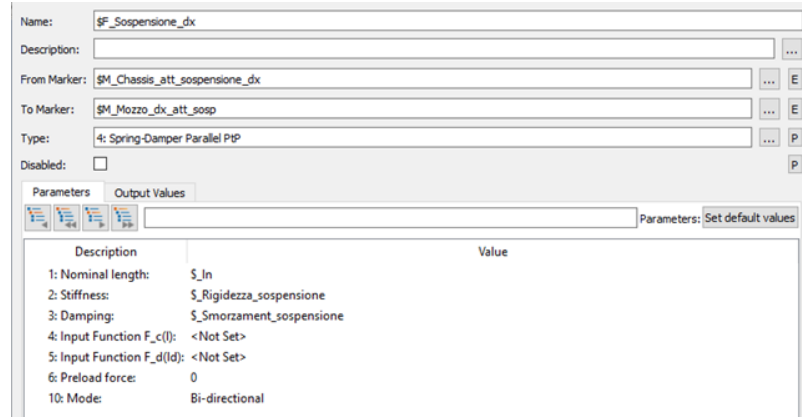


Figure 3.14: Suspension parameters used

this definition, the first three parameters have been used for this treatment; they are useful for defining the resulting force as:

$$F_{ij} = K * (l_{ij} - ln) + C * v_{ij} + F_0 \quad (3.7)$$

Where K is the stiffness of the spring, l_{ij} is the length of the spring at a given instant, ln is the nominal length, i.e., the distance between the two markers (distance magnitude), C the damping value, v_{ij} is the difference in speed between the two markers at a given instant while F_0 represents the spring preload. The From Marker and To Marker have been obtained from the CAD file, the positions of the markers are presented in Table 3.1, the first belongs to the Chassis while the second to the wheel hub; therefore, the suspension was applied between the two bodies. To simulate the tire, the "Pacejka similarity" package was used which allows simulating the tire-asphalt contact in a simplified way compared to the standard package, this choice was made because for the second one all the coefficients of the case should have been known, which they are very difficult to find, for this reason, the first was chosen as the values that were used were taken from the literature. The absolute reference system, which is at ground level, was used as From Marker, while the BRF of the wheel was used as the To Marker. The characteristics of the contact are contained in the "pacejka_similarity_training.tdx" file (paragraph 2.1.2), the road must be entered using parameter number 6; it recognizes the imposed characteristics such as the coefficient of friction and vertical excitation due to roughness, while the reference Joint is that of the "Chassis". In Table 3.2 all the subvar used to build the DM model are inserted, they were of fundamental importance for the definitions of the previously described markers. As the last step for a visual issue, the frame and the driver's seat have been inserted into the model

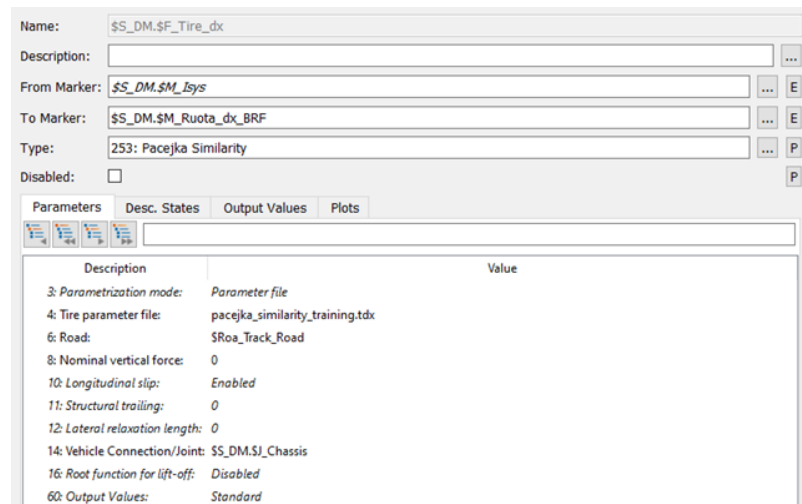


Figure 3.15: Tire parameters used

as an STL file, as mentioned, the geometry is only a question of display as the mass and geometric properties are entered manually.

Table 3.2: Subvar used

Name	Value	U.M.
\$_X_COM	-0.28	<i>m</i>
\$_Y_COM	0	<i>m</i>
\$_Z_COM	0.751	<i>m</i>
\$_Mass_Frame	939	<i>Kg</i>
\$_Frame_Ixx	684.86	<i>Kg * m²</i>
\$_Frame_Iyy	609.81	<i>Kg * m²</i>
\$_Frame_Izz	402.83	<i>Kg * m²</i>
\$_Frame_Ixy	0.91	<i>Kg * m²</i>
\$_Frame_Ixz	-77.01	<i>Kg * m²</i>
\$_Frame_Iyz	0	<i>Kg * m²</i>
\$_X_0	0	<i>m</i>
\$_Z_0	-0.45688	<i>m</i>
\$_asse_anteriore_X	-53.6	<i>mm</i>
\$_interasse_mozzo_Y	1.448	<i>m</i>
\$_interasse_sospensione_Y	1.23	<i>m</i>
\$_D_Ruota	653.9	<i>mm</i>
\$_ln	0.2866803	<i>m</i>

3.4 Data used

As mentioned in order not to make the discussion too long, the construction of the other modules was not carried out as it was very similar in many respects to the one just described, in fact, being the DM the most complex module, it encompasses all the passages present in the other substructures. The only substantial difference lies in the fact that only the DM module has steering wheels, so the handling in other cases is easier. The wheels were not constrained to each other to consider the use of a differential.

Table 3.3: Data used to build the model in terms of inertia and center of mass

Item	Mass (kg)		COM			Inertia Matrix						
			X (m)	Y (m)	Z (m)	Ixx (kg * m ²)	Iyy (kg * m ²)	Izz (kg * m ²)	Ixy (kg * m ²)	Ixz (kg * m ²)	Iyz (kg * m ²)	
Connection Module												
Frame	553		4.11	0	0.49	368.88	318.7	298.11	-0.01	0.68	0	
Wheel Assembly	Wheel_Hub	DX	40	With respect to BRF			10	10	10	0	0	0
		SX	40	With respect to BRF			10	10	10	0	0	0
	Wheel	DX	60	With respect to BRF			2.69	4.71	2.69	0	0	0
		SX	60	With respect to BRF			2.69	4.71	2.69	0	0	0
Driving Module												
Frame	164											
GRP external	275											
Seat	160											
Powertrain	340											
Total	939		0.28	0	0.71	684.86	609.81	402.83	0.91	-77.01	-0.81	
Wheel Assembly	Wheel_Hub	DX	20	With respect to BRF			5	5	5	0	0	0
		SX	20	With respect to BRF			5	5	5	0	0	0
	Wheel	DX	60	With respect to BRF			2.69	4.71	2.69	0	0	0
		SX	60	With respect to BRF			2.69	4.71	2.69	0	0	0
Transit Module												
Transit Module	Frame	1452.000										
	GRP	642.000										
	Battery	260.000										
	cooling frame	12.000										
	Total	2366.000	2.100	0.050	0.920	3647.120	3691.730	2988.780	0.660	-60.220	23.240	
Driving Module 2												
Frame	Frame	164										
	GRP	275										
	Total	439	8.07	0	0.81	486.9	358.89	316.49	0.61	38.19	0.66	
Wheel Assembly	Wheel_Hub	DX	20	With respect to BRF			5	5	5	0	0	0
		SX	20	With respect to BRF			5	5	5	0	0	0
	Wheel	DX	60	With respect to BRF			2.69	4.71	2.69	0	0	0
		SX	60	With respect to BRF			2.69	4.71	2.69	0	0	0
Transit Rear Module												
Transit Rear Module	Frame	1185										
	GRP	642										
	Total	1827	6.09	0.05	1.05	2929.14	2886.28	2500.31	-0.01	-0.25	21.6	

Table 3.3 shows the data extrapolated by Solidworks with the various assumptions made regarding the grouping of elements that are not useful for the simulation and therefore grouped within a single rigid element.

3.5 Assembly generation

A new file has been created to insert the substructures, starting from scratch; the template model has been selected as Automotive track and the body that the software introduces automatically has been eliminated, at this point the first substructure is inserted (the order of the substructures does not change the result).

We have chosen to proceed as in Figure 3.2. Then insert the DM via the "Create" → "Substructure" → "Abs command path" and choose the file in the PC directory. This is done until all the substructures have been inserted. Since the reference system of Simpack and Solidworks do not coincide, as the latter uses the opposite x axis with respect to the former, this was considered in the construction of the model. It was then decided to translate the whole model starting from the zero line so that the Simpack zero coincided with the zero of the CAD software, passing from configuration depicted in Figure 3.16 to Figure 3.17.

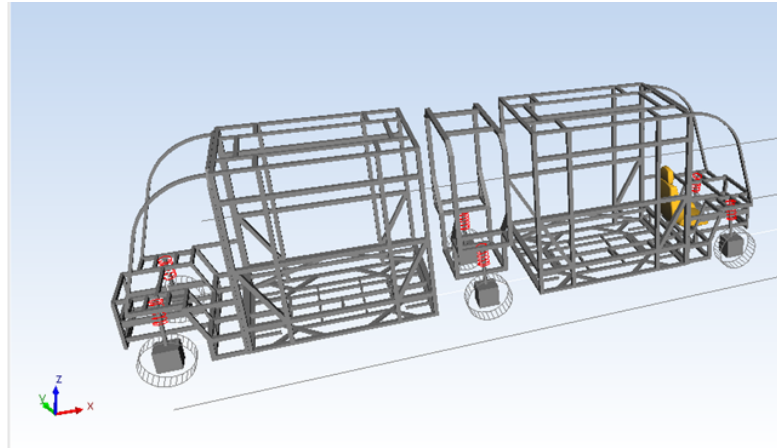


Figure 3.16: Before translation

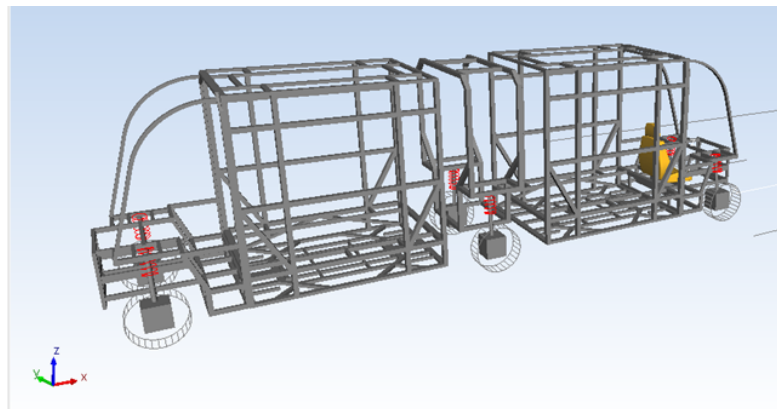


Figure 3.17: After translation

In this way, the same configuration present on Solidworks was obtained but only with the negative x axis. This was all translated by $8,217\text{ m}$. At this point, all that is needed is to connect the substructures together to obtain the complete assembly.

3.6 Configurations studied

The connection of the central module (CM) with the surrounding modules (TM and TrM) are of fundamental importance for the correct functioning of the vehicle and for dynamics in general, especially for the behaviour of the vehicle when cornering. In this regard, two possible solutions have been studied for the upper connections, while, the lower connections has been kept the same for both solutions. The lower configuration is shown in Figure 3.18, it has longitudinal dampers with a certain damping value and a certain inclination (which determines the arm in the various directions); these two parameters are the basis for the optimization of these elements.

The central stiffness represents the spherical joint with very high stiffnesses in the x , y and z directions ($10^8 N/m$), all elements will be subsequently dealt with in detail. The solutions studied for the upper connections are:

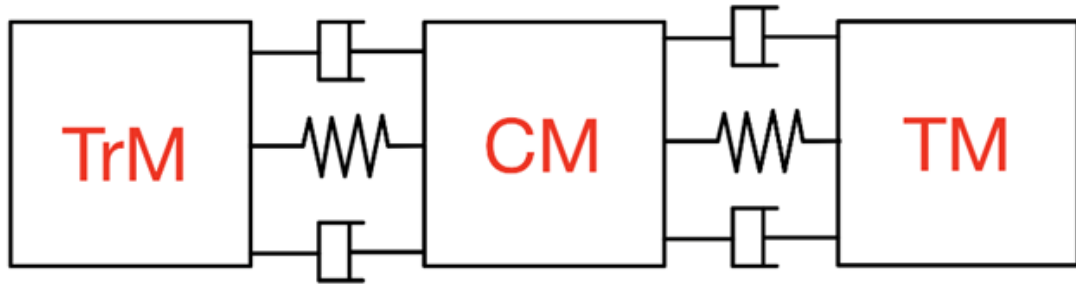


Figure 3.18: Configuration of the lower connections CM-TM/TrM

1. Longitudinal springs with inclined spring (Configuration 1)
2. Longitudinal springs with silentblock (Configuration 2)

Configuration 1 is shown in Figure 3.19, in which the inclined spring is shown in the figure, it has a different stiffness from the longitudinal ones, it has also been parameterized for later optimization. The other elements are always present and are the longitudinal springs and the longitudinal dampers the optimization values will change between the studied configurations as the two cases are very different. In Figure 3.20 configuration 2 is represented in which the silentblock has been simulated as an element having a certain rotation stiffness α and β in parallel to the longitudinal stiffness and the real damper.

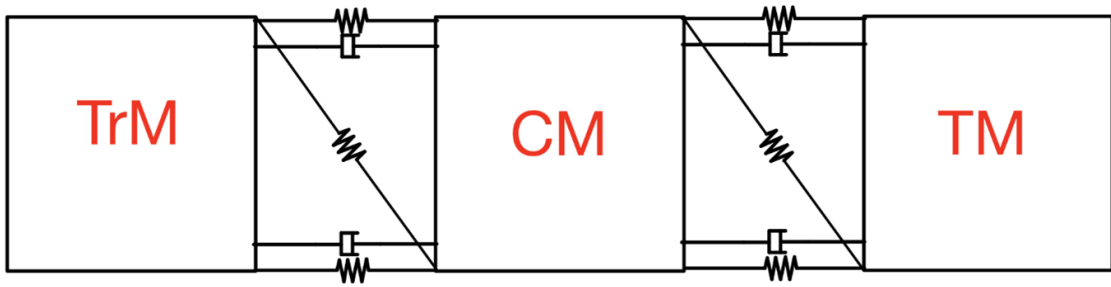


Figure 3.19: Configuration 1

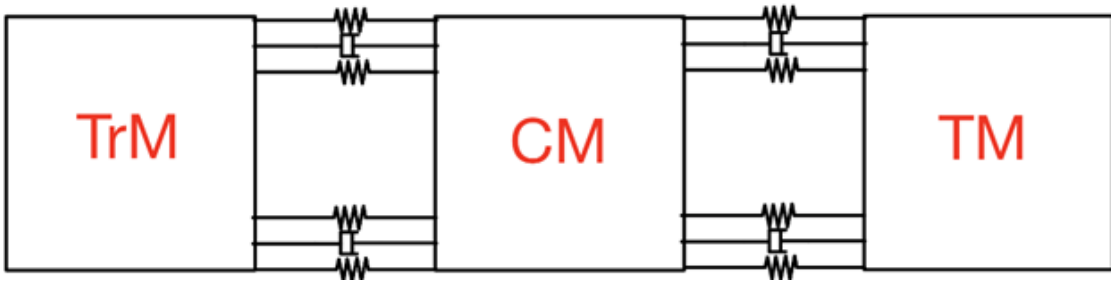


Figure 3.20: Configuration 2

3.7 Connection between modules

To study the dynamics of the vehicle it is necessary to connect the substructures the goal of this paper is precise to optimize the connections between the CM and the surrounding modules. For the study of the connections, it was decided to keep the assembly as a set of substructures, only at the end of the optimizations, it is resolved to simplify operations. The types and methods of connection are of fundamental importance both from the point of view of simulation as the dynamics change significantly as the connections used vary, especially in a vehicle like this in which no module is autonomously stable but becomes stable thanks to connections to the surrounding modules. A fundamental aspect is to study connections that are easily replicable in reality. The connections used between the various modules can be divided into:

- Rigid connection between modules (DM-TM and TrM-DM2)
- Lower CM-TM/TrM connections (Joint and longitudinal dampers)
- CM-TM/TrM longitudinal dampers (upper and lower)
- Upper CM-TM/TrM connections (Configuration 1 and Configuration 2)

The first represents a constraint while the rest are force elements. The difference between the two is that the former adds a kinematic connection by suppressing the degrees of freedom set by the user, while the latter act at the level of dynamics by adding stiffness or damping. In Configuration 1 and Configuration 2 only the elements that distinguish them will be described, that is the inclined stiffnesses for the first and the silent block for the second.

3.7.1 Rigid connection

This constraint allows a rigid connection between the markers, no movement is possible. It was used to connect DM-TM and DM2-TrM in this way simulating the welding that would exist. As mentioned before, if the idea were to always leave zero d.o.f. as a connection element, it would also have been possible to group the TM within the DM (same thing for DM2 and TrM) as the result would be the same. It was decided to take this path as this connection could later be simulated in more detail. In Figure 3.21 you can see the two connections, the connection between

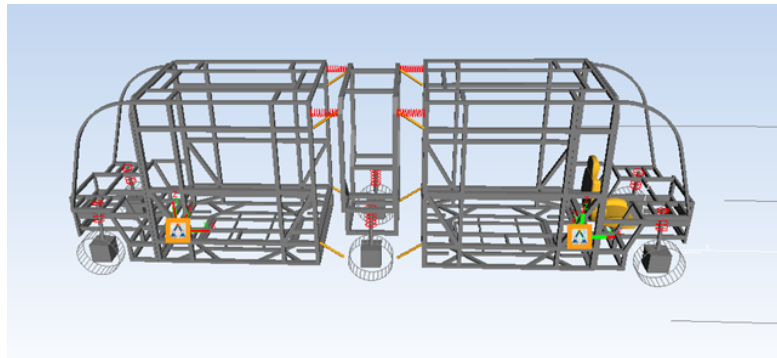


Figure 3.21: Front and rear rigid connection

DM-TM (right) will be explained in detail, in a similar way the left constraint has been created. For the application of the constraint, two markers were created, one belonging to the DM while the other to the TM; these markers were created in such a way that they were coincident, as seen in Figure 3.21. At this point, having the two markers, it is possible to proceed with the application of the constraint through a rigid connection as shown in Figure 3.22. The two markers coincide and are 0.882 m distant from ISYS. The coordinates of interest is the longitudinal one since the y coordinate is zero; the z is indifferent to the result, while, the x coordinate is fundamental as it also geometrically represents the separation between the two modules. As for the rear connection, it is located at the coordinate of -7.334 m .



Figure 3.22: 0 d.o.f. Simpack definition

3.7.2 Lower connections - Joint

The joint is an element, as it was used in this discussion, which connects two independent modules. Especially for how the Trolleybus is structured, this element is fundamental as it allows the vehicle to be functional, as each module for how it is structured could not move because in unstable equilibrium. Therefore, the correct definition of both the permitted degrees of freedom and the position is of primary importance for the dynamics of the vehicle. The joint was simulated thanks to a force element called "Bushing cmp", this universal force element applies spring and damper forces and torques between two Markers in multiple axis directions. This element is defined as cmp, which means that it applies a certain value of stiffness and/or translational or torsional damping between two markers in the components of the axes for which this value of stiffness/damping has been given. Unlike PtPs, which the stiffness value varies in the components remaining constant in the connection between the two points, as the position of the two markers varies; this does not happen about the cmp, on the contrary it works in the opposite way. For the simulation of the joint, after a careful analysis of the mobility that the vehicle must have and after preliminary tests, it was decided to opt for a spherical joint. In this case we have chosen to simulate the joint with a bushing type element even if for this treatment also a constraint type element would have worked as the stiffness of this element is very high which means that the difference with a constraint type is negligible.

The stiffness applied to the joint is 10^8 N/m in the three translations to have the three rotational degrees of freedom free. There is the possibility, as mentioned before, to also impose a certain damping but for this application, for what has been said, it is useless; the first three values shown in Figure 3.23 represent the preloads in the three directions in which the stiffness is present, the study of the preload of

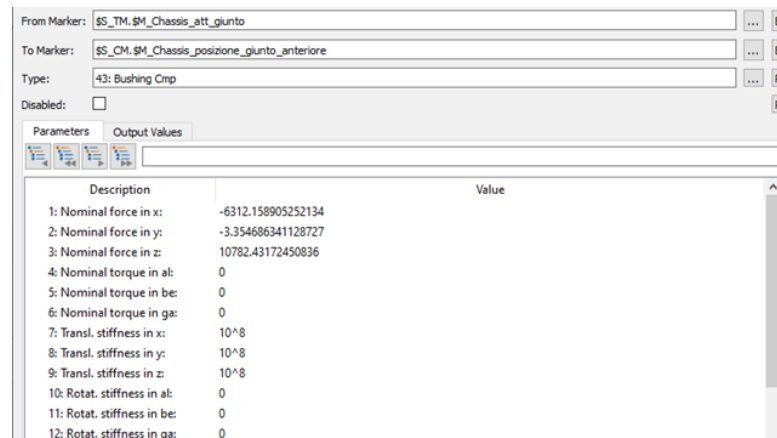


Figure 3.23: Joint Simpack definition

the various elements will be subsequently dealt with in a separate paragraph. The markers used belong one to the TM and the other to the CM and both lie in the same position, the coordinates of these markers have been taken from the CAD file. The longitudinal positions are respectively -3.525 m for the front joint and -4.690 m for the rear joint from the ISYS, considering that the vehicle has been developed in the negative side while the height of the joint is set to 0.374 m ; it must be borne in mind that it is always good have a symmetry along the y -axis, in fact, the joint has been positioned in the middle ($y = 0$) as the vehicle must have the same dynamics whether it curves to the right or to the left. This joint was simulated as a bushing element and once the entire model has been built, thanks to ad hoc tests, the maximum force exchanged by the joint in the three translational coordinates will be determined to size the latter.

3.7.3 Longitudinal dampers (upper and lower)

The longitudinal dampers were used to connect the CM with the surrounding modules (TM/TrM), in detail they were used to prevent the vehicle from reaching dynamic instability, in fact for how the vehicle is built (with two spherical joints that connect the various modules), it is subject to this phenomenon. The instability could be brought about by road conditions or, particularly dangerous is the condition of gusts of crosswind when the vehicle is traveling at high speeds. Therefore, the presence of longitudinal dampers is also essential from the point of view of vibration and comfort. This paragraph explains how it was modeled in a multibody environment. The dampers, initially to carry out the optimization tests on them, were modeled as ideal, subsequently, once the ideal value for the damping coefficient was found, the trend was entered using the input function; this was explained in

detail in Paragraph 2.2. In this section we will show how the real dampers were modeled. They have been inserted as PtP elements. The input function used is the one in Figure 3.24. Once the reference function has been defined, it is inserted

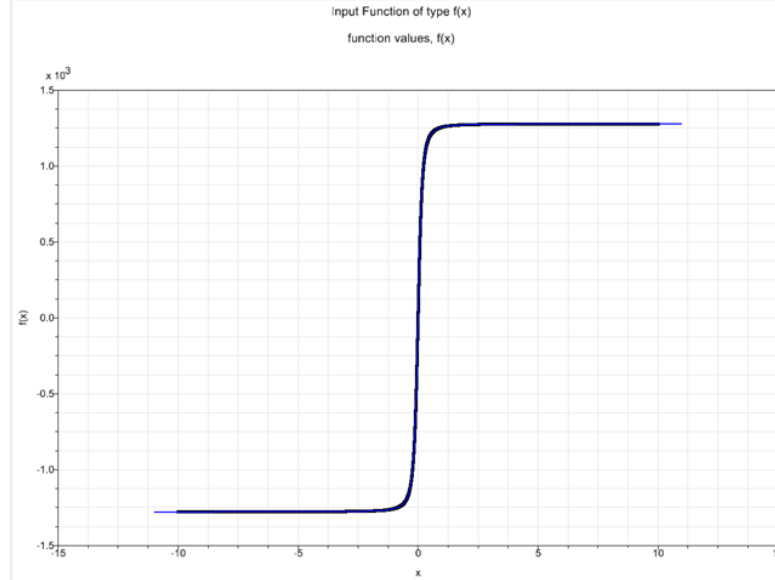


Figure 3.24: Force-speed trend through input function

directly into the force element; for this discussion, the spring-damper serial was chosen to faithfully trace the reality as the stiffness in series with the damping is given by the oil present in the damper. The configuration used is shown in Figure 3.25.

The position of the dampers was parameterized as a function of the angles α and β as shown in Figure 3.25, to then perform a parametric analysis and optimize these two angles and the damping value. Both the lower and upper dampers depend on these two angles in order to make optimization easier, initially the damping coefficients relating to the upper and lower dampers were parameterized separately. The choice of the angles α and β is important as it will determine the optimal position of the longitudinal dampers, the angles are entered as input data and the marker position is returned as output. For the β angle the fixed markers (for the $y - x$ view) are those relating to the TM and the TrM in fact these markers can only translate vertically, forming the α angle. The opposite occurs for the α angle as the fixed markers for the $z - x$ view are those relating to the CM. So α represents a vertical translation of the marker (z -direction) and β instead a horizontal translation (y -direction). Knowing that the distance between the module CM and TM/TrM in the x direction is equal to $l_x = 0.355 \text{ m}$, we obtain that:

$$\Delta y = l_x * \tan(\beta) \quad (3.8)$$

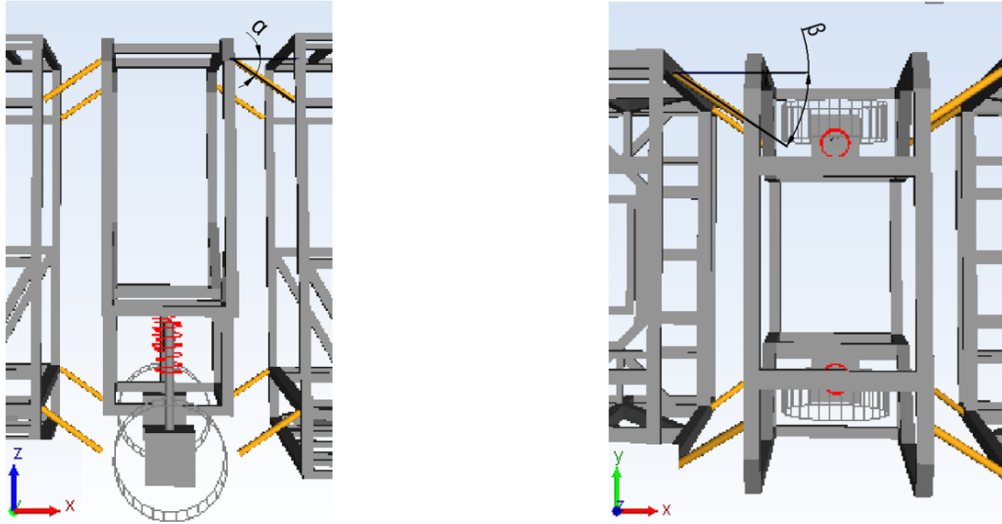


Figure 3.25: α and β definition for longitudinal dampers

$$\Delta z = l_x * \tan(\alpha) \quad (3.9)$$

These quantities are inserted within the markers belonging for the first to the CM and for the second to the TM and TrM. In this way, by varying the angles, different configurations in space can be obtained.

The dampers have been inserted as in Figure 3.26.

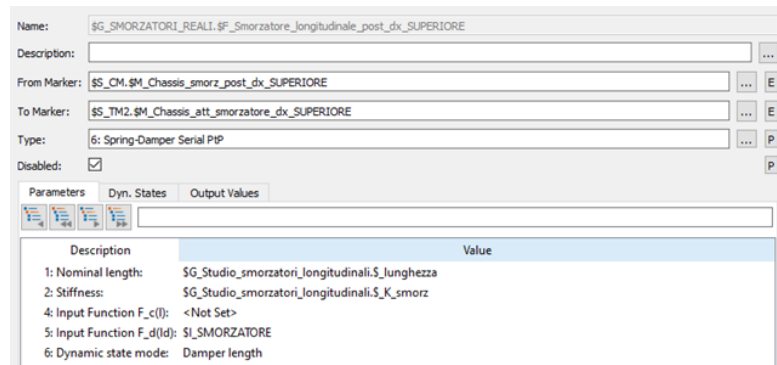


Figure 3.26: Definition of dampers in Simpack

Since the length of the damper depends on the angles α and β , it is possible to obtain the lengths along the three axes, knowing that the longitudinal one is fixed at $l_x = 0.355m$, we obtain:

$$L_n = \sqrt{(\Delta y^2 + l_x^2 + \Delta z^2)} \quad (3.10)$$

While the stiffness has been entered as a parameric value to find the optimal value.

3.7.4 Longitudinal springs

Since the longitudinal springs are present in both configuration 1 and configuration 2, they are grouped in a single treatment for this paragraph, even if they will have different optimization parameters, the construction of these elements is the same in both cases. The stiffnesses implemented in the upper part of the CM are also fundamental for the dynamics of the vehicle as they allow you to correctly perform a steering operation and keep it in position in CM without allowing the pitching of this module. The stiffnesses were placed at the ends of the central element to have an higher arm. In this case the distance between the two markers varies only along the x coordinate, so the angles α and β have not been implemented in the model. We have chosen to proceed in this way since during the curve the stiffness being defined as PtP, does not require an arm in the other directions in the initial condition; in fact, during the curvature of the vehicle, thanks to the definition of the spring in this way and to the fact that the markers also move in the y and z directions (e.g. if superelevation is present) it automatically generates a force in these directions. Also, in this case it was decided to proceed in defining the position of the springs always in a symmetrical way for the reasons described above; the configuration used can be seen in Figure 3.27. Below, based on the

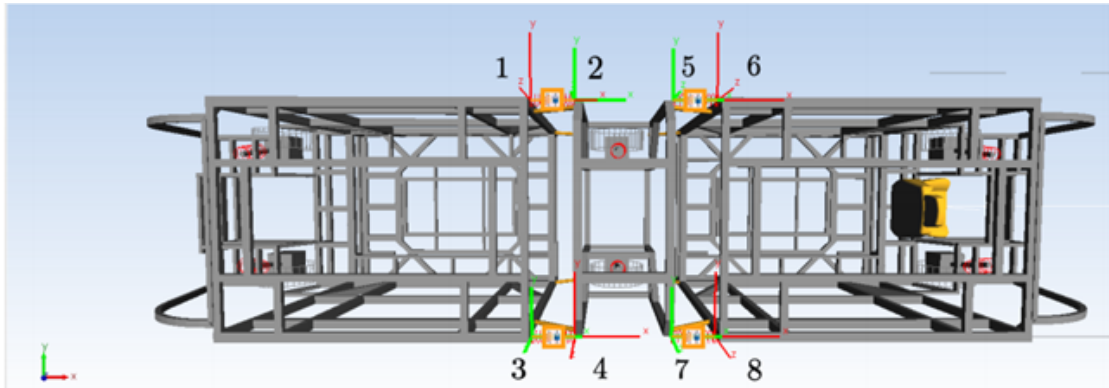


Figure 3.27: Longitudinal springs From (in red) and To (in green) Markers

numbering represented in Figure 3.27, the Table 3.4 has been inserted which shows the position of the markers used to generate the force elements. The positions have been obtained from the CAD drawing. The From markers were given on the TM module as regards the anterior stiffnesses, while belonging to the CM as regards the posterior stiffnesses. As regards the force element, it has been defined as indicated in Figure 3.28 (the creation of the single force element will be explained,

Table 3.4: From and To Markers positions

Marker	ID	x (m)	y (m)	z (m)
1	\$\$_TM2.\$M_Chassis_att_molla_sx	-4.8580	0.96	2.66688
2	\$\$_CM.\$M_Chassis_Molla_post_sx	-4.503	0.96	2.66688
3	\$\$_TM2.\$M_Chassis_att_molla_dx	-4.8580	-0.96	2.66688
4	\$\$_CM.\$M_Chassis_Molla_post_dx	-4.503	-0.96	2.66688
5	\$\$_CM.\$M_Chassis_Molla_ant_sx	-3.713	0.96	2.66688
6	\$\$_TM.\$M_Chassis_att_molla_sx	-3.3580	0.96	2.66688
7	\$\$_CM.\$M_Chassis_Molla_ant_dx	-3.713	-0.96	2.66688
8	\$\$_TM.\$M_Chassis_att_molla_dx	-3.3580	-0.96	2.66688

the other elements have been created by analogy), in which the nominal length which represents the distance between the two markers in static conditions, the stiffness value has been entered in parametric form to optimize this value and the preload as already mentioned will be treated later.

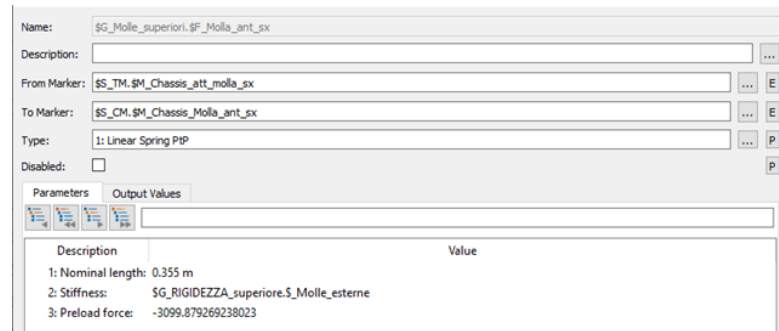


Figure 3.28: Longitudinal springs Simpack definition

Table 3.5, shows the stiffnesses, nominal lengths and preloads of the four longitudinal springs.

Table 3.5: Longitudinal springs stiffnesses, nominal lengths and preloads

ID	Nominal length (m)	Stiffness (N/m)	Preload force (N)
Spring_ant_left	0.355	$2 * 10^5$	-1196
Spring_post_left	0.355	$2 * 10^5$	-1079
Spring_ant_right	0.355	$2 * 10^5$	-1196
Spring_post_right	0.355	$2 * 10^5$	-1079

3.7.5 Configuration 1

To obtain a configuration that can then actually be constructed, the upper springs have been fixed at the ends by means of rubber elements with a certain stiffness to the rotation α (around $x - axis$) and β (around $y - axis$) as shown in Figure 3.29. The rotation around $z - axis$ must be guaranteed as otherwise it would not be possible to make a curve, but the central module would tend to remain rigidly connected to the surrounding modules.

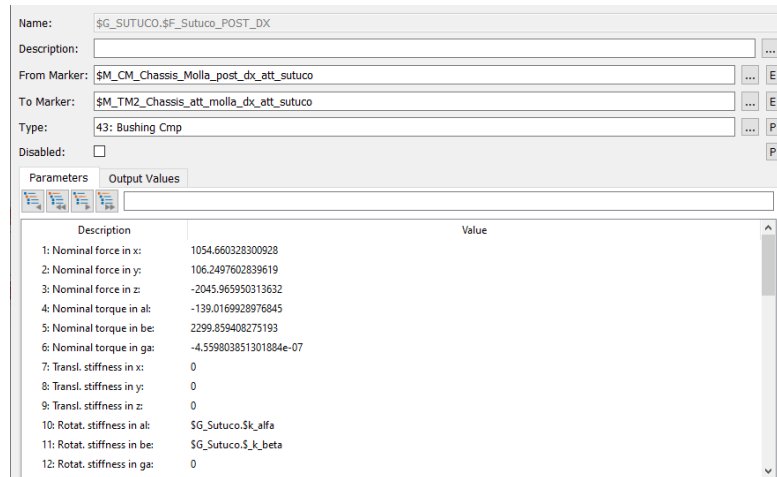


Figure 3.29: Silent block definition in Simpack

The sutuco or silent block has been inserted in the middle of each longitudinal spring in Figure 3.30, so that the stiffnesses obtained are equivalent stiffnesses; this is because the sutuco will be present at the ends of the spring and will connect the spring to the considered module (CM, TM or TrM). As you can see in Figure 3.29 in fields 4 and 5, also in this case the preload values have been entered, as mentioned several times, the explanation of how it works will be proposed later.

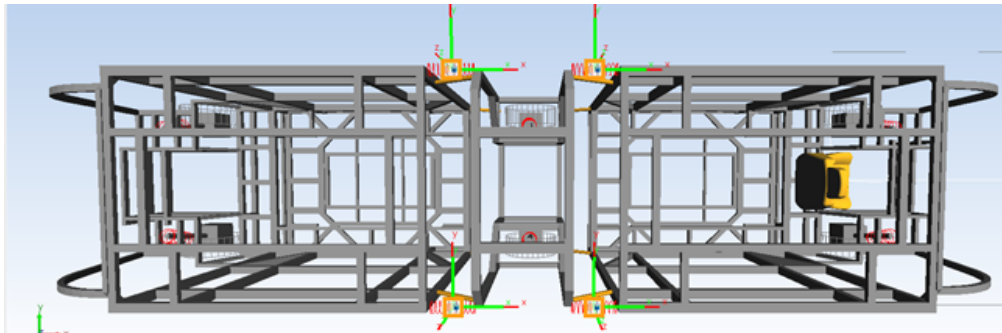


Figure 3.30: Silent block location

The "sutuco" or "silent block" is essentially an anti-vibration element consisting of a part in vulcanized elastomeric material between two metal pipes. Thanks to the rubber, this element acts as a vibration absorber, which in addition to imposing a certain stiffness due to the rubber allows for a higher level of comfort. In this paragraph it will only be explained how this element was simulated, subsequently the value will be derived through tests.

The sutuco was simulated by using two coincident markers, one belonging to the CM while the other belonging to the TM or TrM, the coordinates are visible in Table 3.6.

Table 3.6: Silent block Markers location

ID	x(m)	y(m)	z(m)
Sutuco_post_right	-4.6805	-0.96	2.66688
Sutuco_ant_left	-3.5355	0.96	2.66688
Sutuco_post_right	-3.5355	-0.96	2.66688
Sutuco_post_left	-4.6805	0.96	2.66688

Table 3.6 shows the position in which the silent blocks were simulated, the positions were obtained from the drawing, as mean value of the longitudinal position of the upper springs.

3.7.6 Configuration 2

Both for configuration 1 and configuration 2, the stiffness elements that have been inserted are necessary to guarantee the correct dynamics to the vehicle as they impose a certain rolling stiffness, so without these elements, the central module would tend to be in equilibrium in an improper position, this is mainly due to inertia, so a small variation is enough to change the position of the CM definitively; being the mechanical joint designed to prevent only the translational degrees of freedom.

To ensure the correct rolling behaviour, a spring element has been inserted in an inclined position with very high stiffness, the configuration is that shown in Figure 3.31. The stiffness value of this element is an optimization parameter through subsequent sensitivity analysis. The inclined springs are connected to the attachment points, therefore to the markers, of the longitudinal springs. As can be seen from the Figure 3.32 a linear PtP spring was chosen as the force element, the distance between the two markers was given as the nominal length, the stiffness was entered as a parametric value for the sensitivity analysis while the preload value it was calculated by the software, as explained later.

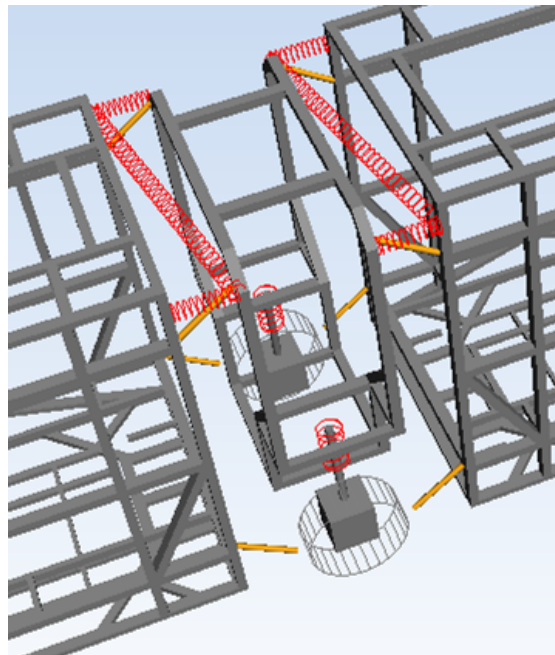


Figure 3.31: Springs - Configuration 2

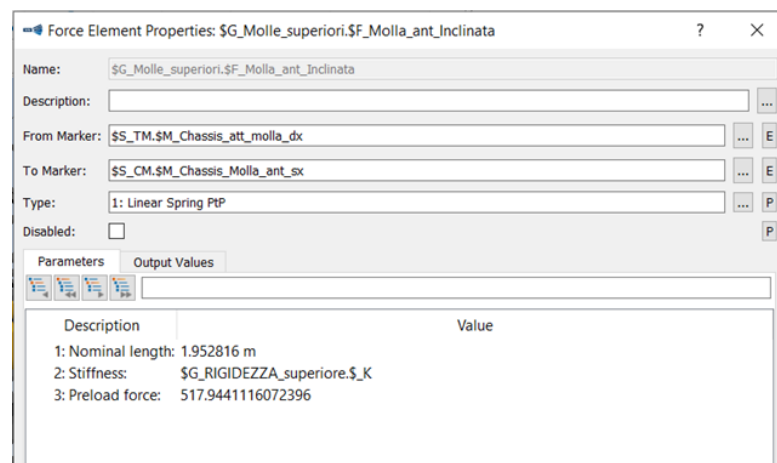


Figure 3.32: Creation in Simpack of the inclined springs elements

This configuration represents only a preliminary analysis of the problem, as it works at the simulation level, but it is very complex to replicate this solution, therefore for the following treatments, especially for the sensitivity analysis, the configuration used is the first.

3.8 Preload

Many Force Elements provide the possibility to define a constant nominal or preload force or torque, which is added to the force or torque from the actual characteristics. The simplest case is a pre-loaded linear spring where :

$$F = kx + F_{preload} \quad (3.11)$$

Preloads are most often used to resemble a pre-stressing of a spring due to the gravity. This is particularly interesting if the spring's initial (unstretched) length is unknown in early development stages, or if the user intends to vary the spring stiffness while keeping the geometric state of the model. The user can specify these preloads directly in the element parameters. The Preload solver calculates the preloads automatically so that the model is in equilibrium, i.e., the residual accelerations become zero or at least very small. The automatic solution is helpful or even indispensable for complex models with many preloads in different directions where a manual calculation is difficult or impossible [26]. To carry out the preload in Simpack, the initial speed V_0 must be zero and there must be no force elements applied to the body. As for the tire module, not all the packages present within the software allow to coexist with the preload command, in fact, the one used for this report does not allow it; in this regard, a different path was followed to be able to use the automatic calculation. This is both because it is useful to understand how to use the preload command in the automotive field, and to be able to deal with even the most complicated models, because carrying out the calculations by hand is very long and complex. Since the tire module used is the problematic regarding preload, constraints have been used to perform it; to do this, a marker has been created belonging to the wheel in the contact position between the wheel and the ground. At this point, we have made the connection Figure 3.33, as marker From we used M_Isys (the absolute reference system) while as To marker M_Ruota the new marker created. This was done for all wheels.

"User Defined" was used as a type of constraint, which allows the user which degrees of freedom to block and which to keep free. In this regard, Table 3.7 will be inserted below to explain how the d.o.f. were chosen.

At this point, all the forces and torques applied to the element are disabled, the initial speed is set to zero and the preload is performed Figure 3.34.

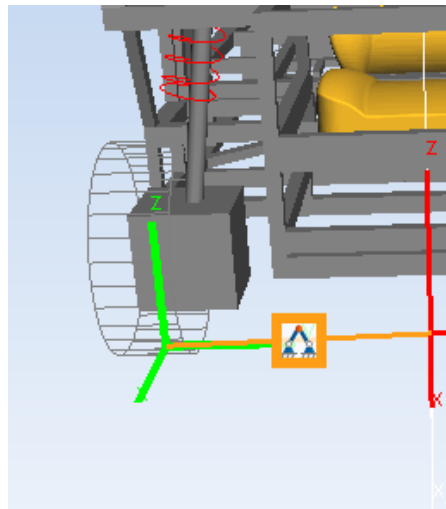


Figure 3.33: Constraint used to lock the wheel

Table 3.7: Free and locked d.o.f. constraint in order to perform preload

Module	Wheel	α	β	γ	x	y	z
DM	Sx	free	locked	free	free	free	locked
	Dx	free	locked	free	free	free	locked
CM	Sx	free	locked	locked	free	free	locked
	Dx	free	locked	free	free	free	locked
DM2	Sx	locked	locked	free	free	free	locked
	Dx	free	locked	locked	free	free	locked

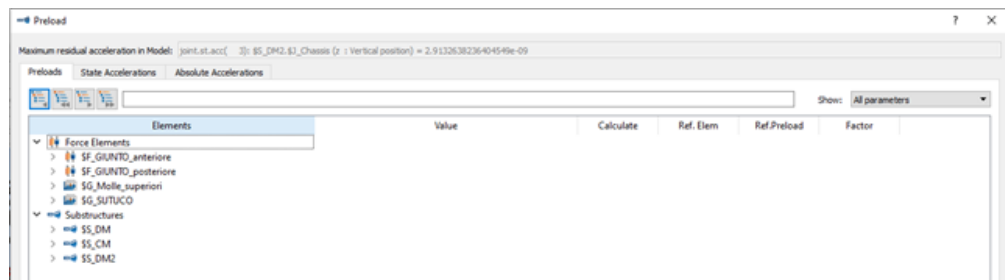


Figure 3.34: Preload calculation

As can be seen from Figure 3.34 the preload was carried out on the two joints, one front and the other rear, on the upper longitudinal springs, on the bushing element representing the sutuco and finally on the suspensions, which are contained in the substructures. As you can see, the residual acceleration is shown at the top, in this case it tends to zero so you can consider the exact calculation, if it were

on the unit the preload would be wrong and the software would have declared a warning.

3.9 Steering system

To simulate the steering, a simplified way was followed that allows recreating the functionality of the latter without studying all the details present in the reality but still reliable as regards the study of vehicle dynamics and especially for the correct choice of parameters of the elements to be sized. The concept used is to have a reference marker that follows the track and another belonging to the local reference system of the module on which the steering will be applied. During the motion, the two markers will deviate generating an angle; the goal is that the vehicle follows the track correctly, therefore, that the range of the angle is as low as possible, which is why torque is applied to the steering axis via a control element. This element also allows you to simulate the advance or delay in the steering of the vehicle. Using this approach, the reference marker does not follow the track perfectly but follows the trajectory due precisely to the delay or advance in the steering Figure 3.35.

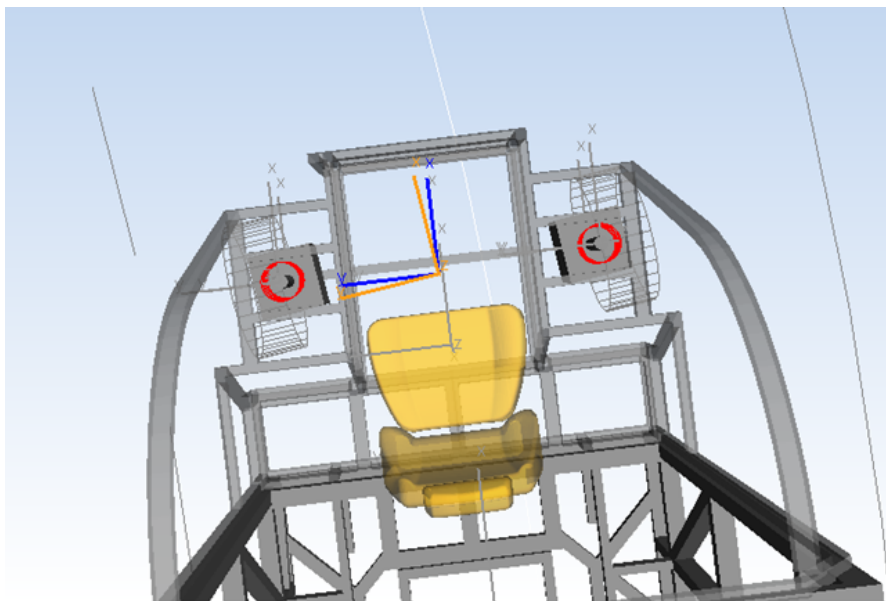


Figure 3.35: Steering marker

Two new markers belonging to the driving module chassis have been created for this model; one called `$M_Chassis` coinciding with the BRF while the other called `$M_Chassis_Steering` which is the reference marker. Four elements were used to create the steering:

- Sensor
- Controller
- Marker
- Constraint

The sensor used is called “Automotive Track Sensor”; this sensor element measures kinematic road vehicle measurements as input to the control loop pipeline. The parameters used for this sensor are depicted in Figure 3.36.

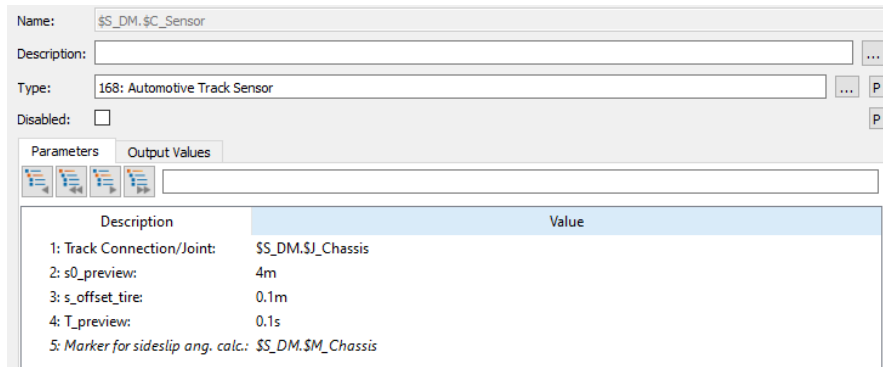


Figure 3.36: Steering Sensor definition

The first parameter is necessary as it allows to obtain the position of the Joint in the s direction, the fourth represents a useful time factor for the calculation of the second parameter through the relation:

$$s_{preview} = s_{vehicle} + s_{prev} + T_{prev} * \dot{s}_{vehicle} \quad (3.12)$$

The first, second and fourth parameters are useful for determining the steering delay, while the third is a useful parameter to calculate the effective rotation of the steering wheel in the geometric position in which it is placed. The arm of the applied torque is automatically calculated by the software knowing the relative position of the two markers.

The control used is called "Track Controller", this control element is used to control the position and velocity of a vehicle along the track, it operates as a steering controller and uses one input. The output is the steer angle; it is determined by the input to the controller, lateral displacement, via the transfer function 3.13. The input control element is given by the Sensor previously described, while the other parameters are described by the Figure 3.37. Using the Simpack notation the control element is defined as:

$$F(p) = C * \frac{K_p + \frac{K_p}{T_i * p} + K_p * T_d * p}{(1 + T_1 * p) * (1 + T_2 * p)} \quad (3.13)$$

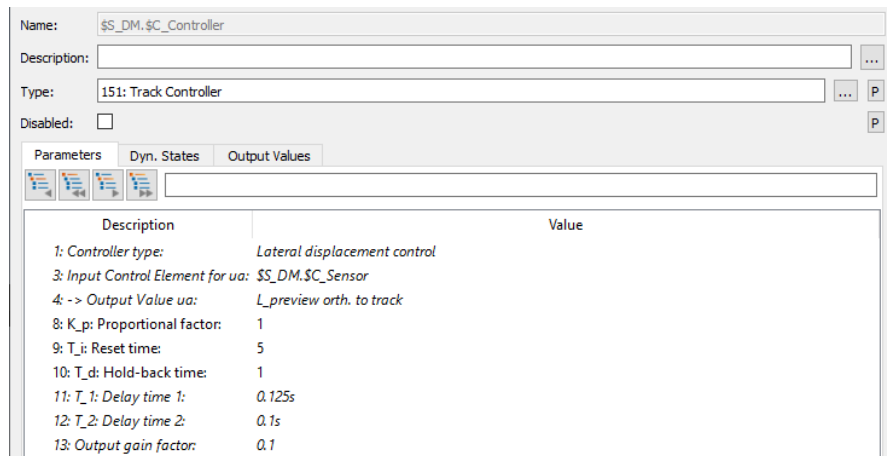


Figure 3.37: Steering Controller definition

where:

$$F(p) = \frac{del(p)}{dy(p)} \quad (3.14)$$

with:

del	steer angle [rad]
dy	lateral displacement [m]
C	Output gain factor

Once the sensor and controller have been defined, you can proceed with the creation of the steering. Initially, the reference marker is defined which, as previously mentioned, was called \$M_Chassis_Steering and is presented in Figure 3.38. From Figure 3.38 it can be seen that the axis around which the rotation takes place is indicated and also the previously defined Control Element is supplied as a parameter from which y is extracted, i.e. the value of the function, then the Steering angle and ua i.e. the current lateral displacement. Up to now, the control elements and the reference marker have been defined, now it is necessary to insert in the model a constraint that allows performing a rotation on the hub of the front wheels, having two degrees of freedom: one of vertical translation and one of rotation around z (the latter allows you to steer). Figure 3.39 shows the left constraint, that is the one that connects the From Marker which is the \$M_Chassis_Steering with the To Marker which is the \$M_Mozzo_sx; the first being the main one, if it rotates, thanks to how the constraint has been defined, the hub also rotates, thus acting as a steering wheel. The same approach by analogy was used for the right side of the front. In Figure 3.39 we can see that the Constraint has been defined by the user by selecting the locked and free degrees of freedom based on what to simulate.

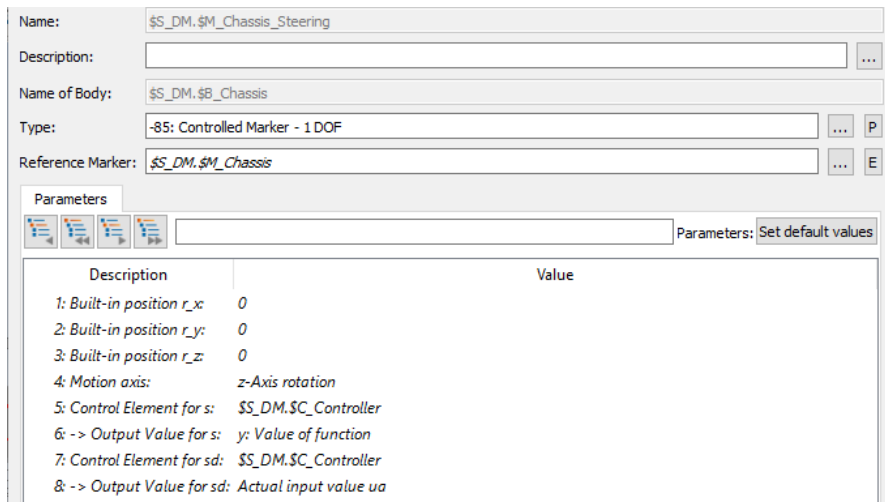


Figure 3.38: Steering marker definition

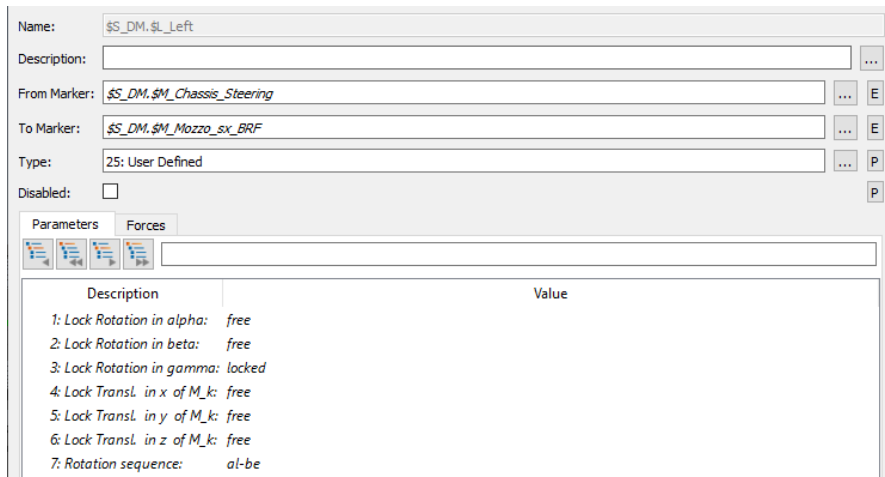


Figure 3.39: Steering Left Constraint definition

3.10 Speed control

To study vehicle dynamics, this paragraph will explain the implementation of a speed profile within the Simpack software. The profile studied is the one represented in Figure 3.40.

This trend is followed thanks to a proportional type of control and is applied through a force element as torque to the wheels. The torque is applied individually to the drive wheels and not directly to the front axle to have them decoupled and allow cornering behaviour in which the wheels have different speeds, which happens

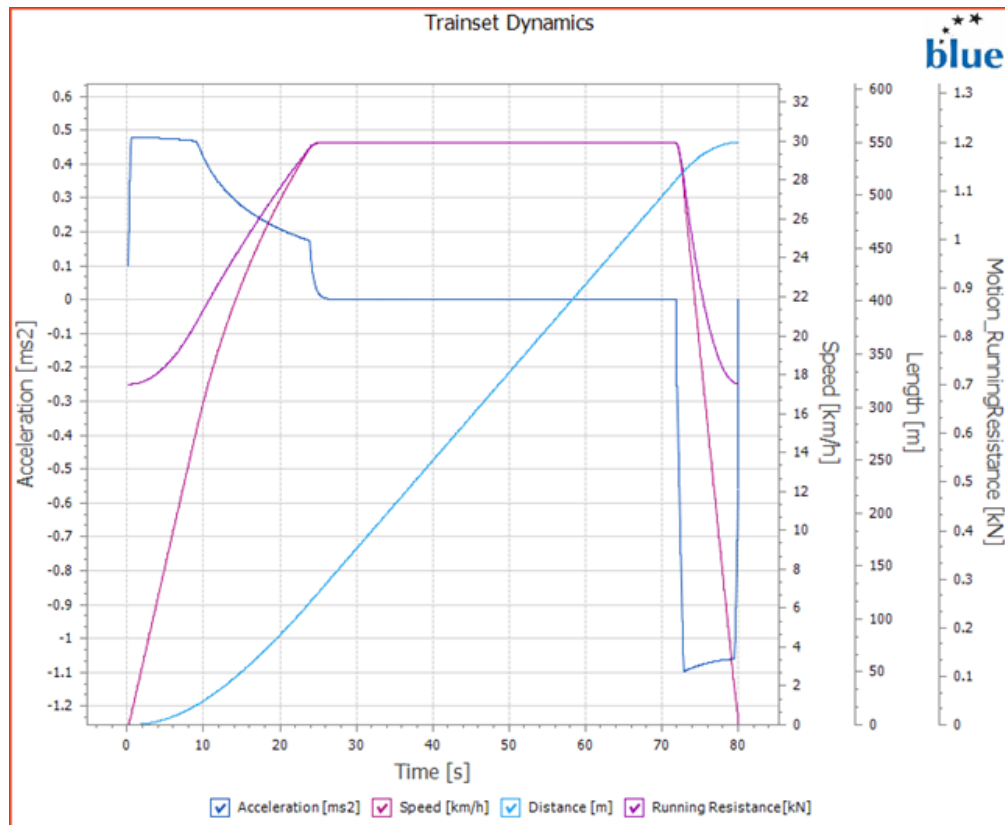


Figure 3.40: Reference transient dynamics

thanks to the use of the differential. The procedure used was to import a text file into the work environment containing the coordinates of the various points that form the trend represented in Figure 3.40 using an input function Figure 3.41. Subsequently, an excitation from the input function was generated, in which the generic function $f(x)$ is expressed as a variable as a function of time $f(t)$ Figure 3.42. An excitation describes a typical time, distance or frequency-dependent function that can be used to excite the mechanical or mechatronic system. The speed profile to follow was given as input, the acceleration is automatically calculated by the software as a time derivative of the speed. Subsequently, a "u-Vector Element" is created using the "create" command at the top right of Figure 3.42. The u-Vector connects excitations to the modelling elements that finally bring the excitations, i.e., the movement or the force or torque, into the model. The name "u-Vector Element" is derived from the fact that these elements can be considered as components of a vector u , which is a commonly used name for input vectors in mechatronic system simulations. This u-vector acts as a reference when calculating the speed error as the difference between the current speed and the target speed.

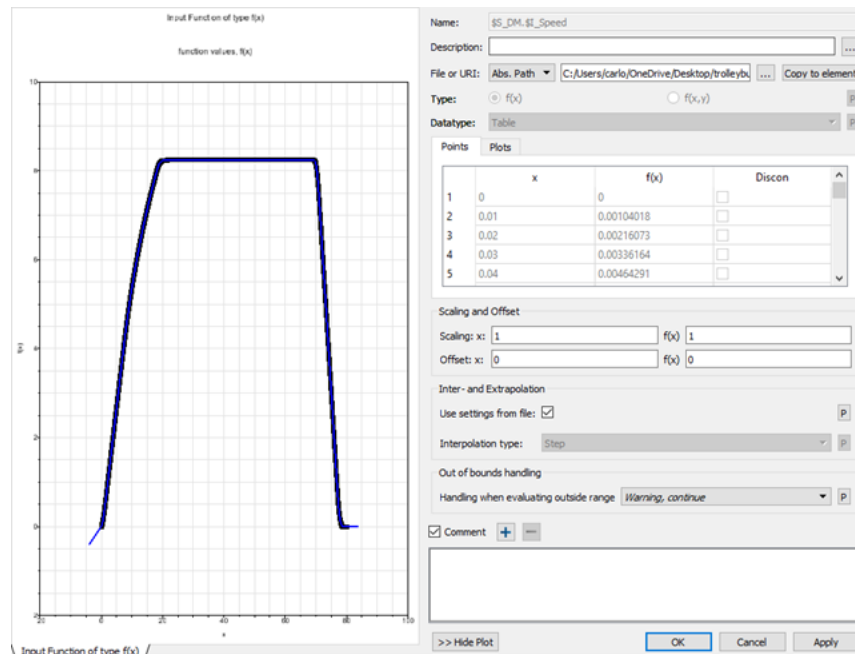


Figure 3.41: Speed profile input function

To perform the correct speed control, "Control Elements" was used, specifically four elements were created:

- Reference speed
- Feedback speed
- Error
- Proportional control

The reference speed is taken from the u-vector previously described and refers to the speed profile that was given in input. The speed (in the longitudinal direction) of feedback is read from the state of the Joint that has been chosen, in this case, the Joint of the DM. The error is calculated simply as the difference between the two previously described speeds. At this point, the type of control is selected, in this case, proportional and the gain is assigned as shown in Figure 3.43, the error is provided as the input value.

Once the type of control has been decided, the next step is to create a force element that allows you to follow the speed profile.

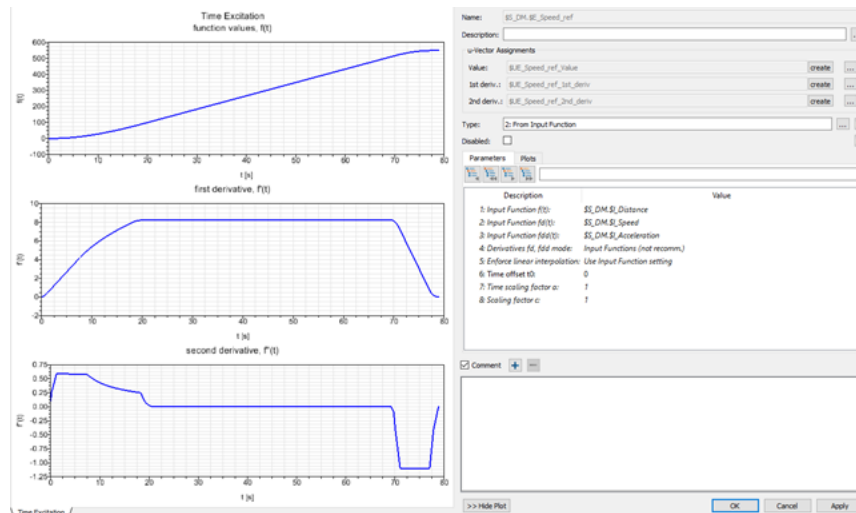


Figure 3.42: Speed profile function of time

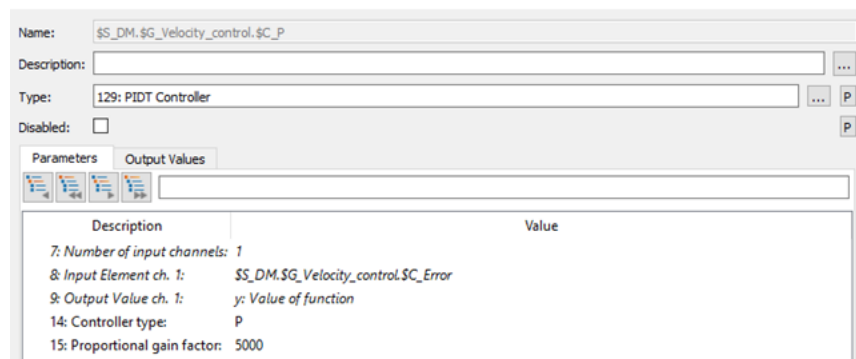


Figure 3.43: Proportional controller

A torque is applied in the BRF of the two-wheel drive separately as they are decoupled. As can be seen in Figure 3.44, the torque has been selected as the force element and the y axis which represents the degree of freedom possessed by the wheel as the application axis. The figure shows the treatment relating to the left wheel, the right wheel has been treated by analogy. The first parameter represents the control element used, while the second parameter concerns the data to be extracted from the first parameter; in this case, it represents the output of the proportional control. In the last field, -1 was put as a negative torque is obtained concerning the inertial reference system and consequently, positive torque is applied to the wheel by action-reaction.

Figure 3.45 shows the trend of the position, speed, and acceleration of the Joint of the DM.

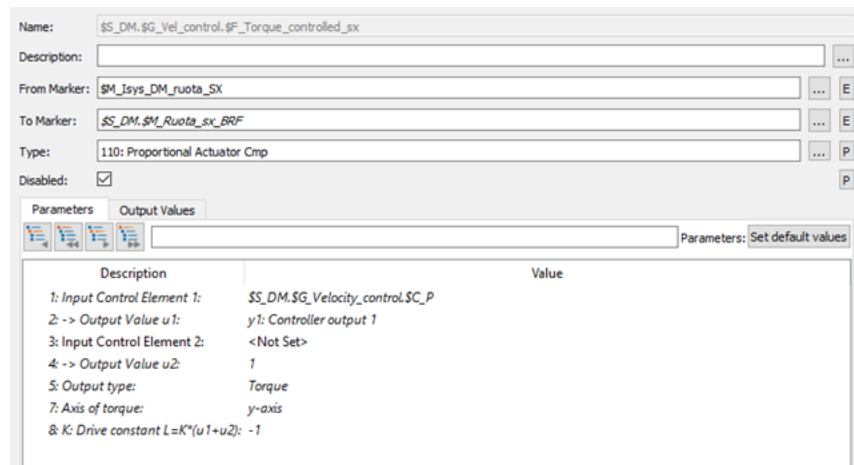


Figure 3.44: Proportional actuator

The trend of the curves faithfully follows the graph given in input; the acceleration presents a very high oscillation initially due solely to the fact that as regards the tire package on Simpack it is not possible to start with zero speed; a very low initial speed was therefore given so as not to affect the desired trend ($v_0 = 0.03 \text{ m/s}$). Since the path in which the test was carried out is straight, the

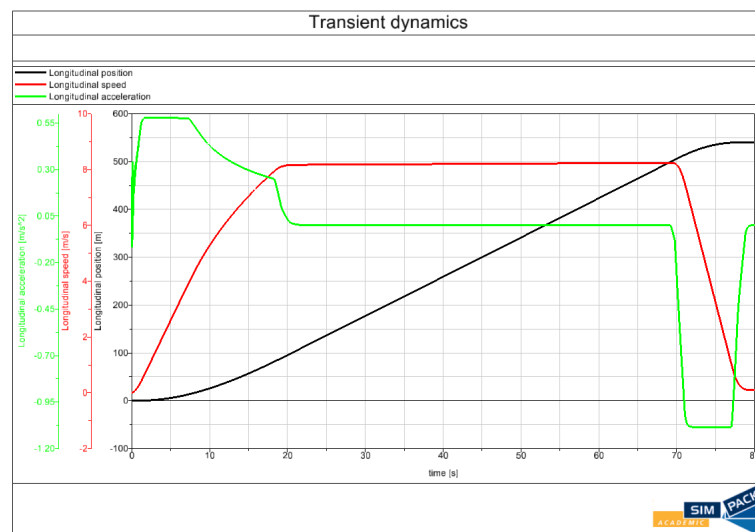


Figure 3.45: Measured vehicle dynamics performance

torque trend follows the one in the figure, if the profile deviates from linearity, the torque trend would change in proportion to the changes in the path.

Chapter 4

Optimisation

In this chapter the connecting elements between the CM and the TM/TrM will be dimensioned, to do this a sensitivity analysis is performed using the Simpack software based on tests built ad hoc for the various connecting elements. The tests are carried out using the paths described in paragraph 2.4. The sensitivity analysis is useful to optimize a certain input value based on the output results, for this work the DOE (Design Of Experiment) interface was used; this environment allows you to set the range of values for the chosen input parameter and the desired results are extracted in terms of graph and value, the latter are obtained using filters that starting from the graph with a trend of the quantity that varies over time they extract the desired value (for example the maximum in absolute value, RMS etc.). In addition to extracting a specific value of the graph considered to make an immediate comparison, the post-processing environment can be used to compare the trend of the graphs of a variable, this happens when it is not useful to extract a single value, but it is necessary to know the trend as, for example, comparing the trajectory to the variation of the longitudinal stiffnesses. The difference between extracting a specific value and plotting the results is that the former, thanks to the Simpack post-processing environment, allows to obtain all the required result combinations as the software estimates the result based on the analyses carried out with a certain level of probability; the latter instead allows only to plot the trends of the simulated configurations.

The goal of this paragraph is to determine the best position and value of dampers, longitudinal springs, and silent block and then subsequently, using this configuration, perform the sizing of the two connection joints, respectively the front and rear one. From the joint definition, i.e., ensuring rotations around the three axes, an element is needed that controls these degrees of freedom. Initially the joint was designed so that only pitch and yaw were allowed, in this way, however, having infinite rolling stiffness, any excitement of this type could break the connecting element, so it was decided to continue the treatment using a spherical joint. The

elements that control the various degrees of freedom are those previously defined, in detail, the longitudinal springs have the primary task of conferring the correct dynamics in the curve by controlling the rotation around z in addition to the translation in x . Being defined as PtP, as already mentioned in paragraph 3.7.4, despite for how they have been built they do not have an arm to compensate for the rotational degree of freedom around z , during the curve the vehicle settles in in such a way that the two markers of the spring (From and To), arranges generating an angle (as in Figure 4.1) so that they impose a stiffness. In addition, the spring elements also allow you to control pitch as they are defined. The silent block elements, on the other hand, are simulated to obtain rolling and pitching stiffness. The dampers are defined in such a way as to perform an action for all six degrees of freedom of the vehicle being inclined in the $y - x$ and $z - x$ planes thanks to angles α and β .

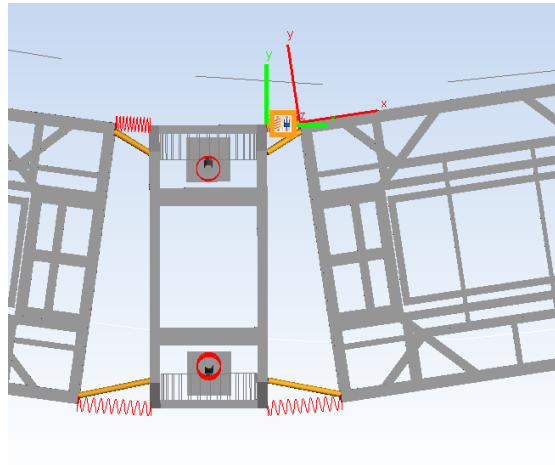


Figure 4.1: Longitudinal springs top view

The optimization was performed on the output results, based on the specific element on which the reference results were chosen on the correct choice of the parameters of the connecting elements. The tests used are:

- Longitudinal springs in Castelfidardo roundabout
- Silentblock in a double curve
- Silenblock in a vertical slope
- Lateral excitation on a straight road

To analyze the influence of the different variables on the chosen output, the Simpack DoE interface is used which allows analyzing the influence on the output

values of the values supplied in input in the sensitivity analysis. In this part, we will explain how it works so that you can understand how to interpret the results.

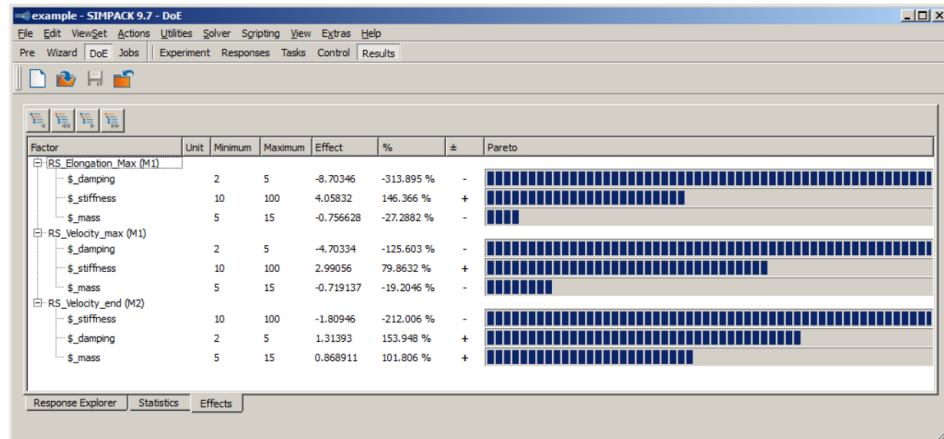


Figure 4.2: Sensitivity analysis post-processing

Figure 4.2 shows the sensitivity analysis in the Simpack environment, in detail the effect of the various input data on the output values is represented. The first column represents the extracted result (the prefix RS_ represents the DoE response) and the subproducts represent the chosen Subvar that play the role of DoE input data, these are made to vary from a maximum value to a minimum value, represented respectively by the column four and three. The effect (column five) is the variation of the output value from the minimum value to the maximum value of the Subvar considered, with all other variables kept constant. A positive effect means that the result increases passing from the minimum to the maximum value of the data considered. Column six represents the relative effect. This is the absolute effect related to the respective nominal (not original) factor value, i.e., to the mean of their minimum and maximum value. thus, the relative effects strongly depend on their nominal factor values, which might be surprising when comparing the effects of different factors directly. While the last column considers the (relative) size of the effect shown as the Pareto bar. Later, it will be explained in detail how the parametric analysis takes place within the Simpack software via the DOE interface.

4.1 DoE in Simpack

This paragraph will describe in detail the creation of a new space to carry out a sensitivity analysis in a multibody environment. First of all, starting from the model from which you want to carry out the analysis, you go from the Pre

environment to the DoE environment and clicking the icon with the white sheet of paper creates a new file with the ".doespck" extension. When creating a new file, the "DoE configuration" must be specified, which represents the name of the file we want to create, in this case, a folder is chosen to save the file. At this point it is necessary to specify the "DoE directory", it represents the folder in which all the simulations that are carried out in this environment are saved, for this reason, a new folder is created; usually, the folder is created within the same path in which the file with the ".doespck" extension is present, in order not to generate confusion. At this point, it is possible to set the sensitivity analysis. Figure 4.3 represents the workspace, this figure represents the "Experiment" in which the experiment is set up; it is composed on the left of the "Target models" which are the models from which we start to carry out the simulations, sometimes several models may be required in parallel to carry out the analyzes; for example, referring to this thesis, it may be useful to set two models in parallel representing two different paths at different speeds and to vary the same variables in parallel during the analysis for a more detailed study of the problem. On the right, all the SubVars have been created within the model and they are the basis for this type of analysis, in fact by performing a drag and drop they can be inserted into the "Factors" window and can decide how to change the parameter within the simulation.

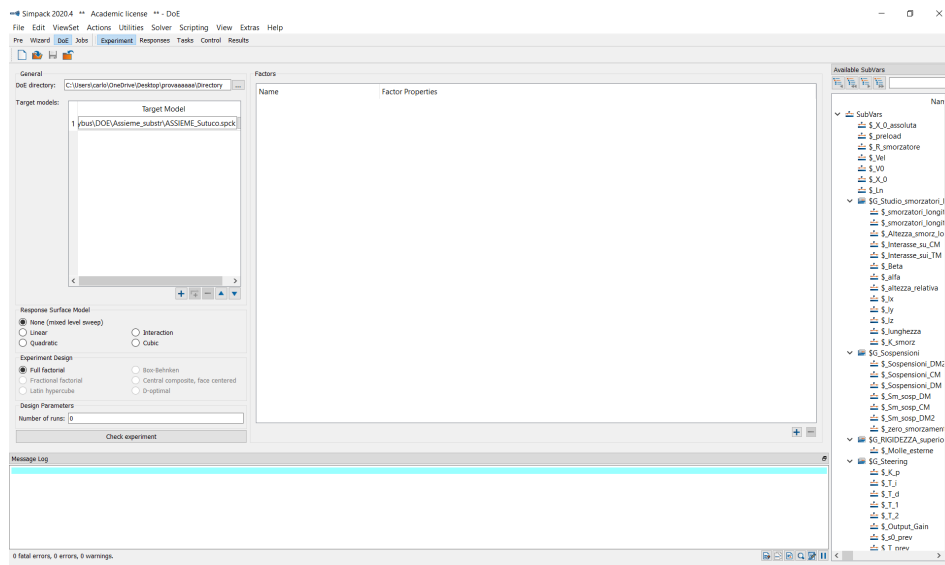


Figure 4.3: Experiment workspace

The Figure 4.4 shows how it is possible to vary the factor considered. It is possible to set a variety of parameters from a minimum value to a maximum value, useful for the analysis of the influence of the variables in which the software based on the number of simulations, makes the value vary within the desired

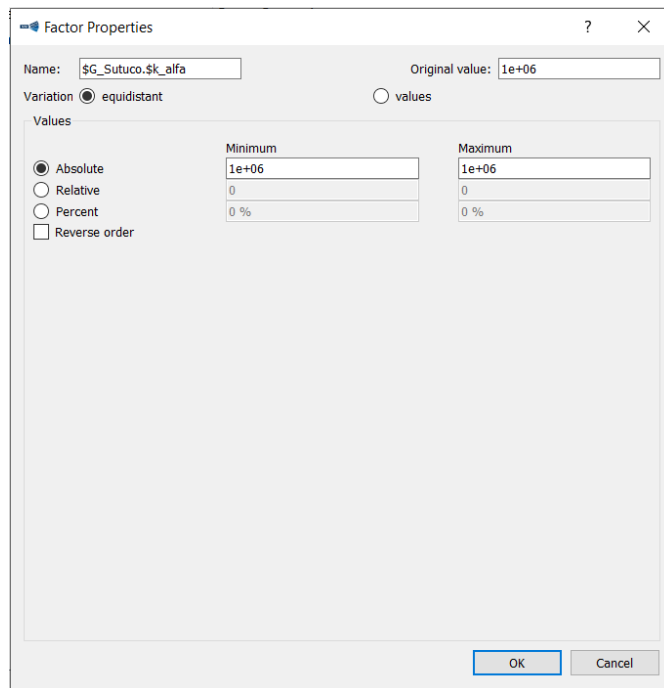


Figure 4.4: Input values properties

range through an equidistant variation or employing manually set values. The equidistant variation can be set following a range of absolute, relative or percentage values based on what is selected. In Figure 4.3 at the bottom left there is the part relating to "Experiment Design and Response Surface" in which you set the type of interaction between the various factors and the number of simulations thanks to the "Number of runs" part. At this point you can move on to define the "Responses" section in which the desired results are extracted from the simulation in the form of values, sometimes this is not possible and therefore this part is not compiled (when it is not necessary to compare the single value, but it is useful to compare the trend in the form of a graph). This section uses the parameters that are created in the pre-processing environment directly on the model. To extract a result, it is necessary to define (in the main model) the output to be extracted in the form of a graph thanks to the "Result Elements" and through a filter, you will find a value that is used to be compared in the different simulations. This treatment is the same that is carried out within the post-processing, to extract the classic results present in this environment, a result element is created in the model (pre-processing) and the type is set to "General", at this point based on the number of outputs to be extracted, enter the number in "Number of Result channel" as you can see in Figure 4.5. Once the output element has been created, a filter is performed which is useful for extracting a value to be compared. To do this, always

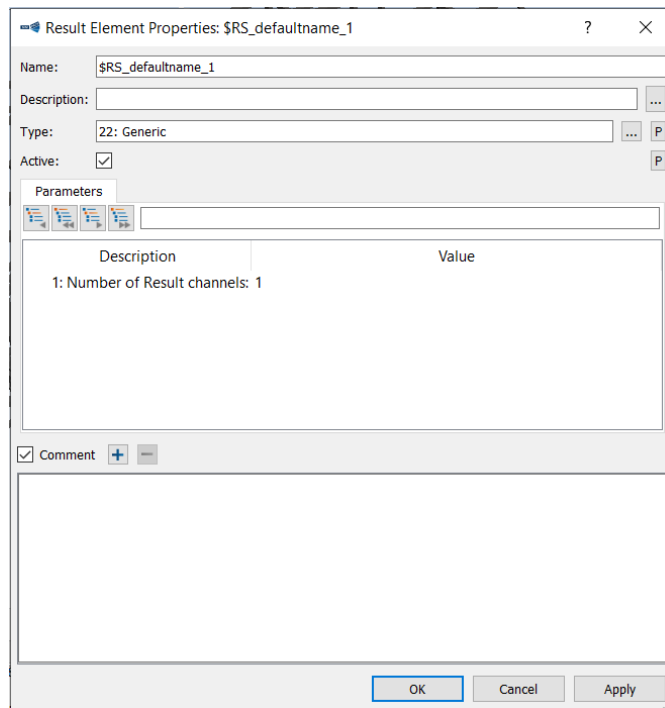


Figure 4.5: Result Element Properties

in the main model, the "Create Filter" command is executed, and this element is the same as inserting the filters into the post-processing, an example of a filter is the absolute maximum value of a function. Once these two elements (Result Element and filters) have been done, a new element is created in the "Responses" section in the DoE environment, the result element and the filter are inserted as shown in Figure 4.6, they are inserted again thanks to a "drag and drop". If there are more target models, select the desired one and set the DoE Response to it.

Once you have entered several adequate responses for the simulation, you go to the Task section, in this sub-ViewSet the user defines the different solvers and the related activities that will be performed on the target models during each execution. These activities perform the various simulation phases and generate the required responses and/or other results. The single DOE jobs execute, for the different target models according to their order in the experiment section table, the tasks in the specified sequence. For this thesis, the activities illustrated in Figure 4.7 were mainly used; time integration represents the resolution of the model, like what happens in the pre-processing environment for solving the model. The second means that the DoE response is measured that the results that have been set in the previous section are measured and in addition to these all-other responses are also calculated as in the target model, another option is to measure only what is

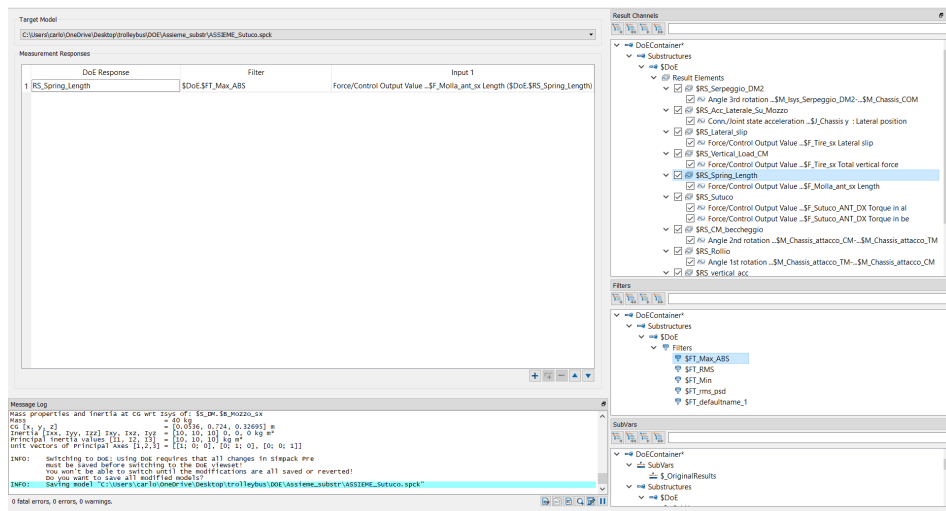


Figure 4.6: Responses workspace

extracted from DoE, significantly reducing calculation times.

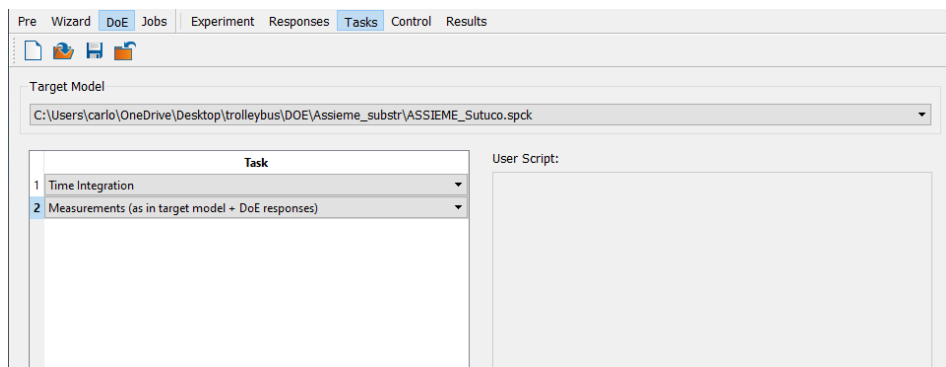


Figure 4.7: Tasks workspace

At this point in the "Control" section, it is possible to start the simulation, it will be performed according to the interaction model between the various SubVars set in the Experiment section. Once the simulation is finished, it is possible to analyse the results by evaluating the response (extracted values), the statistics that is the reliability of a combination of input data that is obtained by interpolating the outputs and finally analysing the effects of the individual input data on the output results as described in Figure 4.2.

4.2 Longitudinal springs

The choice of the stiffness parameter for the longitudinal springs is the first to be made as it influences the other elements to be optimized, consequently it is chosen as the main element; in particular, it influences the pitch, therefore it interacts with the stiffness value of the silent block. So the spring is first optimized in a flat track (without cant and vertical slope) where neither pitch nor roll is present and then the elements of the silent block are sized. In this way the stiffness of the latter with respect to pitch will be optimized starting from the longitudinal spring element already fixed and adapting to it the stiffness of the silent block. Longitudinal springs are fundamental because they keep the CM in the correct position while driving, moreover they are necessary when the vehicle is cornering because the higher the stiffness the more the vehicle tends to behave as a single body; therefore it is not correct to impose a too high stiffness value because the shortening of the springs allows a correct dynamic while cornering because only the DM has steering wheels; the configuration obtained thanks to the springs allows not to have a too high lateral slip and to correctly execute the corner. So the stiffness has been optimized according to different specifications, the lateral slip has been analyzed first because a wrong stiffness value (too high) leads the central module to translate almost rigidly in the curve, on the other hand a too low stiffness value can lead the surrounding modules to collide with each other or even to "crumple" during the steering operations. The stiffness value has been optimized for the Castelfidardo traffic circle, which represents the worst condition for this type of element since the lower radius of curvature that the vehicle has to make is very small (13 m), therefore it can be considered a reliable result. For this test, the track used does not have a cant, so the stiffness values of the silent block do not affect the test if a roll stiffness value is set such that the vehicle settlement is correct and a high roll angle is formed. The values used for the Subvar connection are given in the table 4.1. The stiffness of the spring was made to vary as shown in the Table 4.2: The

Table 4.1: Connection Subvars used to optimize longitudinal springs

SubVars	Value	U.M.
Silentblock		
$\$_k_alfa$	1.00E+06	Nm/rad
$\$_k_beta$	1.00E+06	Nm/rad
Longitudinal Dampers		
$\$_Longitudinal_Dampers_Lower$	5000	Ns/m
$\$_Longitudinal_Dampers_Upper$	5000	Ns/m
$\$_Alfa$	0.35	rad
$\$_Beta$	0.35	rad

Table 4.2: Variation of longitudinal springs stiffness for the analysis

\$G_Longitudinal_Springs.\\$_Value	U.M.
2.00E+04	N/m
4.00E+04	N/m
6.00E+04	N/m
8.00E+04	N/m
2.00E+05	N/m
4.00E+05	N/m
6.00E+05	N/m
8.00E+05	N/m
2.00E+06	N/m
4.00E+06	N/m

same stiffness value was applied to each longitudinal spring so that it behaves the same whether the vehicle is cornering to the right or the left. From the simulation performed it was noted that the first two stiffness values are too small, at this point the third is chosen as the optimum stiffness value following the order of Table 4.2. The value was chosen as a reduced stiffness value leads to great benefits in terms of lateral slip and curve trajectory. As a demonstration, a comparison is inserted on the various output values between the chosen value ($6.00E + 04 N/m$) and the maximum value shown in the Table ($4.00E + 06 N/m$). From Figure 4.8 it can be seen that a very high stiffness value leads (as can be seen in the graph at the top right) to have a rigid connection between the various modules and this leads as a direct consequence to having a very high lateral slip (graph top left) since the CM translates stiffly when cornering, this also leads to an incorrect trajectory of the vehicle as you can see from the graph at the bottom right. As for the yaw angle (bottom left) for the higher stiffness value, the same trend will be obtained for all modules as, as mentioned, the vehicle tends to behave as a single body, while for the lower value you will have the same curve, with different amplitudes out of phase in time, as it should be; the yaw angle is calculated by the software concerning the s coordinate of the path. It is noted that the first two values of Table 4.1 lead to errors in the integration, which means that the stiffness is too low. For this reason, you can choose the value of $6.00E + 04 N/m$ but as you can see from the length of the spring it is still possible to reduce the stiffness, for this reason, the value of $5.00E + 04 N/m$ is used which represents the minimum value limit of possible stiffness for longitudinal springs.

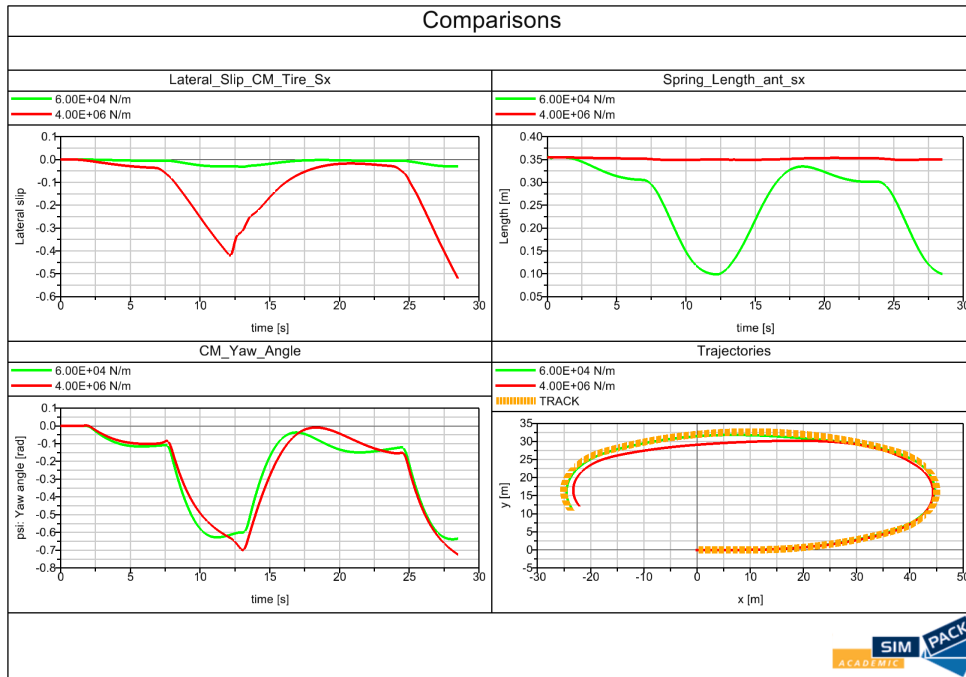


Figure 4.8: Post-processing comparisons by varying stiffnesses

4.3 Silent block

The silent block is fundamental to give the vehicle the correct dynamics as it is the only linking element that imposes a roll stiffness, this is of fundamental importance especially to obtain a correct configuration while driving, going to compensate for the adjustment phases that would occur without it. For this reason, the track along which the vehicle is simulated for this element has a superelevation to optimize the rolling stiffness, so a test is performed on a track with a certain vertical slope, in detail the track changes from z null coordinate to an increasing coordinate in space with a certain percentage of inclination to optimize the pitch stiffness.

4.3.1 Rolling stiffness

For this discussion, the element will be mainly sized to optimize the maximum percentage load acting on the wheel during the curve (not exceeding the maximum value of 60%). It is calculated using the following relationship:

$$\frac{Q - Q_0}{Q_0} \tag{4.1}$$

90

Where Q is the maximum load of the wheel when cornering (or minimum according to the wheel being considered), while Q_0 represents the load along the straight. Furthermore, in the choice of the optimal configuration, the lateral slip and the length of the spring were also used in the comparison, since in the case of superelevation the stiffness value influences the roll, a comparison of the roll angle relative to the DM2 module is presented. be the one most affected. The same treatment was carried out for the track with vertical slope by evaluating the influence of the pitching stiffness. The test is carried out in the double curve track, explained in paragraph 2.4 at a constant speed of 15 m/s . In this case only a variation of the stiffness around α is considered as in this test the pitch is not excited. For this reason, since there is only one free parameter to be optimized, it makes no sense to make a comparison as in Figure 4.2. The values of the connection Subvar in this test have been reported in the Table 4.3. Furthermore, the variation

Table 4.3: Subvars used for the analysis

SubVars	Value	U.M.
Longitudinal Springs		
$\$_{Molle_esterne}$	5.00E+04	N/m
Silentblock		
$\$_{k_beta}$	2.50E+05	Nm/rad
Longitudinal Dampers		
$\$_{Longitudinal_Dampers_Lower}$	5000	Ns/m
$\$_{Longitudinal_Dampers_Upper}$	5000	Ns/m
$\$_{Alfa}$	0.35	rad
$\$_{Beta}$	0.35	rad

of the free parameter has been reported in Table 4.4. The graphs are shown below

Table 4.4: Variation of the parameter $\$_{k_alfa}$ for the optimization analysis

$\$_{k_alfa}$	U.M.
1.00E+04	Nm/rad
2.50E+04	Nm/rad
5.00E+04	Nm/rad
7.50E+04	Nm/rad
1.00E+05	Nm/rad
2.50E+05	Nm/rad
5.00E+05	Nm/rad
7.50E+05	Nm/rad
1.00E+06	Nm/rad
2.50E+06	Nm/rad

to determine the correct stiffness value since for the results useful for this treatment (first the percentage of load that weighs on the wheel) it is not possible to extract a single parameter for comparison. A wide variation of the free parameter was carried out to identify within which range of values the optimal one was contained. In the following graphs, the two threshold values regarding the stiffness of the silent block have been highlighted (greater line thickness). Figure 4.9 shows the vertical load on the left wheel, it can be seen from the graph that for stiffnesses lower than $1.00E+05 \text{ Nm/rad}$ the value is too small and there are very high oscillations even as shown note from the roll angle Figure.

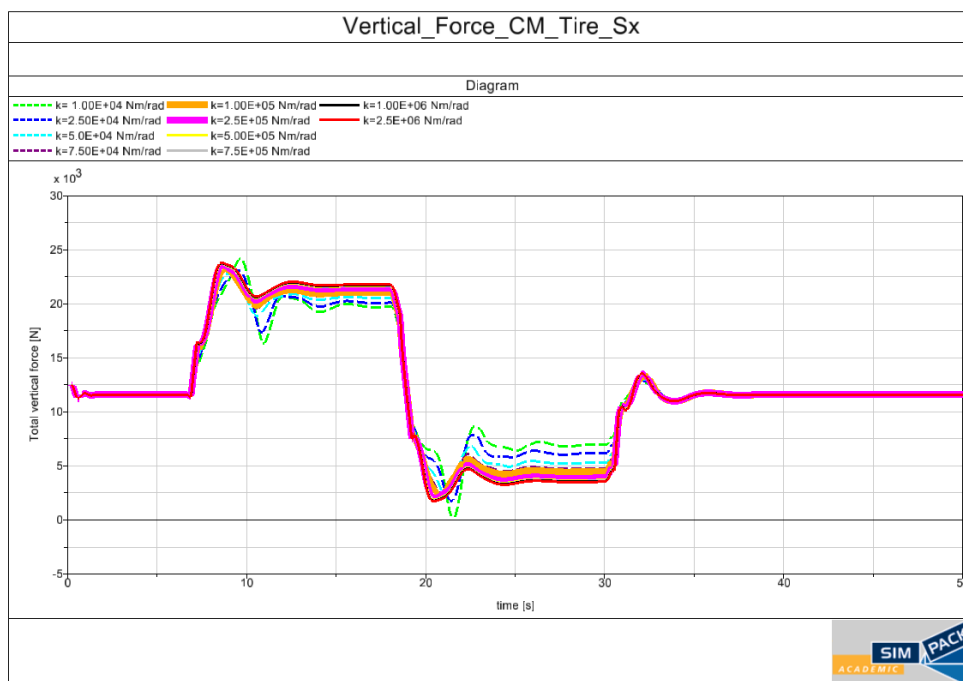


Figure 4.9: Vertical force on the wheel as the stiffness varies

From Figure 4.9 it can be seen that for a stiffness greater than $2.50E+05 \text{ Nm/rad}$ the trend of the characteristic does not vary too much, for a correct choice of the parameter, therefore, it is also necessary to graph the trend of rolling angle as the time changes. It is also noted from this graph that the trend of the vertical load grows and reaches a peak and then stabilizes, this represents the step that goes from zero superelevation to the maximum one. Precisely for this reason, low stiffness leads to oscillations around the equilibrium value, however, leading to a very high acceleration in the body. From the graph of Figure 4.10 it is possible to better understand which are the correct values for the determination of the optimal stiffness, in detail, the two threshold characteristics have been highlighted

(through a greater line width). In fact, a value lower than $1.00E + 05 Nm/rad$ (dotted lines) leads to oscillations in the curve, for this reason, all values lower than the one considered are discarded, on the other hand, a value higher than $2.50E + 05 Nm/rad$ does not influence the trend of the graph. Based on these configurations, a stiffness value of $1.00E + 06 Nm/rad$ was chosen, above all since in the Castelfidardo roundabout track, when cornering, the element tends to have a roll angle that influences the stiffness value of the longitudinal springs. For this reason, it was decided to proceed with the preliminary choice made in the optimization of the longitudinal elements, in this way the vehicle dynamics will be correct.

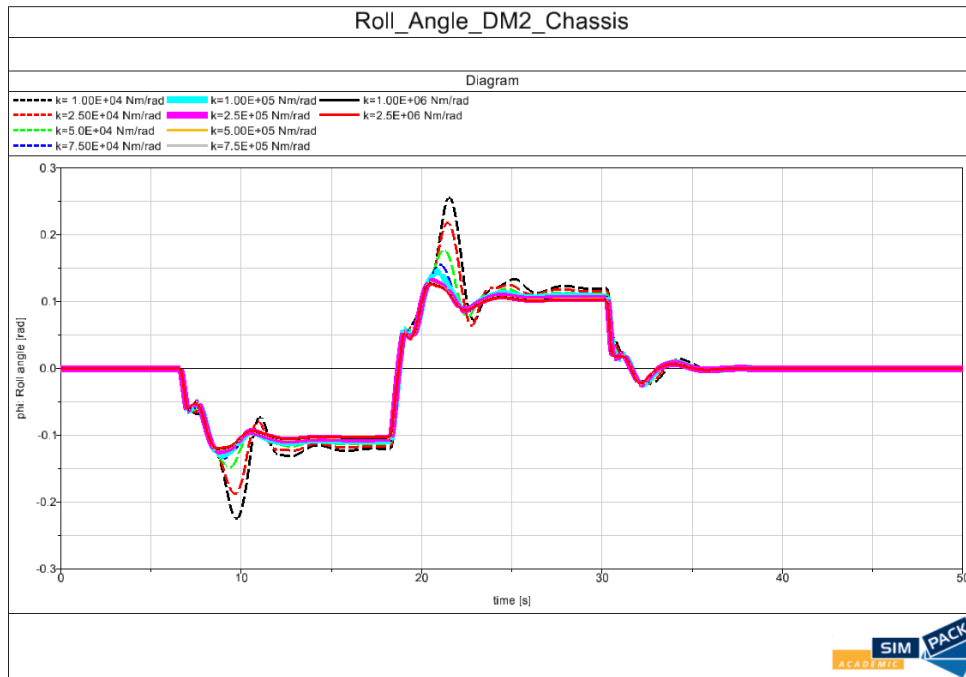


Figure 4.10: Roll angle as the stiffness varies

To validate the choice, the comparison of the stiffnesses is also included as regards the lateral slip and the length of the spring (the left front spring has been chosen), the graphs are shown in Figure 4.11. For this approach, a trend of the input parameters was used such that it was possible to identify a range of values within which to perform another sensitivity analysis, it can be said that this method is a kind of convergence to the optimal result, in this the value entered in the first operation to determine the optimal configuration was deemed sufficient. From Figure 4.11 it can be seen that the above considerations are also valid for these quantities.

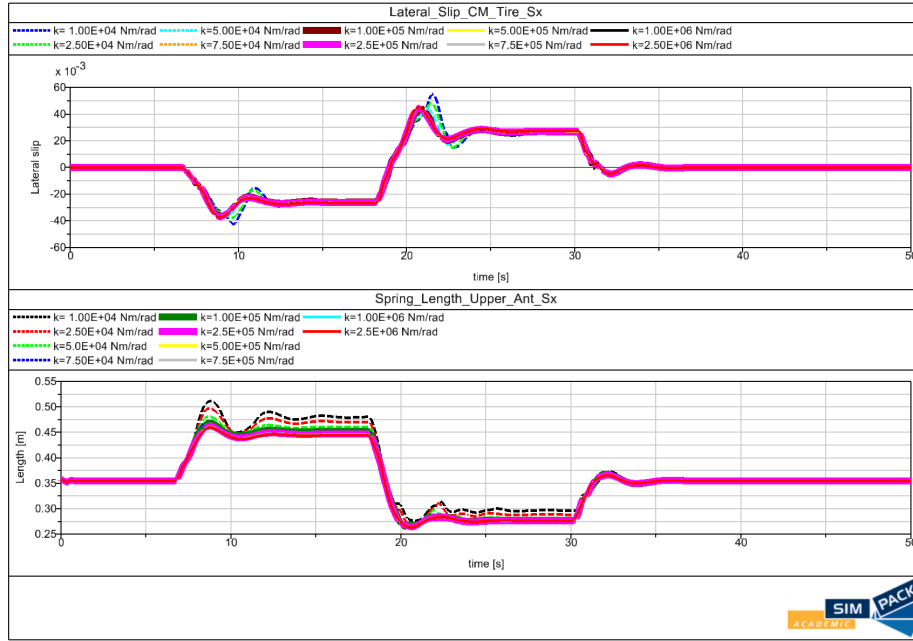


Figure 4.11: Lateral slip and spring length as the stiffness varies

4.3.2 Pitch stiffness

To optimize the silent block element in the β direction, a test was performed with a variable slope and making sure that the change in slope was strong, this is described in the paragraph 2.4 where the vertical slope is described. The test is performed on this track at a speed of 15 m/s kept constant along the track. The speed is very high for the type of test performed, but it was used to emphasize the results as the optimization does not have a dependence on speed. As for the data for the tests, the initial ones are kept and the optimized ones are updated, consequently, it turns out that the Subvars used in the connection are the ones described in Table 4.5. As regards the variation of the free parameter, the same as the previously optimized parameter is used, it is shown in Table 4.6; the only difference is relative to the last value, which has been replaced by a very high one, useful for emphasizing the differences. To optimize this element, it was decided to improve the vertical load on the wheels as much as possible, therefore a pitch stiffness value was determined such that the curve was approximately constant. To understand the behaviour of the vehicle on this track, it is useful to compare the results between the smallest and largest stiffness values (the latter practically represents a rigid connection between the parts). In this regard, the study of the load developed on the wheels of the central module is of fundamental importance since it is the most stressed for this characteristic. In detail, a very high stiffness value, as mentioned, tends to behave

Table 4.5: Connection subvar used

SubVars	Value	U.M.
Longitudinal Springs		
$\$_{Molle_esterne}$	5.00E+04	N/m
Silentblock		
$\$_{k_alfa}$	1.00E+06	Nm/rad
Longitudinal Dampers		
$\$_{Longitudinal_Dampers_Lower}$	5000	Ns/m
$\$_{Longitudinal_Dampers_Upper}$	5000	Ns/m
$\$_{Alfa}$	0.35	rad
$\$_{Beta}$	0.35	rad

Table 4.6: Variation of the parameter $\$_{k_beta}$ for the optimization analysis

$\$_{k_beta}$	U.M.
1.00E+04	Nm/rad
2.50E+04	Nm/rad
5.00E+04	Nm/rad
7.50E+04	Nm/rad
1.00E+05	Nm/rad
2.50E+05	Nm/rad
5.00E+05	Nm/rad
7.50E+05	Nm/rad
1.00E+06	Nm/rad
1.00E+10	Nm/rad

rigidly and therefore when the vehicle approaches the clear transition between two different inclinations, the front and rear wheels are in contact with the ground while the central module tends to detach from the ground. Below, an example is reported (Figure 4.12), in which this behaviour has been exaggerated a lot to make the problem understood the CM will never detach from the ground in this type of track. The opposite situation is that with too low stiffness, in this case instead the forces relative to the other modules are discharged on the wheels of the central module, in fact by discharging them, however, the CM will reach a much higher load than the nominal one. These two behaviours can be understood in Figure 4.13. In Figure 4.13 it can be seen that the green curve representing the lowest stiffness value among those considered, in correspondence with the slope change tends to grow a lot, for the above reasons; in contrast, the red curve represents a very high stiffness value which tends to make the vehicle stiff due to the degree of freedom of pitching. The vertical load trends on the DM and DM2 modules are shown below in Figure 4.14. It can be seen from the graphs that for high stiffness

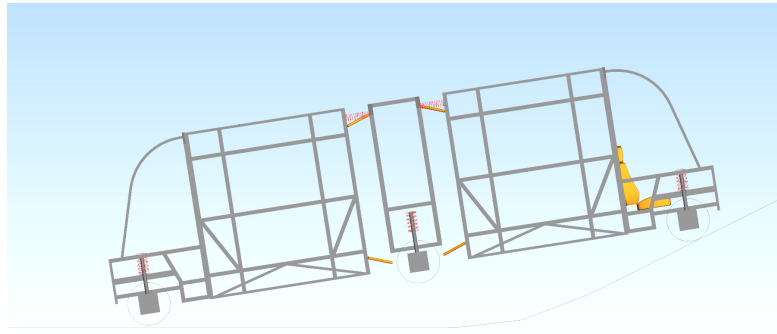


Figure 4.12: Vehicle behaviour approaching vertical slope



Figure 4.13: Influence of the maximum and minimum stiffness parameter on the vertical load (CM)

values the DM2 and DM modules tend to have a higher vertical load as it unloads less on the CM which tends to detach from the ground, the opposite behaviour is obtained with a lower stiffness value. At this point you can choose the stiffness value such that the trend of the load on the CM is as constant as possible, this being the most critical module.

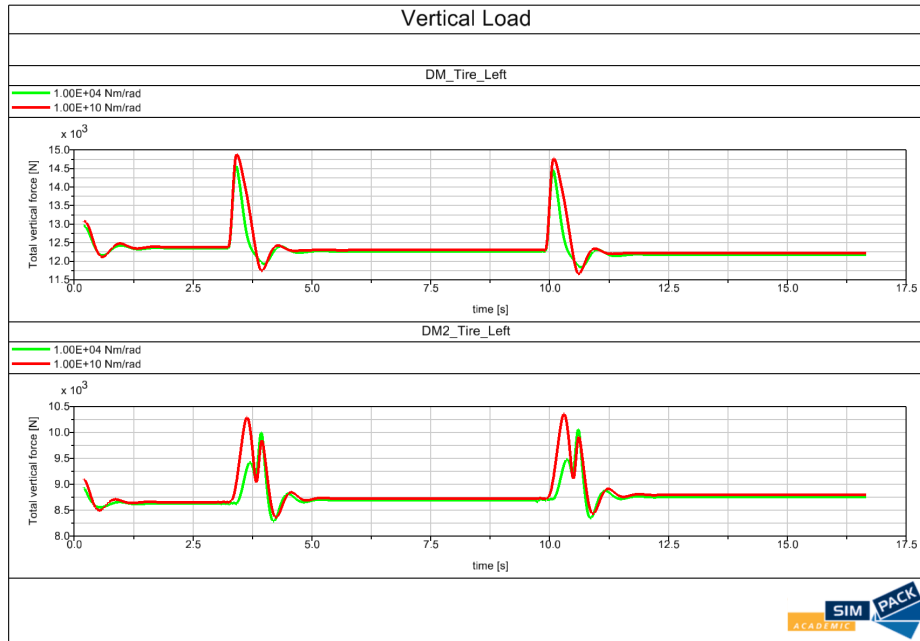


Figure 4.14: Influence of the maximum and minimum stiffness parameter on the vertical load (DM and DM2)

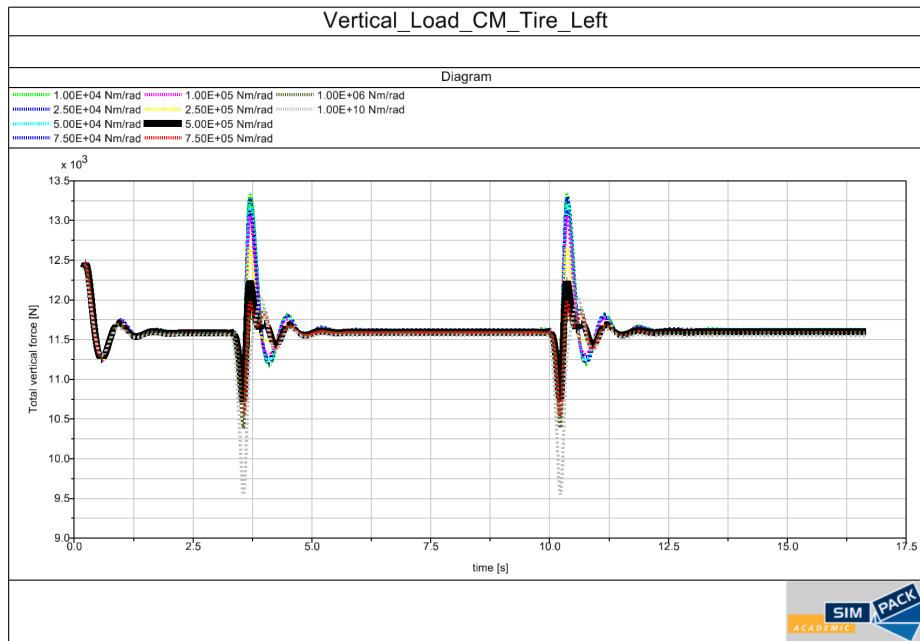


Figure 4.15: Influence of stiffness parameter on the vertical load (CM)

Figure 4.15 shows the trends of the vertical load on the left tire of the central module with the stiffness values that vary according to Table 4.6, the best value that allows satisfying the reasoning made has been highlighted.

In the figure it can be seen that the trend chosen is the one in a continuous line while the others are dashed, as you can see the trend chosen is the one that keeps the vertical load as constant as possible, so the optimal value for the stiffness of the silent block in direction β turns out to be $5.00E + 05 \text{ Nm/rad}$. The value of $7.50E + 05 \text{ Nm/rad}$ is more unbalanced as it tends to discharge more on the other modules as can be seen from the peak it reaches.

4.4 Longitudinal dampers

To optimize these elements, the “Normal” track was used which provides a straight road travelled at high speed (30 m/s), a speed control is imposed using torque to the wheels to ensure that it remains constant. Under these conditions, a step excitation with a maximum force of 25 KN is applied in the position of the connection module, on the axis of the wheels (Figure 4.16). This was done in such a way as to induce a yaw excitation, in fact for how the vehicle is made an excitation on the CM causes the vehicle to sway, the dampers are optimized to reduce as much as possible both the amplitude and the duration of the oscillation. The higher the value of the damping coefficient, the more the behaviour improves for the variables listed above, but in this way, a much higher damping force is required as with the same relative speed having a higher damping coefficient, the force determines it is superior. The approach for this type of element is to first determine a range within which the optimization of the element can be found and subsequently within this variation of values a parametric analysis is set to determine the optimized value of the key parameters of the longitudinal dampers. For the first treatment, it was decided to impose a subvar that would represent the damping coefficient of both the lower and upper dampers, keeping the angles α and β at zero for simplicity, in this case the task is only to identify a possible range of values.

In the Figure 4.16, we note that the excitation starts from zero and arrives linearly at the desired value of 25 KN represented by the subvar "\$_Val_serp", in this case, the input function is shown, then it is processed through excitation in which the values are set as a force as a function of time, a u-vector is generated from it and it is applied as input to the force element (93: Force/Torque by u (t) Cmp), in which a follow track belonging to an Isys while the "To Marker" belongs to the chassis of the CM. The two markers have been designated to be coincident with coordinates $x = -4.11 \text{ m}$, $y = 0 \text{ m}$, $z = 0.32695 \text{ m}$. The data of the connection subvars used during the simulations are those optimized so far and are represented in Table 4.7.

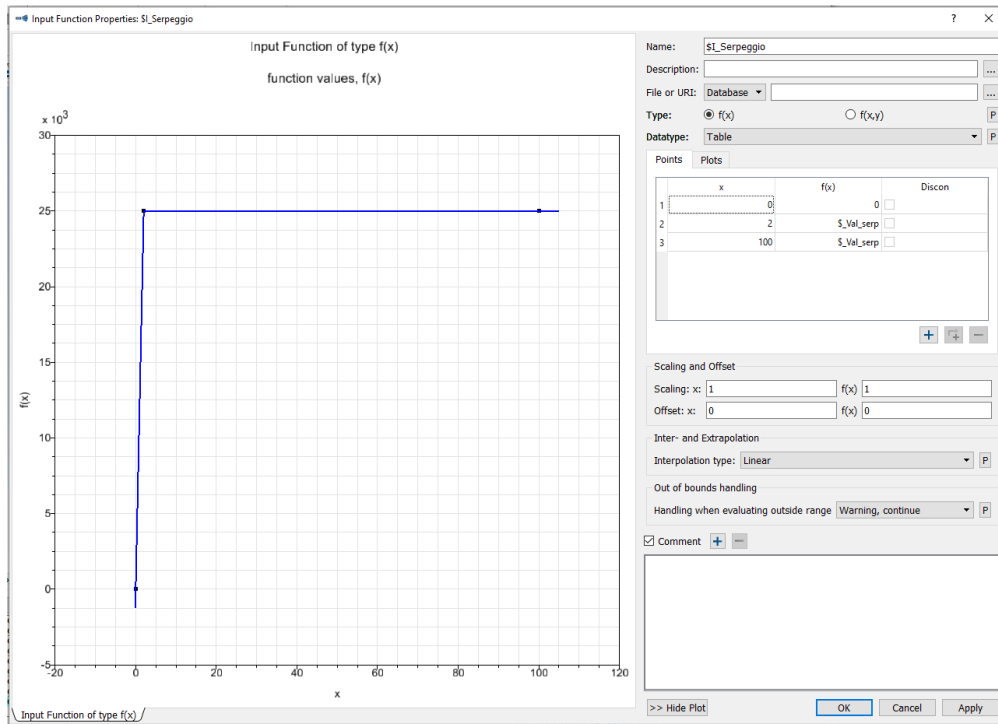


Figure 4.16: Step excitation to optimize longitudinal dampers

Table 4.7: Values of optimised SubVars for longitudinal dampers

SubVars Group	SubVar	Value	U.M.
Longitudinal Springs			
\$G_RIGIDEZZA_superiore	\$_Molle_esterne	5.00E+04	N/m
Silentblock			
\$G_Sutuco	\$_k_alfa	1.00E+06	Nm/rad
	\$_k_beta	5.00E+05	Nm/rad

At this point, a parametric analysis can be set to vary the damping coefficient, as mentioned, the same value has been applied to the upper and lower dampers to make the analysis faster. The variation of this variable is represented in Table 4.8. As a result, the yaw angle of the CM is considered, the module is indifferent to the purposes of the analysis as the behaviour is similar in all units except for a shift in time (or space). The connection joint between the chassis of the CM and the absolute reference system has six degrees of freedom, however, as previously said, they are referred to the track, consequently, the results relating to the yaw angle have been taken from this "dummy" joint, so the data refer to the reference frame jointed to it and not to the absolute reference system. It can be seen from

Table 4.8: Variation of damping coefficient

Damping coefficient	U.M.
0.00E+00	Ns/m
1.00E+04	Ns/m
2.00E+04	Ns/m
3.00E+04	Ns/m
4.00E+04	Ns/m
5.00E+04	Ns/m
6.00E+04	Ns/m
7.00E+04	Ns/m
8.00E+04	Ns/m
9.00E+04	Ns/m

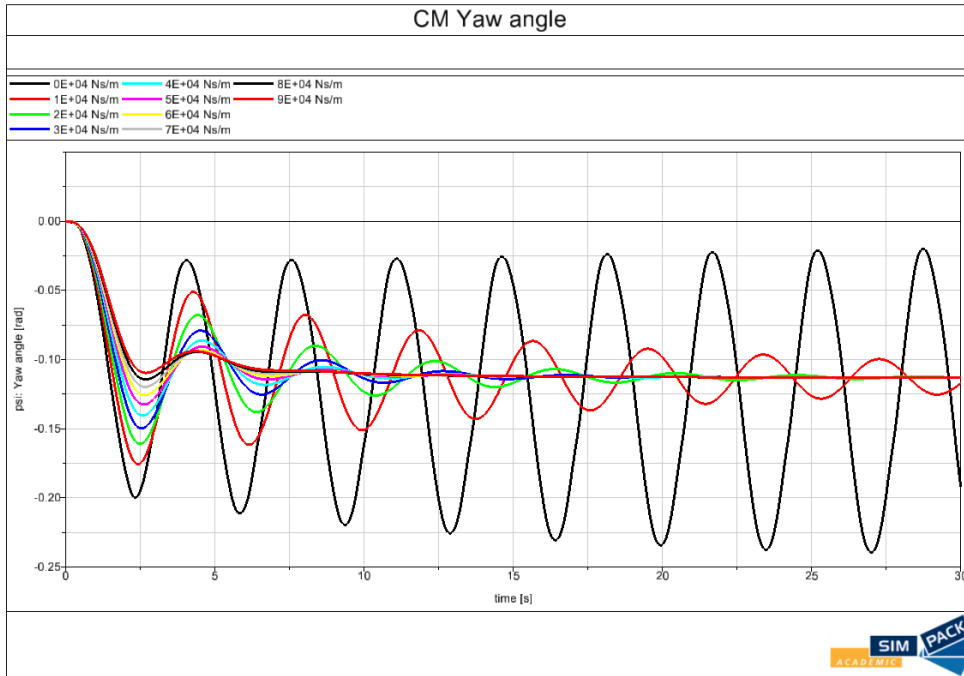


Figure 4.17: Yaw angle response to step excitation

the graph in Figure 4.17 that for a null damping value, the amplitude increases over time, leading the vehicle to instability. Instead, as can be expected as this value increases, the trend of the oscillations is more and more damped, and one passes from an under-damped system response to an over-damped response for very high coefficients like $9.00E + 04 \text{ Ns/m}$. To the detriment of these considerations, the trend of the force of the upper, front right damper over time is shown below

(Figure 4.18). It is noted that as the damping coefficient value increases, the force value that the damper must impose also increases, in the figure the condition with zero coefficient is not represented as clearly the force value will be zero. After

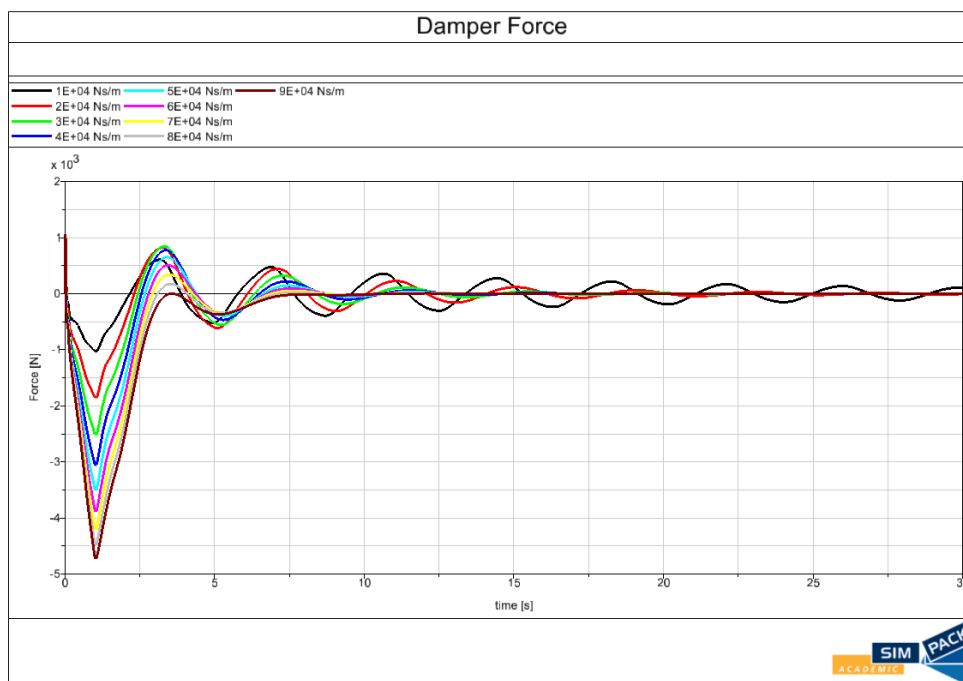


Figure 4.18: Damper force response to step excitation

these considerations, it is decided to opt for a range that varies from 0 Ns/m to $1.00E + 04 \text{ Ns/m}$ (Figure 4.19) as the maximum force exchanged is very low and it still avoids the resonance of the vehicle. The test carried out appears to be a critical condition as a higher value of lateral force leads to instability of the vehicle with any damping coefficient value. In this regard it is sufficient to choose dampers such that there is no instability; in any case, the vehicle during the running operation does not have very high performance, so this treatment is conservative. The same analysis is carried out with the variation of the values indicated above, as the maximum damping value was chosen at the value of 7000 Ns/m which represents a good compromise. Subsequently, a parametric analysis is carried out as the damping coefficients vary between a minimum and maximum value and as the angles α and β vary, reaching the best condition and analysing the influence of the different variables on the selected outputs. The analysis was carried out primarily to avoid yaw instability phenomena, in which the angle between the modules progressively grows; subsequently, the longitudinal damper element is optimized to reduce as much as possible both the oscillations and the maximum

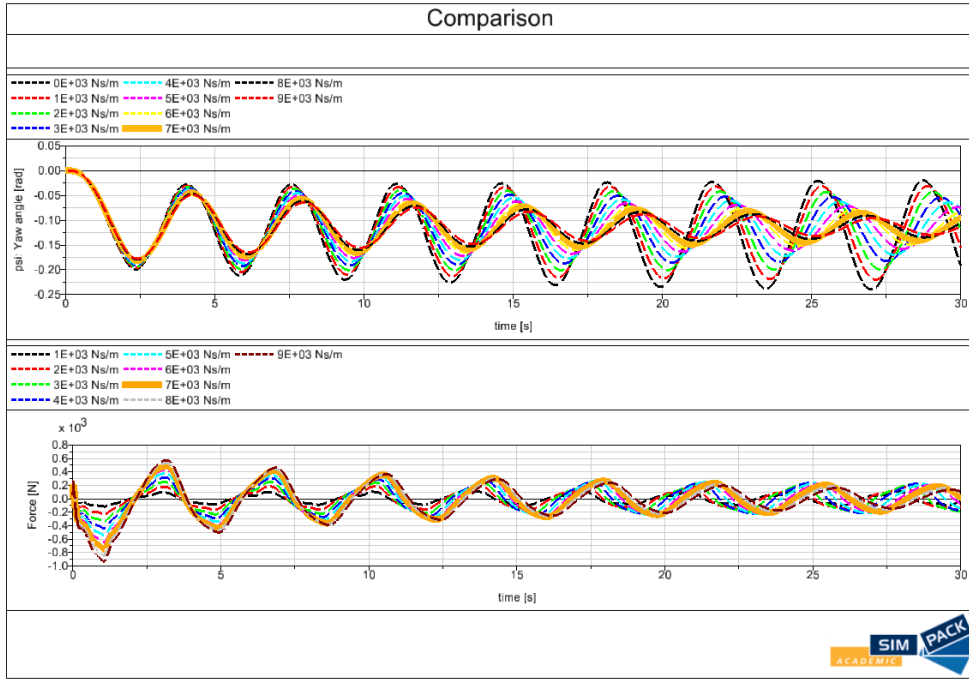


Figure 4.19: Comparison varying damping coefficient

angle (yaw) that is generated following the excitation, thus improving the lateral slip parameters of all three macro groups.

The test was carried out by imposing as a filter the maximum in the absolute value of the angle of yaw of the joint both anterior and posterior, simulations were performed simultaneously with the variation of the parameters represented in Table 4.9, in this way it is possible to sort the results starting from the smallest extracted value, making the analysis faster in choosing the best configuration. Subsequently, a comparison is made on the trend of the angle of the front joint (for the rear one it would be very similar) between the configuration in terms of α , β and damping coefficients chosen as the best and the one that gives the worst result. The excitations to which the vehicle is subjected are applied in one plane only; in this way, the yaw behaviour is maximized at the expense of rolling and pitching, in this regard the best configuration is chosen with an angle α and β different from zero to compensate for the excitement coming from the other axes. This setting was chosen because the yaw is the degree of freedom that most influences the dynamics of the vehicle, as it is constituted.

Figure 4.20 shows the influence of the various input values on the set output values (yaw, pitch, roll). The explanation of the subvar is described in Table 4.10.

Although as mentioned, the excitations occur on a single plane, they affect

Table 4.9: Parameters used for the sensitivity analysis of longitudinal dampers

α [rad]	β [rad]	C_{top} [Ns/m]	C_{low} [Ns/m]
0	0	0	0
0.1	0.1	1000	1000
0.2	0.2	2000	2000
0.3	0.3	3000	3000
0.4	0.4	4000	4000
0.5	0.5	5000	5000
0.6	0.6	6000	6000
0.7	0.7	7000	7000

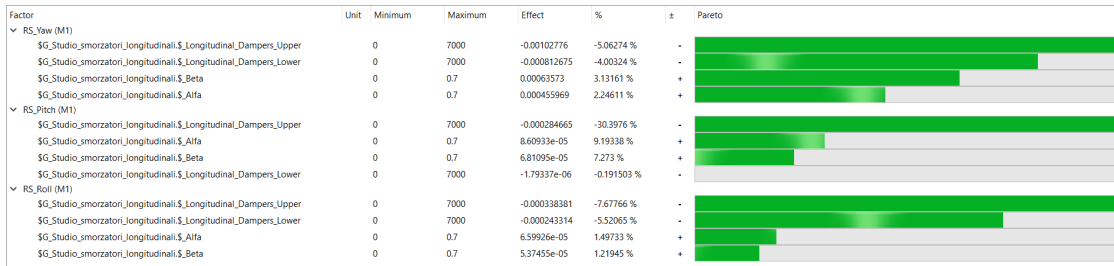


Figure 4.20: Longitudinal dampers sensitivity analysis post-processing

the vehicle going to excite the elements in the other planes, obviously in a very limited way but useful, however, to understand how the input parameters affect the outputs. In detail, the values that have a negative effect mean that they have a beneficial effect on the result because it means that by passing from the minimum value to the maximum, the amplitude of the oscillation is reduced having set as a filter the maximum in the absolute value of the function over time. Taking the yaw as a reference, it can be seen that increasing the value of the damping coefficient reduces the amplitude of the oscillation while as regards the inclination of the damper (angles α and β) it has a negative effect as reduces the arm by imposing less resistance. The same approach for comparing the effect of the parameters can be used for the other outputs. It is noted that in all three cases an inclined damper has a detrimental effect on the results, for this reason, it is decided to set the values of α and β to zero. Once the simulation was carried out, the results were sorted from the maximum value to the minimum value of the yaw angle. The values found are those shown in Table 4.11.

Table 4.10: Input subvars explained

Name	Meaning	U.M.
\$G_Studio_smorzatori_longitudinali.\$_Longitudinal_Dampers_Upper	Upper longitudinal damper coefficient	Ns/m
\$G_Studio_smorzatori_longitudinali.\$_Longitudinal_Dampers_Lower	Lower longitudinal damper coefficient	Ns/m
\$G_Studio_smorzatori_longitudinali.\$_Alfa	Angle formed in plane z-x	rad
\$G_Studio_smorzatori_longitudinali.\$_Beta	Angle formed in plane y-x	rad

Table 4.11: Optimized configuration for longitudinal dampers

C_upper [Ns/m]	C_lower [Ns/m]	α [rad]	β [rad]
7000	7000	0	0

4.5 Final configuration

Once all the optimization analyzes have been carried out using the constructed tracks, we come to the definition of a final configuration in which each element is sized correctly. In this regard, in Table 4.12 all the connecting elements are inserted with the corresponding values assigned deriving from the analyzes previously carried out. The choice of this configuration allows subsequently to go to find the forces exchanged on the joint.

Table 4.12: Optimized connection subvar values

Element	Subvar	Value	U.M.
Silentblock	\$_k_alfa	1.00E+06	Nm/rad
	\$_k_beta	5.00E+05	Nm/rad
Longitudinal dampers	\$_Longitudinal_Dampers_Lower	7000	Ns/m
	\$_Longitudinal_Dampers_Upper	7000	Ns/m
	\$_Alfa	0	rad
	\$_Beta	0	rad
Longitudinal springs	\$_Molle_esterne	5.00E+04	N/m

Knowing the values of the angles α and β , at this point the position of the upper and lower longitudinal dampers can be derived as presented in Table 4.13. As you can see, the values of the single damper do not vary in space (y and z) as the angle in those directions for the optimized configuration is zero. From the table it can be seen that the dampers have a fixed dimension from the vehicle's symmetry axis as regards the y direction; this value, in fact, represents the maximum achievable, this was done to obtain as much useful arm as possible in order to react in correct way to the excitations deriving from the external environment.

Table 4.13: Longitudinal dampers positions

Element	Position	Marker	x [m]	y [m]	z [m]
Longitudinal dampers	Upper_anterior_right	From TM	-3.358	-0.9	2.66688
		To CM	-3.713	-0.9	2.66688
	Upper_anterior_left	From TM	-3.358	0.9	2.66688
		To CM	-3.713	0.9	2.66688
	Upper_posterior_right	From CM	-4.503	-0.9	2.66688
		To TrM	-4.858	-0.9	2.66688
	Upper_posterior_left	From CM	-4.503	0.9	2.66688
		To TrM	-4.858	0.9	2.66688
	Lower_anterior_right	From TM	-3.358	-0.9	0.374
		To CM	-3.713	-0.9	0.374
	Lower_anterior_left	From TM	-3.358	0.9	0.374
		To CM	-3.713	0.9	0.374
	Lower_posterior_right	From CM	-4.503	-0.9	0.374
		To TrM	-4.858	-0.9	0.374
	Lower_posterior_left	From CM	-4.503	0.9	0.374
		To TrM	-4.858	0.9	0.374

4.6 Choice of the mechanical joint

Following the optimization of all the connection elements, the analysis of the forces exchanged on the joint can be performed to size this element. In this discussion, as mentioned, a speed trend will be considered (described in paragraph 3.10), which contains the acceleration and speed trend that the vehicle will have to replicate in the track tests. To extract the trend of the forces over time, the test is performed on a road with a slope of 4% with the required speed (and therefore acceleration) trend, this slope was chosen as it represents the maximum reached during the test; the data of the connection subvars used are the optimized ones. Figure 4.21 and Figure 4.22 show the trends along with the translational coordinates of the forces exchanged by the front and rear joint respectively, they represent the maximum value in operation. The discontinuity presented at 5 s is due to the step that is formed when passing from zero slope to the set slope. In detail, the time interval represents the space travelled from the starting point to the point where the position of the joint coincides with the step. The trend of the force in the z direction in a track without vertical slope would be practically flat, the slope of the track leads to a greater discharge on the joint both front and rear. Regarding the force in the x direction, on the other hand, it faithfully follows the acceleration trend followed by the vehicle, but it will be scaled with respect to the flat condition, because also in these conditions the forces involved are more burdensome. In the y direction, on the other hand, as expected, the equilibrium condition is 0 N since the vehicle

is symmetrical and the road is straight. In this regard, it was decided to extract the maximum value exchanged on the joint in that direction, to obtain a trend of forces in all directions. The worst condition is the curve made in the roundabout at a constant speed. It is represented in Figure 4.22.

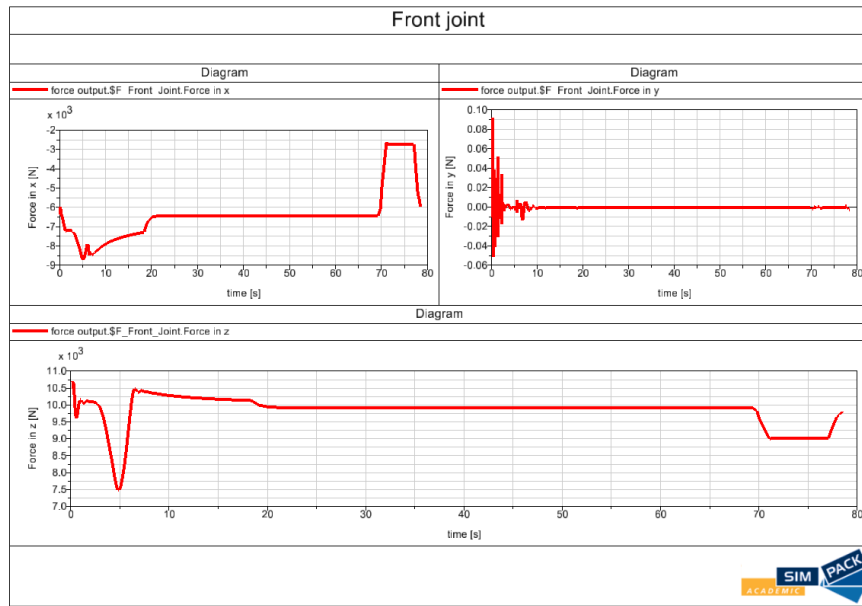


Figure 4.21: Trend of the forces exchanged by the front joint over time

Figure 4.23 shows the trend of the force in the y direction for the front and rear joint, it can be seen that both have approximately the same difference in values between the maximum and the minimum. Finally, therefore, it is possible to define the maximum forces exchanged in the various directions for both the front and rear joint. In this case, obviously, a single joint will be dimensioned which will be used as a front and rear connection. The values are presented in the Table 4.14.

Table 4.14: Maximum force in each direction for joint characterization

	Coordinate	Value [N]
Joint	x	8750
	y	3500
	z	10750

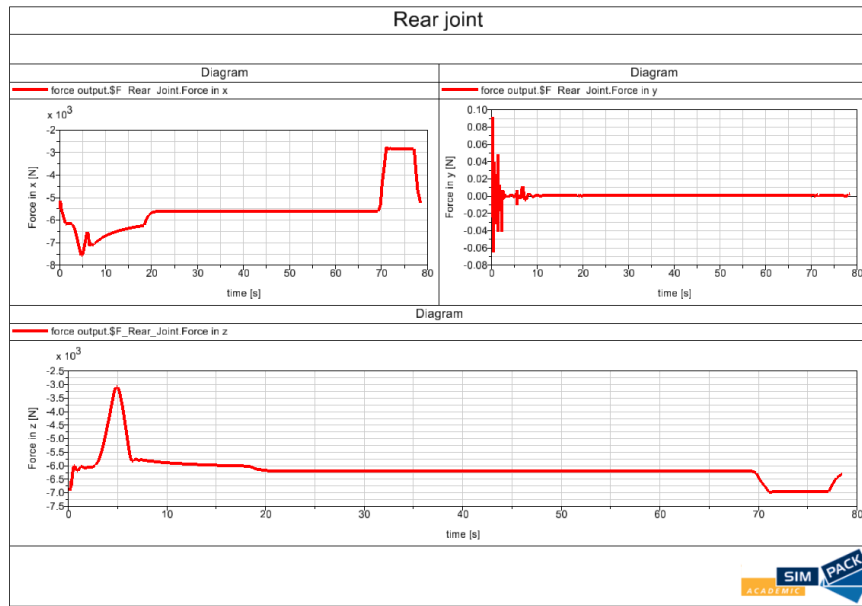


Figure 4.22: Trend of the forces exchanged by the rear joint over time

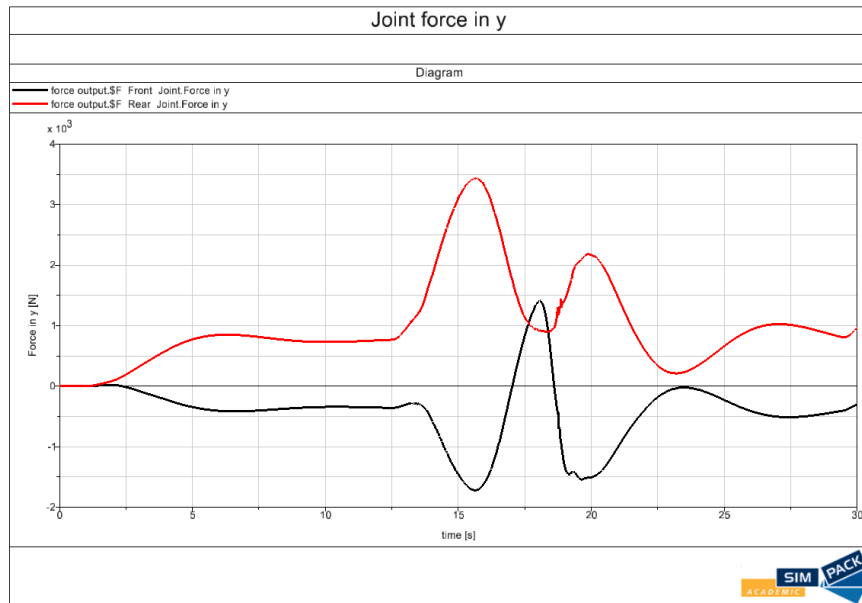


Figure 4.23: Front and rear joint force trend in y direction

4.7 Active dampers

As a further step, it has been decided to insert active dampers in the treatment, instead of the already present passive longitudinal dampers. This choice is dictated by the fact that being the vehicle in question a prototype, initially during the tests will certainly be used passive dampers to reduce the cost, then it can be performed an improvement by inserting the active dampers, to increase the performance in terms of comfort and dynamics of the vehicle. Active dampers use separate actuators, which apply a force that opposes movement to improve comfort and dampen oscillations much more quickly. This technology is very effective from a practical standpoint, but it is very expensive and requires constant maintenance. The active dampers have been placed in the longitudinal direction as a connection between the CM and the TM/TrM, this way has been followed initially by imposing a PID (Proportional-Integrative-Derivative) control on the relative speed, as an error has been given the speed difference at the ends of the damper so that the control tends to impose a zero speed, this strategy has been followed by placing a control force at each point where there is a damper. Obviously, the speed cannot be zero, because otherwise the vehicle dynamics would vary, and the steering operations could not be performed correctly because it would tend to remain rigid. Therefore, it was not possible to give a too high proportional control, in this way the high frequency oscillations are eliminated, and the travel comfort is improved. Using this technique, it is possible to choose an active damper, or ask the manufacturer for a custom-built damper having the damping force trend as a function of speed (the force coming from the PID while the speed calculated from the relative positions of the markers). For this type of treatment, we used the element "Expression" thanks to which it is possible to monitor the trend of the relative speed between two markers in time. For each damper has been calculated the relative speed in time as the instant-by-instant difference of the speed of the two markers at the extremes of the damper. This instantaneous value is defined as the error of the PID as the goal is to impose a zero relative velocity, for this purpose we created the control element using as feedback value the one extracted from the expression and inserting this value directly into the control as the difference in speed as mentioned represents the error. At this point a PID type control is set, from which the constants are then calibrated. To make a comparison between the two types of dampers two different models were used one containing the active dampers and the other the real ones. The first test was carried out on the track called "Castelfidardo roundabout", where there is a tight curve to verify that the vehicle dynamics do not vary too much in the two conditions, especially to verify that the value of the proportional control is not too high and does not stiffen the trolleybus too much. This test was conducted using a vertical excitation due from the road, the vehicle travels along the track at a constant speed of 5 *m/s*. The

second test was performed once the ideal PID parameters were found and is done to show the actual benefits they bring to both the vehicle dynamics and the comfort level of the vehicle. On a straight road an excitation is set through an impulsive type of torque value in all three rotations, this to analyze the system response; the torque results to be $20 \text{ KN} * m$ and the speed of the track is constant at 30 m/s , so the test conditions are decidedly adverse, to highlight more the differences. In normal conditions, in fact, the benefits of using active dampers for longitudinal connections are negligible.

Figure 4.24 shows the type of impulse so that is applied to the rotational degrees of freedom, it is noted that the excitation is of the step type, that is, in an infinitesimal time, it passes from zero to the maximum set value. To impose the excitation on the vehicle, a force element was used inside which the vector deriving from the excitation is inserted, inside which the input function represented in the figure is inserted. Being a force element needs of two markers, which are coincident in the centre of mass CM (the From marker is a follow track belonging to Isys while the To marker belongs to the chassis of the connection module). To choose

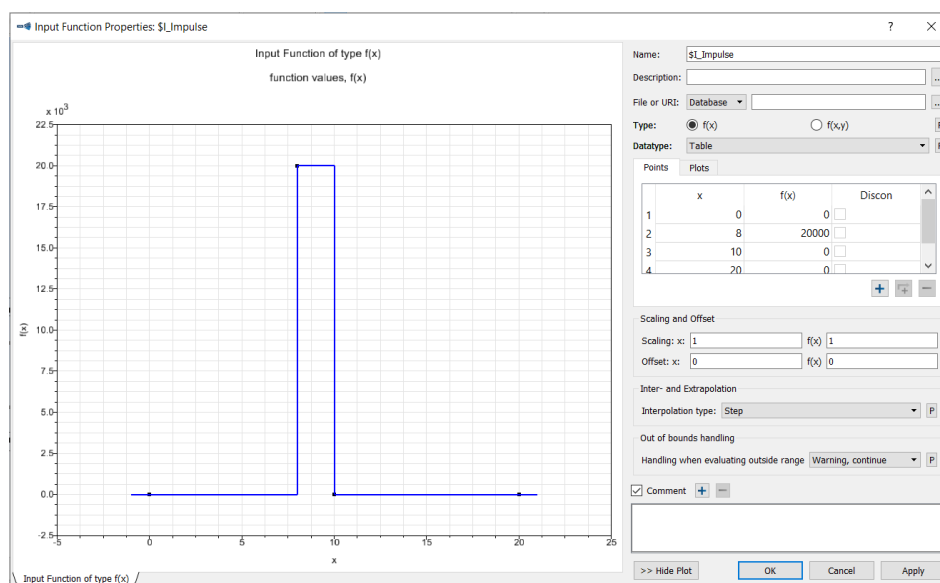


Figure 4.24: Impulse applied through input function

the values of the coefficients of the control used, a further test was used in which the same force element described above is created, with the difference that in this case a step type excitation is used to record the PID control. The maximum value of the step represents $20 \text{ KN} * m$ and is always applied through a force element between two coincident markers on the CM, in this case only the degree of freedom of the yaw is excited as the dampers are mainly used for damping in this rotation.

From the tests carried out, a control of the PD type was opted for, because it better suits the problem. For this control type the coefficients are defined. The time-continuous form function is defined as:

$$y(s) = \frac{K(1 + T_D s)}{1 + T_1 s} * u(s) \quad (4.2)$$

Where K represents the proportionality factor that has been optimized to 15000, T_D is the derivative time constant fixed at 2, finally, T_1 represents the delay time. Figure 4.25 shows the comparison between the active and passive damper in response to the step excitation. Since yaw is the exciting degree of freedom, it

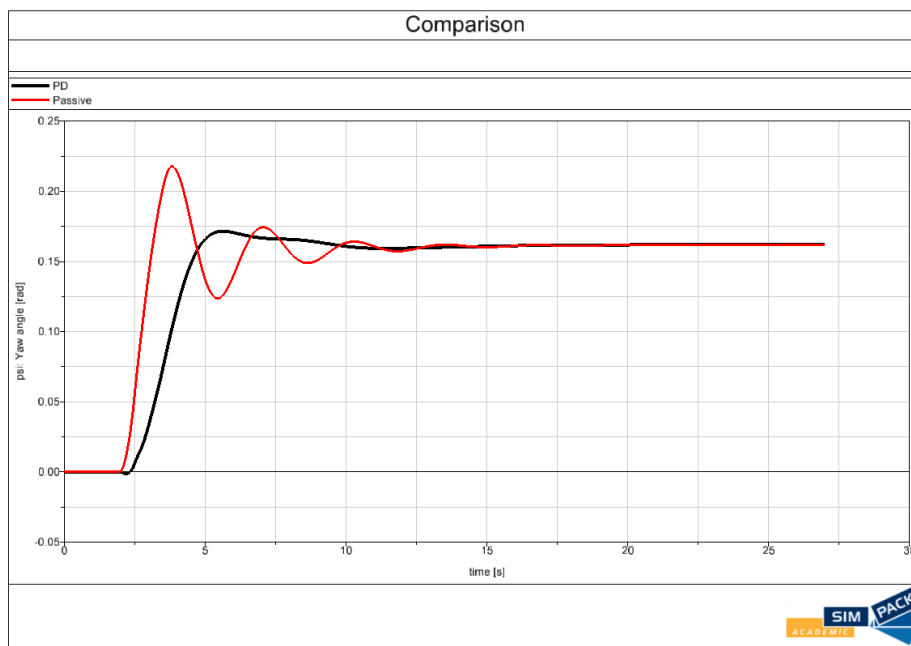


Figure 4.25: PD calibrated compared with passive dampers

is also the one taken into consideration in post-processing analyzes. You can see the difference between active and passive dampers, the first in fact has a lower maximum amplitude and moreover avoids the onset of oscillatory phenomena, which means that it is more stable and with a higher level of comfort.

First test

The first test is useful in the first instance to determine if the proportional control is too rigid and therefore if the trajectory travelled in the curve respects in principle that with the passive dampers, subsequently having imposed a vertical excitation

on the road, the results are extrapolated in terms of comfort always through a comparison between the two cases (active or passive) as the acceleration RMS. Figure 4.26 shows the trajectory followed by the two cases considered and it is

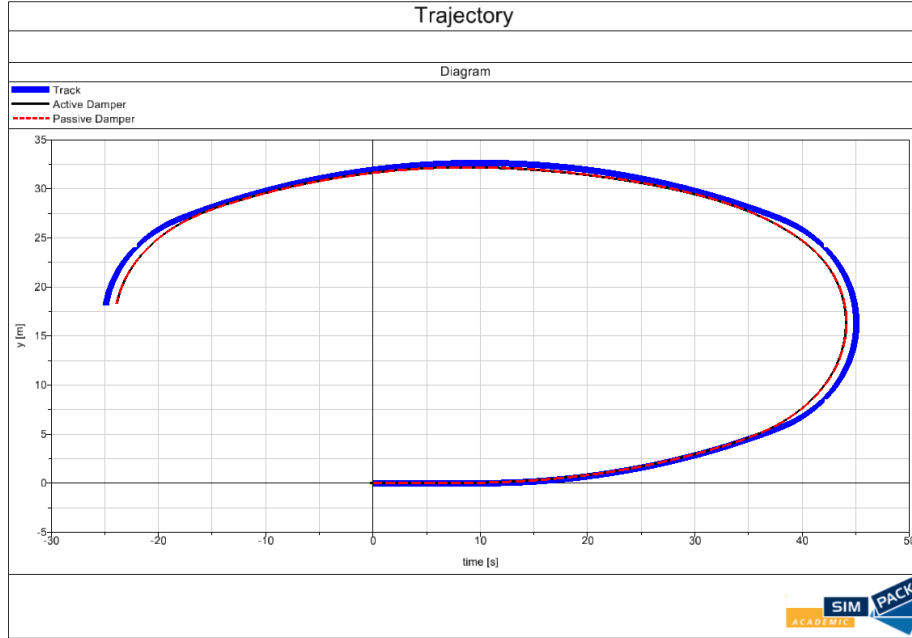


Figure 4.26: Trajectory comparison

noted that it practically coincides, which means that the result is to be considered exact for this parameter, subsequently, the acceleration is extracted on the same path. Since it is very difficult to compare the acceleration trend in the two cases due to the imposed excitation, it was decided to use a filter in post-processing that calculates the RMS on the single function, this measurement is the most significant as regards accelerations as it also considers the history of the function over time and provides an amplitude value directly related to the energy content of the vibration. It is defined as:

$$RMS = \sqrt{\frac{1}{T} \int_0^T x^2(t) dt} \quad (4.3)$$

Where $x(t)$ is the signal as a function of time and T is the duration of the signal. At this point the comparison between the two cases is shown in Figure 4.27, the modules considered in the discussion are those in which the axle with wheels is present (DM, CM, DM2).

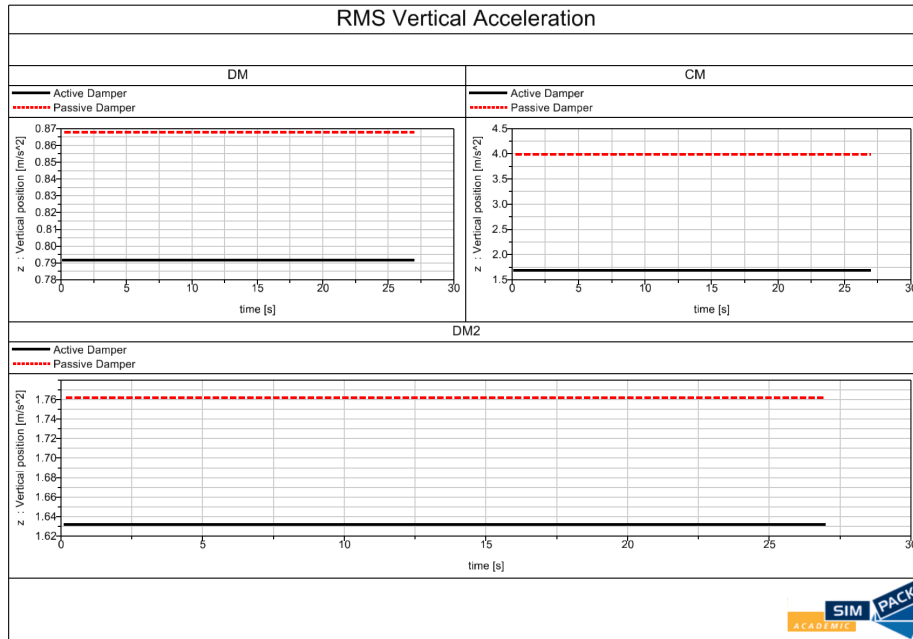


Figure 4.27: R.M.S. vertical acceleration of the different modules

It is noted that the active dampers have a beneficial effect on comfort in all the modules considered, the most evident is the vertical acceleration on the CM which represents the module most stressed, using the active dampers a value in line with the other modules is reached.

Second test

The second test has been previously described, the results are extracted in terms of roll , pitch and yaw angles as these are the degrees of freedom affected by the impulse that has been applied, to induce further instability the track has been travelled at a very high speed. In particular, the output data is extracted from the connection module, which, as noted previously, represents the most requested. In Figure 4.28 you can see the differences in terms of variation of the angles over time, it is clear that the active dampers achieve better results from all points of view, but it is also noted that the difference between the results is not so large as to prefer the one with respect to each other, especially bearing in mind that the following project represents a prototype, which means that operation is also guaranteed through the passive dampers and also allows, in the preliminary phase, to carry out the necessary tests safely and also at a cost inferior. In fact, it must also be considered that the vehicle in question has been designated for a maximum speed of 35 – 40 *Km/h*, so at those speeds the variation in results between the

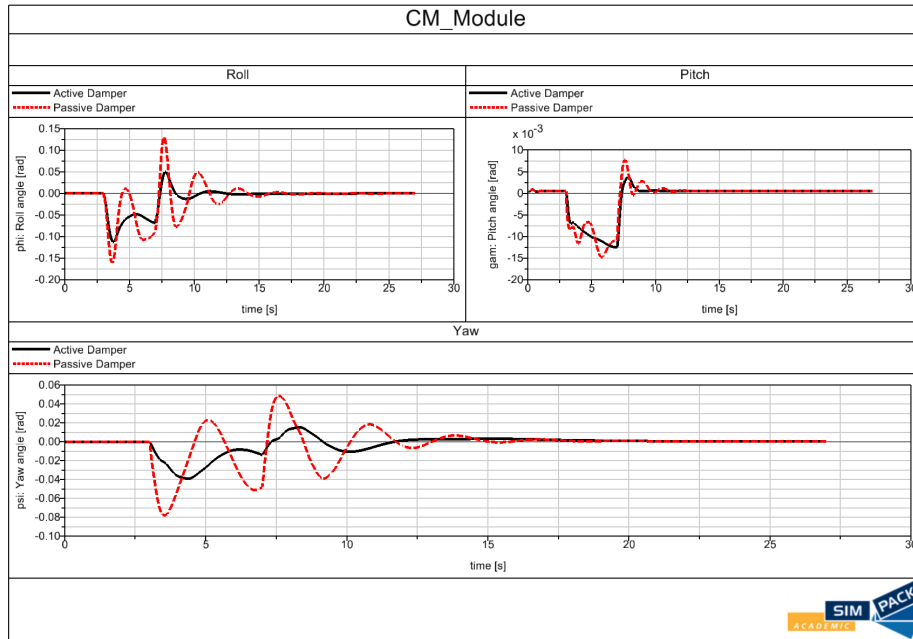


Figure 4.28: Roll, pitch and yaw angle responses to the impulse

two cases is negligible, this is mainly due to the longitudinal springs, which have been designated ad hoc and were not present in the original project but necessary to achieve the desired result, moreover, also saving in terms of cost.

Chapter 5

Conclusion

From the thesis work it is possible to extract what were the main objectives on which the guideline for the development of the paper was followed. This work was carried out in order to complete the following objectives:

- construction of the model using a multibody software;
- construction of the tracks where the vehicle will be tested;
- study and optimization of the elements of connection of the vehicle.

For the construction of the model using multibody software has been followed the classic approach that characterizes this type of code, in which the elements are grouped and simulated as rigid bodies, this drastically decrease the number of degrees of freedom within the model; this was done starting from the CAD file, assigning the material to the various bodies, and extracting the inertia matrix. The simplifications made to the model, such as the steering or the modeling of the tire-asphalt contact, are in line with both the nature of the results to be extracted and to the very limited performance of the vehicle. The objectives set have been achieved, the study of the connections has led to modify the initial design, adding several different types of connections. The most important element has been the joint since the choice of the degrees of freedom of the same, influences the choice of the connection elements useful to control the movement of the vehicle. After a careful analysis of the degrees of freedom that the trolleybus should have, a spherical joint was chosen to allow all three rotations. Compared to the initial project, the upper stiffnesses and the silent blocks have been added, particularly useful for the reaction to pitching and cornering dynamics. Furthermore, active dampers have been studied, initially a priority for the company, but after a detailed analysis it was decided to simply use passive dampers as the difference between the two is negligible for the normal driving conditions of the vehicle in question

with a significant saving in terms of initial investment and maintenance. Future developments concern the implementation of a more accurate model starting from the connections studied in this paper which are optimized. Such development would result useful for possible future improvements, mainly from the performance point of view. In fact, being this a prototype, it is tested at very low speeds and accelerations; this leads to different approximations. In fact, with the increase in performance both the contact model and the creation of the vehicle in Simpack must be more accurate; at this point it becomes interesting with higher performance the implementation of active dampers. Finally, to validate the model, once it has been simulated in detail, a last step can be to import the trolleybus frame into the multibody environment as a modal superelement, in order to take into account the flexibility of the body.

Bibliography

- [1] «World Health Organization. Global Status Report on Road Safety;WHO: Geneva, Switzerland, 2018; ISBN 978-9241565684.» In: () (cit. on p. 1).
- [2] De Jong Yeong, Gustavo Velasco-Hernandez, John Barry, and Joseph Walsh. «Sensor and Sensor Fusion Technology in Autonomous Vehicles: A Review». In: *Sensors* 21.6 (2021). ISSN: 1424-8220. DOI: 10.3390/s21062140. URL: <https://www.mdpi.com/1424-8220/21/6/2140> (cit. on pp. 2–5).
- [3] Sean Campbell, Niall O’Mahony, Lenka Krpalcova, Daniel Riordan, Joseph Walsh, Aidan Murphy, and Conor Ryan. «Sensor technology in autonomous vehicles: A review». In: *2018 29th Irish Signals and Systems Conference (ISSC)*. IEEE. 2018, pp. 1–4 (cit. on p. 4).
- [4] Babak Shahian Jahromi, Theja Tulabandhula, and Sabri Cetin. «Real-Time Hybrid Multi-Sensor Fusion Framework for Perception in Autonomous Vehicles». In: *Sensors* 19.20 (2019). ISSN: 1424-8220. DOI: 10.3390/s19204357. URL: <https://www.mdpi.com/1424-8220/19/20/4357> (cit. on p. 4).
- [5] *GNSS+INS Systems*. <https://novatel.com/an-introduction-to-gnss/chapter-6-gnss-ins/gnss-ins-systems>. 2021 (cit. on p. 5).
- [6] Abdulhakam AM Assidiq, Othman O Khalifa, Md Rafiqul Islam, and Sheroz Khan. «Real time lane detection for autonomous vehicles». In: *2008 International Conference on Computer and Communication Engineering*. IEEE. 2008, pp. 82–88 (cit. on pp. 6, 9).
- [7] «B. M. John, N. Donald, “Application of the Hough Transform to Lane detection and Following on High Speed Roads”, signal & system Group, Department of Computer Science, National University of Ireland, 1999,pp. 1-9.» In: () (cit. on p. 8).
- [8] Joseph Redmon, Santosh Divvala, Ross Girshick, and Ali Farhadi. «You only look once: Unified, real-time object detection». In: *Proceedings of the IEEE conference on computer vision and pattern recognition*. 2016, pp. 779–788 (cit. on p. 10).

-
- [9] Joseph Redmon and Ali Farhadi. «YOLOv3: An Incremental Improvement». In: *arXiv* (2018) (cit. on p. 11).
- [10] «R. Wolcott and R. Eustice, “Visual localization within LiDAR maps for automated urban driving,” IEEE International Conference on Intelligent Robots and Systems, pp. 176–183, 10 2014». In: () (cit. on p. 11).
- [11] «I. Zolanvari, S. Ruano, A. Rana, A. Cummins, A. Smolic, R. Da Silva, and M. Rahbar, “DublinCity: annotated LiDAR point cloud and its applications,” 09 2019.» In: () (cit. on p. 11).
- [12] «A. Hata and D. Wolf, “Road marking detection using LiDAR reflective intensity data and its application to vehicle localization,” 10 2014, pp. 584–589». In: () (cit. on p. 11).
- [13] Wikipedia contributors. *Simultaneous localization and mapping — Wikipedia, The Free Encyclopedia*. https://en.wikipedia.org/w/index.php?title=Simultaneous_localization_and_mapping&oldid=1027469336. [Online; accessed 25-June-2021]. 2021 (cit. on p. 11).
- [14] Jorge Fuentes-Pacheco, José Ruiz-Ascencio, and Juan Manuel Rendón-Mancha. «Visual simultaneous localization and mapping: a survey». In: *Artificial intelligence review* 43.1 (2015), pp. 55–81 (cit. on p. 12).
- [15] Liangkai Liu, Sidi Lu, Ren Zhong, Baofu Wu, Yongtao Yao, Qingyang Zhang, and Weisong Shi. «Computing Systems for Autonomous Driving: State-of-the-Art and Challenges». In: *IEEE Internet of Things Journal* (2020) (cit. on p. 12).
- [16] Pan Zhao, Jiajia Chen, Yan Song, Xiang Tao, Tiejuan Xu, and Tao Mei. «Design of a control system for an autonomous vehicle based on adaptive-pid». In: *International Journal of Advanced Robotic Systems* 9.2 (2012), p. 44 (cit. on p. 12).
- [17] Jing Yang and Nanning Zheng. «An expert fuzzy controller for vehicle lateral control». In: *IECON 2007-33rd Annual Conference of the IEEE Industrial Electronics Society*. IEEE. 2007, pp. 880–885 (cit. on p. 12).
- [18] Noor Hafizah Amer, Khisbullah Hudha, Hairi Zamzuri, Vimal Rau Aparow, Amar Faiz Zainal Abidin, Zulkifli Abd Kadir, and Muhamad Murrad. «Adaptive modified Stanley controller with fuzzy supervisory system for trajectory tracking of an autonomous armoured vehicle». In: *Robotics and Autonomous Systems* 105 (2018), pp. 94–111 (cit. on p. 12).
- [19] Francesco Borrelli, Paolo Falcone, Tamas Keviczky, Jahan Asgari, and Davor Hrovat. «MPC-based approach to active steering for autonomous vehicle systems». In: *International journal of vehicle autonomous systems* 3.2-4 (2005), pp. 265–291 (cit. on p. 12).

- [20] Xiujian Yang, Juntao Song, and Jin Gao. «Fuzzy logic based control of the lateral stability of tractor semitrailer vehicle». In: *Mathematical Problems in Engineering* 2015 (2015) (cit. on p. 13).
- [21] Aleksander Hac, Daniel Fulk, and Hsien Chen. *Stability and Control Considerations of Vehicle-Trailer Combination*. eng. SAE International, 2008 (cit. on p. 14).
- [22] Kyong-il Kim, Hsin Guan, Bo Wang, Rui Guo, and Fan Liang. «Active steering control strategy for articulated vehicles». eng. In: *Frontiers of information technology & electronic engineering* 17.6 (2016), pp. 576–586. ISSN: 2095-9184 (cit. on p. 14).
- [23] MFJ Luijten et al. «Lateral dynamic behaviour of articulated commercial vehicles». In: *Eindhoven University of Technology* (2010) (cit. on p. 14).
- [24] *BLUE Trolley Bus*. <http://blue-group.it/blue-trolley-bus/> (cit. on p. 15).
- [25] Hans Pacejka. *Tire and vehicle dynamics*. Elsevier, 2005 (cit. on pp. 20, 21).
- [26] Simpack help (cit. on pp. 31, 71).
- [27] Transportation Officials. *A Policy on Geometric Design of Highways and Streets, 2011*. AASHTO, 2011 (cit. on p. 33).